Evolutionary, Structural and Functional Characterization of X-palindromic Regions and Their Associated Genes

by

Alyssa Kruger

A dissertation submitted in partial fulfillment
of the requirements for the degree of
Doctor of Philosophy
(Human Genetics)
in the University of Michigan
2020

Doctoral Committee:

Assistant Professor Jacob L. Mueller, Chair
Professor Sally A. Camper
Assistant Professor Sue S. Hammoud
Professor John V. Moran
Professor Patricia J. Wittkopp

Alyssa Kruger

krugeran@umich.edu

ORCID iD: 0000-0001-6682-0990

Dedication

To my parents, who have supported all of my aspirations.

To Max, for the endless support and encouragement.

Acknowledgements

There are many individuals that have supported me throughout my PhD who I would like to thank. First, my PhD advisor Jake Mueller for being a supportive advisor, for your constant enthusiasm for science and for our bench conversations discussing peculiar results and oftentimes crazy scientific ideas. Conducting research has informed the way I look at science and the world around me. Additionally, I would like to thank: The Mueller lab members for creating a collaborative and supportive environment; Pam and Michele for your guidance during my first years in the lab; Jamie and Emma for your enthusiasm for research; Martin for your endless positivity and willingness to help; Callie for our bay conversations about science and life outside the lab; Dr. Turtinen for giving me my first research opportunity at the University of Wisconsin-Eau Claire and for answering every question, no matter how small; The Genetics Training Program community, NSF and Rackham for professional and financial support; My friends and family for supporting me on this adventure and for always being a phone call away; and Max for your willingness to discuss science, endless support and sense of adventure.

Table of Contents

List of Tables

List of Figures

Abstract

The mammalian sex chromosomes are enriched in large (>10kb), nearly identical (>99%) segmental duplications containing testis-expressed gene families. These genomic regions are highly variable in size, ranging from a single duplication present in a palindromic orientation (singleton palindrome) to vast duplications consisting of 10-100s copies present in both palindromic and tandem orientation (palindrome array, or ampliconic array). Both singleton palindromes and palindrome arrays harbor palindrome-associated testis-expressed gene families. In contrast to the majority of single copy sex-linked genes which are post-meiotically silenced, palindrome-associated gene families are expressed post-meiotically. Palindrome-associated gene families independently evolved, with only 30% shared between humans and mice. Furthermore, palindrome-associated gene families are rapidly evolving at the sequence level and can vary substantially in gene copy number, which are hallmarks of genes involved in fertility and speciation. These observations suggest that palindrome-associated genes have evolved mechanisms to evade the post-meiotic gene silencing which single copy X- and Y-linked genes are subject to and that palindrome-associated gene families play important post-meiotic roles in male fertility. In this thesis, I explore the evolutionary history, the importance of palindrome structure, and the functions of genes harbored within palindromes.

Using genetically engineered mouse models, I manipulated the structure and copy number of segmental duplications in two singleton palindromes (*Mageb5* and *4930567H17Rik*) and two palindrome arrays (*Slx* and *Slxl1*). My studies demonstrate the post-meiotic expression of

palindrome-associated genes correlates with gene copy number and is not dependent on their palindromic orientation. The singleton palindrome gene families, *Mageb5* and *4930567H17Rik*, are not dosage sensitive as males with a single copy of either gene exhibit no defects in fertility or spermatogenesis as compared to wild-type males. My investigation of *Slx* and *Slxl1* gene families reveal they are *Mus*-lineage specific, partially redundant, and essential for male fertility. The complete deletion of both *Slx* and *Slxl1,* results in post-meiotic spermatogenetic defects and male infertility. Additionally, alterations in *Slxl1*, but not *Slx*, gene copy number distorts the ratio of male to female offspring. This unequal transmission of X and Y chromosomes is indicative of meiotic drive, the non-Mendelian transmission of chromosomes. We hypothesize that *Slxl1* competes with a related palindromic array associated gene family on the Y-chromosome, *Sly*, as alterations in the ratio of *Slxl1* to *Sly* copy number impact the offspring sex ratio. We believe meiotic drive contributed to the massive amplification of *Slxl1* and *Sly* on the mouse sex chromosomes. As selfish elements, duplications of *Slxl1* and *Sly* enhanced not only their own transmission but the transmission of the entire X- or Y-chromosome, respectively, resulting in the massive co-amplification of *Slxl1* and *Sly*.

In sum, my studies highlight the structural and functional diversity of palindrome-associated genes in the context of spermatogenesis. Furthermore, this work outlines an approach that can be used to study and characterize additional palindrome-associated gene biology within the *Mus*-lineage as well as other species.

Chapter 1

Introduction[1]

Thesis Overview

The mammalian sex chromosomes are enriched for genes with testis-biased expression [1-4]. In male mammals, the X and Y chromosomes are present in only one copy (hemizygous) which is in contrast to autosomes. This provides a selectively advantageous environment for the acquisition and retention of genes involved in male-specific processes. In males, the hemizygosity of sex-linked genes allows new recessive mutations to be readily selected for, while new recessive mutations on autosomes are masked. Therefore, new sex-linked recessive mutations, when beneficial, can be readily selected for [1, 5]. Consequently, many X- and Y-linked genes are important for spermatogenesis—the process by which testicular germ cells undergo meiosis to reduce their ploidy and undergo substantial post-meiotic cellular reorganization to produce a sperm able to navigate and fertilize an egg [6].

Intriguingly, in mammals many X- and Y-linked protein-coding genes with testis-biased expression are contained within large (>10kb), highly identical (>99% nucleotide identity), segmental duplications in palindromic orientation [7-9]. Many palindrome-associated genes are expressed post-meiotically, in contrast to single-copy X- and Y-linked genes that are transcriptionally repressed [7]. Palindrome-associated genes come in two varieties, singleton

[1] The section titled Meiotic Drive is in preparation for submission as a review article

palindromes and palindrome arrays. Singleton palindromes consist of a single duplication in palindromic orientation (Figure 2-1B), whereas palindrome arrays contain greater than two duplications in palindromic and tandem orientation (Figure 3-7A). Palindrome arrays can be vast, containing 10s-100s of duplications, which collectively comprise multiple megabases of sequence. While palindrome-associated genes are enriched on the sex chromosomes in mammals, the collection of palindrome-associated genes have independently evolved between mammals [8, 9].

To date, explorations into individual palindrome-associated genes are limited. First, the identification and assembly of palindromic regions is challenged by the large size and high level of sequence identity between the segmental duplications. Therefore, short-read based sequencing approaches (e.g. Illumina sequencing) currently cannot be used to accurately assemble palindromic regions and instead require laborious and time-consuming clone-based sequencing approaches [10-13]. Furthermore, functional investigations of palindrome-associated genes are limited to a lineage-specific understanding because of the independent acquisition and rapid evolution of these genes in mammals [8].

Studies on X- and Y-linked palindromes indicate that the high level of nucleotide identity (>99%) between duplications is maintained through gene conversion in mice and primates, respectively [14, 15]. The maintenance of gene sequences suggests that palindrome-associated genes may have functionally significant roles; however, functional insights are limited. In humans, naturally occurring deletions on the Y chromosome remove a collection of palindrome-associated genes and are associated with male infertility [16, 17]. These deletions, known as

AZFb and AZFc deletions, remove a collection of genes making it unclear if an individual gene or subset of genes is essential for fertility [16, 17]. In mice, a single family of palindrome arrays, *Slx* and *Slxl1* on the X and *Sly* on the Y chromosome, has been studied [18-20]. Knockdown of *Sly* or *Slx/Slxl1* results in post-meiotic defects, male infertility and sex ratio distortion [18-21]. *Slxl1* versus *Sly* mediated sex ratio distortion is the result of meiotic drive, the non-Mendelian transmission of alleles, which in this case is specific to the X and Y chromosomes. The individual contributions of these genes to infertility, sex ratio distortion and spermatogenic development are not known.

In this thesis, I will evaluate the significance of the palindromic orientation and dosage of two singleton palindrome genes (Chapter 2) as well as the evolutionary and functional role of two palindrome array genes (Chapter 3). Given the finding that *Slxl1* and *Sly* are implicated in meiotic drive (Chapter 3), the remainder of the introduction will discuss the advancements and principles governing other meiotic drive systems which will serve to inform future experiments surrounding *Slxl1* versus *Sly* meiotic drive.

Meiotic Drive

Germ cells are the only cells in the body that contribute their DNA to the next generation. A feature distinguishing germ cells from somatic cells is their ability to undergo meiosis, the process by which a cell divides to produce haploid gametes (*e.g.,* eggs, sperm and spores) (Figure 1-1). The union of gametes leads to the formation of a zygote, which ultimately will develop its own gametes. Meiotic chromosome segregation give chromosomes a 50% chance of being transmitted to each offspring. However, germ cells are susceptible to hijacking by selfish

genetic elements—DNA sequences that increase their associated chromosomes transmission to more than 50% of offspring. The wide-variety of selfish genetic elements has been reviewed elsewhere [22-24]. This review will focus on meiotic drive: selfish genetic elements (meiotic drivers) that act to increase chromosome transmission from meiosis to the formation of the zygote. We define meiotic drive broadly as chromosome transmission biases occurring during female and male germ cell development, as well as in spores (*e.g.,* yeast and other fungi) [25-27].

In its most simplified form, meiotic drive systems require two components, a meiotic driver and a substrate the meiotic driver utilizes to bias chromosome transmission that can evolve suppressors (Figure 1-1). One of the two components must be a *trans*-acting factor (RNA or protein), in order to bias transmission of one chromosome over the other. The *trans*-acting factor biases chromosome transmission via interaction with either another a *cis*-acting element (DNA) (Figure 1-1A) or another *trans*-acting factor (Figure 1-1B). In many cases, the two components are in tight genetic linkage (on the same chromosome with low/no recombination between them), allowing the two components to co-evolve at the DNA sequence level without being separated via recombination. A universal requirement for meiotic drivers is a DNA sequence (either *cis*- or *trans*-acting) difference that distinguishes the driving chromosome from its wildtype non-driving counterpart. These fundamental principles of meiotic drive systems are shaped by whether a germ cell undergoes symmetric or asymmetric meiosis.

Within a species, meiotic drivers generally function exclusively in the female or male germline, but not both [26, 28]. Specifically, we propose that it is the asymmetry (female) or symmetry

(male) of meiosis that defines the biological and mechanistic constraints placed on the evolution of meiotic drivers (Figure 1-1). Females undergo asymmetric meiosis, producing a single egg and polar bodies, which are meiotic products that are not transmitted to the next generation (Figure 1-1). In asymmetric meiosis, meiotic drivers act within a cell to increase segregation of a particular chromosome homolog to the single egg (Figure 1-1A). Males, and spore producers, undergo symmetric meiosis producing four haploid sperm (or spores) during each meiotic division. In symmetric meiosis, meiotic drivers act between cells to establish a fitness differential between sperm or spores (Figure 1-1B). Here we discuss recent advancements in understanding asymmetric and symmetric meiotic drive with a particular focus on the mechanistic constraints governing these systems.

Asymmetric meiosis

In asymmetric meiosis, chromosome segregation into the egg is spatially determined and half of the genome never segregates to the egg. In mice, meiotic spindle poles are initially at the center of the cell and then migrate to the periphery. At the periphery, chromosomes attached to the outward facing spindle (cortical pole) are extruded to a polar body and those attached to the inward facing spindle (egg pole) are retained in the egg (Figure 1-1A) [29]. Meiotic drivers act to bias the orientation of chromosomes toward the egg pole, ensuring its transmission to offspring. To accomplish this phenomenon, two features are needed: (i) a *cis*-acting DNA sequence difference that differentiates the chromosomes, and (ii) a *trans*-acting molecule that differentiates the egg from the cortical pole to spatially orient the chromosomes [30, 31]. *Cis*-acting DNA sequences within or near the centromere acts as the attachment point between a chromosome and spindle pole; thus, alterations in these sequences contribute to meiotic drive (also known as

centromeric drive). There is evidence for centromeric drive in mice (*Mus* hybrids) [31-33], *Drosophila* [34] and monkeyflower (*Mimulus* hybrids) [35, 36]. Similar spatial principles also govern chromosome fate in maize, where differences in *cis*-acting non-centromeric DNA sequences cause meiotic drive [37-40]. Below we further discuss centromeric drive in mice and non-centromeric drive in maize, the systems with the greatest mechanistic understanding.

Centromeric Drive

Centromeric meiotic drive results from *cis*-acting DNA sequence differences in and around the centromere that differentially establish kinetochore-spindle pole interactions and bias a chromosomes segregation (Figure 1-1A, 2A, B). The differential recruitment of proteins between chromosome pairs can affect the segregation of chromosomes to either the egg or cortical spindle pole, ultimately leading to meiotic drive (Figure 1-2A, B). The chromosome bound to the egg pole is referred to as the "driving" chromosome, whereas the chromosome bound to the cortical pole is the "non-driving" chromosome. In mouse, there are two well-characterized cases of centromeric drive, which are studied by crossing different mouse strains to generate hybrid mice [31-33]. Both cases rely on underlying differences in centromere sequences (*cis*-acting elements) and differences in spindle functions (*trans*-acting factors) to influence a chromosomes orientation and fate (Figure 1-2A, B) [30-33]. The two cases differ by the timing at which the driving chromosome reorients relative to spindle migration (Figure 1-2A, B) [30, 31].

In one case of hybrid mouse centromeric drive, chromosomes re-orient prior to spindle migration [31]. In this case, differences in the underlying centromeric sequence differentially establish the kinetochores of driving vs non-driving chromosomes. These *cis*-acting sequence differences

coupled with differentially established *trans*-acting factors at the spindle poles facilitate meiotic drive [31]. More specifically, the microtubule organizing centers (MTOCs) differ in their size, and because MTOCs give rise to the spindle poles, the spindles also exhibit different densities (Figure 1-2A); however, it is unclear how MTOCs of different densities are established, as they are composed of a number of *trans*-acting proteins [31]. Similarly, the underlying centromeric and pericentromeric sequence differences in the centromeres in hybrid mice are not known, but they differentially recruit *trans*-acting proteins resulting in different sized kinetochores (Figure 1-2A) [31]. Interactions between the spindle poles and kinetochores are most stable when proportional—when the larger kinetochore is attached to the denser spindle pole (Figure 1-2A) [31]. When disproportionate, the interaction is unstable and leads to the recruitment of proteins, in an aurora kinase-dependent manner, which are involved in correcting erroneous microtubule interactions [31]. The correction of erroneous microtubule interactions enables the chromosomes to re-orient to form more stable kinetochore-spindle interactions during prometaphase (Figure 1-2A) [31]. When the spindle poles migrate to the cortex, the denser spindle pole preferentially faces the cortex causing the chromosome with the larger kinetochore to be extruded into a polar body (Figure 1-2A) [31]. Overall, it will be important for future studies to determine the molecular basis of the instability between the smaller kinetochore and dense spindle pole and how the denser spindle pole is preferentially directed to the cortex and thus extruded to the polar body, perhaps through cortical signaling.

In the second hybrid mouse centromere drive system, the chromosomes re-orient after the spindles have migrated to the cortex [30]. Similar to the previous example of centromeric drive, *cis*-acting centromeric and pericentromeric sequence differences exist and differentially establish

trans-acting kinetochores. In this case of centromeric drive, the spindle poles are differentiated by cortical signaling which results in an enrichment of tyrosination on the cortical spindle microtubules [30]. While tyrosination is known to be dependent on CDC42 cortical signaling, the proteins linking CDC42 and tubulin tyrosine kinase (TTL), which catalyzes tyrosination of α-tubulin, remain unknown. Smaller kinetochores interact more stably with microtubules with tyrosination than larger kinetochores do (Figure 1-2B) [30]. This difference in stability occurs because larger kinetochores recruit more BUB1 kinase and consequently more microtubule destabilizing proteins, including MCAK (meiotic centromere associated kinesin) (Figure 1-2B) [41]. MCAK, a microtubule depolymerase, acts more efficiently on microtubules with tyrosination. Therefore, larger kinetochores with more MCAK form less stable interactions with the tyrosinated cortical microtubules and re-orient to the egg pole, promoting their segregation to the egg (Figure 1-2B) [41, 42]. A greater understanding of this model could be gained by determining the underlying centromeric sequence differences via long-read sequencing and the factors involved in TTL recruitment [43, 44]. As different hybrid mice utilize different mechanisms to favorably re-orient driving chromosomes and bias their segregation to the egg, it is likely that many other cases of centromeric drive exist both within the *Mus*-lineage and across other animals, each with their own corresponding mechanism [31, 33, 41]. Detection of these systems is dependent on the strength of drive, hybrid background and the ability to decipher homologous chromosomes.

Non-centromeric drive

Non-centromeric drive is defined as female meiotic drive that involve *cis*-acting sequences outside of the native centromere and pericentromeric region that bias a chromosomes segregation

to the egg. Examples of non-centromeric drive include mouse *R2d2* [45, 46], HSR(homogeneously stained region) [47] and *Om* (ovum mutant) [48, 49] and rice (*O. sativa*) *S5* [50, 51]. However, the non-centromeric drive system with the greatest mechanistic understanding is knob-mediated meiotic drive in maize. A variant form of maize chromosome 10 (Ab10) contains additional repetitive heterochromatic sequences outside the centromere known as knobs, which function as *cis*-acting neocentromeres and interact with spindle microtubules independently of a kinetochore (Figure 1-2C) [39]. Similar to mammalian oogenesis, a single egg is ultimately produced from meiosis in maize. However, instead of polar bodies, meiosis results in four meiotic products (*i.e*., a meiotic tetrad), but only the distal cell will ultimately become the egg. Chromosomes with heterochromatic knobs migrate faster along the outer spindle poles, promoting their segregation to the distal cell (Figure 1-2C) [37, 40]. Knob-mediated meiotic drive is dependent on a *trans*-acting kinesin protein known as Kinesin driver (KINDR), which is encoded on Ab10 and localizes specifically to *cis*-acting 180 bp knob repeats on both Ab10 and other chromosomes [38]. KINDR binds knobs and moves knob-containing chromosomes towards the outer spindle pole in the direction of chromosome segregation (Figure 1-2C) [38]. The Rhoades model of knob-mediated drive depicts knobs segregating to the distal and proximal cells of the meiotic tetrad aided by a recombination event between the centromere and knob (Figure 1-2C) [52]. The factors that cause KINDR to move knob-containing chromosomes towards the outer spindle poles, as opposed to the inner spindle poles, are not known. While KINDR and 180 bp repeats on Ab10 are genetically linked, KINDR acts in *trans* and therefore all other chromosomes containing the 180 bp repeat are preferentially segregated. This ongoing meiotic drive has resulted in the new acquisition of 500Mb of repetitive sequence in the Maize genome [38]. Maize also contains TR-1 neo-centromeric repeats, which are

functionally distinct from180-bp repeat drive, and may serve to suppress 180-bp drive [37, 38, 53, 54]. Future work can explore the mechanism by which KINDR navigates to the outer spindle poles and the components involved in TR-1 meiotic drive.

Symmetric meiosis

Symmetric meiosis leads to four meiotic products, sperm or spores, half of which contain the meiotic driver. To bias transmission in a symmetric meiotic drive system, gametes with and without the driver must be phenotypically distinct from each other (*e.g.,* carrying an X or Y chromosome, Figure 1-1B). Phenotypic differences between gametes with and without the selfish genetic element manifest in one of two ways. First, if gametes with and without the selfish genetic element are equally present, they exhibit a functional difference (*e.g*., reduced motility of sperm). Alternatively, gametes lacking the driver fail to develop and are underrepresented (*e.g*., sperm- or spore-killing). Fundamental to both scenarios, is a molecular difference (DNA, RNA, and/or protein) distinguishing drive and non-drive containing gametes (Figure 1-1B, Figure 1-3, Figure 1-4).

As symmetric meiotic drive systems rely on the presence molecular differences (*e.g.,* carrying an X or Y chromosome), they function after homologous chromosomes have been separated in meiosis I. However, during spermatogenesis, meiotic and post-meiotic germ cells are connected in syncytium by cytoplasmic bridges, which enable the sharing of *trans*-acting factors (RNA and protein gene products) [55-58]. Gene product sharing makes genetically distinct cells (*e.g.,* X- versus Y-bearing sperm) phenotypically or functionally diploid, mitigating molecular distinctions at the RNA and protein level [55, 56, 59]. Therefore, to generate and maintain

phenotypic differences between sperm (*e.g.*, with or without a meiotic driver), implies there is spatial regulation between connected cells. This spatial regulation between cells is governed by the restriction of *trans*-acting factors transit via cytoplasmic bridges. We therefore define *trans*-acting factors as *intercellular* when they are shared through cytoplasmic bridges and are present in the cells where they are not transcribed/translated (Figure 1-1B, green mRNA and protein). In contrast, we use *intracellular* to define *trans*-acting factors which are not shared across cytoplasmic bridges (Figure 1-1B, grey mRNA and protein). Despite the prevailing view that cytoplasmic bridges facilitate *trans*-acting factor sharing, certain factors are not shared, indicating that sharing through cytoplasmic bridges can be a regulated process [60-64]. We highlight both a male and spore-producer for two models of symmetric meiotic drive (target-killer and poison antidote), placing particular focus on the mechanism of meiotic drive and the *intracellular* versus *intercellular* regulation of *trans*-acting factors.

Target-Killer

In the target-killer model, the driving chromosome encodes a *trans*-acting killer that acts intercellularly on a target in the non-drive containing cell to disrupt a cellular process (*e.g.,* developmental arrest, perturbed motility, apoptosis, etc.). Unlike the killer, the *cis*-acting or *trans*-acting target is encoded on the non-driving chromosome and must exist intracellularly to only disrupt the non-drive containing cell. In order to prevent the killer from self-destructing, the killer and target must remain on distinct haplotypes (Figure 1-3A). To prevent the killer and target from being on the same chromosome (haplotype), the target and killer need to be in tight genetic linkage (the two loci map to positions that are in close proximity to each other in the genome), making recombination events between the killer and target loci on distinct haplotypes

infrequent (Figure 1-3A). The killer can be expressed before meiosis as long as the target is not present and vice versa (Figure 1-3A). If the target itself is a stretch of DNA or expressed before meiosis not only must it remain intracellular, but expression of the killer after meiosis I is necessary for the killer to exclusively target non-drive containing cells (Figure 1-3A). Below we will discuss two target-killer systems, the *Drosophila melanogaster Segregation Distorter* (*SD*) [65] and the fungus *Podospora anserina Het-s* [66-68]. Another relevant target-killer system is *Sa* drive in *Oryza sativa* [69].

Drosophila melanogaster—Segregation Distorter

Segregation Distorter (SD) is an autosomal meiotic drive system present on chromosome 2 in *Drosophila melanogaster*. Males heterozygous for SD (denoted SD) and wild type chromosome 2 (denoted SD^+) transmit SD up to ~95% of the time. Meiotic drive results from the disrupted development of sperm carrying SD^+ (wild type chromosome 2) [65]. SD encodes an intercellular *trans*-acting killer, a truncated duplicate of wild type RanGAP (Ran GTPase activating protein) that is expressed before meiosis and mislocalizes to the nucleus, known as Sd-RanGAP (Figure 1-3B) [70, 71]. The truncated Sd-RanGAP acts intercellularly by targeting a *cis*-acting 120-bp pericentric repeat known as *Responder* (*Rsp*) [72-74]. Though *Rsp* is present on both SD and SD^+ (wild type) chromosomes, the sensitivity of *Rsp* correlates with repeat copy number—SD^+ is sensitive as it contains many copies (>700 copies, Rsp^S allele), whereas SD is insensitive as it contains few copies (<20, Rsp^I allele) (Figure 1-3B) [65, 72-74]. Both the proximity of SD to the centromere and the presence of inversions suppress recombination between the killer *Sd-RanGAP* and the target Rsp^S, which keeps *Sd-RanGAP* and Rsp^I physically linked and prevents the killer from targeting itself [65].

How Sd-RanGAP disrupts SD^+ cellular development is unknown, and likewise, it is unclear if Sd-RanGAP interacts with Rsp^S directly or indirectly [65]. Multiple models for SD have been proposed and all assume a disruption in nuclear transport arising from a disrupted RAN gradient, normally established by the cytoplasmic localization of wild type RanGAP and nuclear RanGEF (Figure 1-3B) [26, 65, 75]. However, Sd-RanGAP mislocalizes to the nucleus and nuclear mislocalization of wild type RanGAP is sufficient to cause drive. This result implicates the nuclear localization of Sd-RanGAP in the mechanism underlying SD drive [76]. Phenotypically, SD^+ sperm fail to undergo chromatin compaction, a process necessary for proper sperm development (Figure 1-3B) [77]. One possible mechanism linking these two observations is that *Rsp* derived piRNAs are needed to silence the *Rsp* locus in order to undergo proper chromatin compaction, and disruptions in nuclear transport prevent production and/or localization of piRNAs silencing complexes [26, 76]. It is unclear whether piRNA production and trafficking rely on the RAN gradient. If piRNA regulation is dependent on a RAN gradient, then it is surprising that more widespread problems do not arise as piRNAs play a critical role in transposon silencing [78]. Though Sd-RanGAP likely affects all sperm, as it is expressed before meiosis (intercellular), disrupted *Rsp* silencing would have greater effects on high copy number Rsp^S than low copy number Rsp^I. Supporting this mechanism, small *Rsp* RNAs are associated with the germline specific piRNA silencing proteins [79]. Additionally, mutations in the PIWI protein, Aubergine, enhance the SD phenotype, implicating piRNA based silencing as a component of SD the mechanism [80]. Future work is necessary to test this model and could explore whether transcriptional silencing of *Rsp* is sufficient to suppress meiotic drive.

Podospora anserina—Het-s

Het-s drive in the fungus *Podospora anserina* utilizes two different alleles of the same protein, HET-s (killer) and HET-S (target) [66]. These two alleles (*Het-s* and *Het-S*) are brought together when two different strains of *P. anserina* fuse [66]. HET-s can undergo a conformational switch to form a prion (killer) that is toxic when it interacts with its target, HET-S (Figure 1-3C) [66] . It is not known what causes HET-s to switch from the wild type to prion form. This interaction causes HET-S protein integrate into and destabilize the plasma membrane of *het-S* spores (Figure 1-3C) [67]. Given the similarity in sequence between *Het-s* and *Het-S,* it is surprising that HET-s is not toxic by itself. One possibility for evading self-toxicity is that the transmembrane domain of HET-s is less able to permeate the plasma membrane. Furthermore, meiotic drive only occurs when the *Het-s* genotype comes from the female strain, because the cytoplasm is almost entirely maternally inherited (Figure 1-3C) [66]. Since *Het-s* and *Het-S* are transcriptionally silenced until after meiosis when individual spores are formed [68], the maternal transmission of the cytoplasmic contents ensures HET-s segregates to all resulting spores to function intercellularly. When *Het-s* and *Het-S* are expressed in individual spores, *Het-S* spores produce HET-S protein which is intracellular and complexes with the maternally transmitted HET-s prion, specifically killing *Het-S* spores (Figure 1-3C) [68]. Future work could examine the differences between *Het-S* and *Het-s* to understand the difference that enable HET-s to form a prion as well as the basis for its toxicity in the presence of HET-S.

Poison-Antidote

In the Poison-Antidote model, the driving chromosome encodes both a poison and an antidote in tight genetic linkage. The poison acts intercellularly and is toxic to all cells. The antidote

neutralizes the effects of poison but must act intracellularly to preferentially spare the cell containing the driving chromosome. Tight genetic linkage between the poison and antidote prevents recombination and the driver from poisoning itself. The poison can either be shared across cytoplasmic bridges following meiosis or be expressed during meiosis I and persist into non-driving cells after meiosis to poison them. Importantly, if expressed before or during meiosis I, the poison cannot function until after homologous chromosomes have separated or the poison will self-destruct (Figure 1-4A). In contrast, the antidote is expressed after the driving and non-driving chromosome separate (meiosis I) and passage through cytoplasmic bridges must be prevented for the antidote to act intracellularly (Figure 1-4A). Poison-Antidote male meiotic drive systems, include: the mouse *t*-haplotype [62, 81-87], *Neurospora intermedia Sk-2* and *Sk-3* [88-90]*, Podospora anserina Spok* genes [91, 92]*, Schizosaccharomyces pombe wtf* genes [93-97] and *Oryza sativa qHMS7* [98]. Below we discuss the male *t*-haplotype and yeast *wtf* poison-antidote systems.

Mouse t-haplotype

The mouse *t*-haplotype is a well-studied mammalian poison-antidote meiotic drive system on chromosome 17. The *t*-haplotype contains four inversions that suppress recombination between it and wild type chromosome 17, keeping antidote and the poisons in tight genetic linkage. Males heterozygous for the *t*-haplotype (*t*) and wild type chromosome 17 (+) can transmit the *t*-haplotype up to 99% of offspring [99]. Preferential transmission of the *t*-haplotype arises from multiple intercellular poisons which collectively dysregulate cellular signaling pathways and disrupt sperm motility [81-87]. Specifically, poison induced dysregulation is thought to converge on post-meiotically expressed intracellular wild type SMOK1 (Sperm motility kinase 1), which

results in disrupted sperm motility. In contrast, *t*-haplotype SMOK1 (TCR) functions intracellularly as an antidote (Figure 1-4B), sparing *t*-haplotype carrying sperm (Figure 1-4B) [62, 87]. It remains to be determined whether the swimming defects are specific to sperm carrying wild type chromosome 17 [100].

SMOK1 dysregulation occurs by the combined efforts of poisons encoded on the *t*-haplotype known as *t*-complex distorters (*Tcd*) [83-86]. *Trans*-acting *Tcd*s have been identified as the duplicated *Tagap1* (*Tcd4*), overexpressed *Fgd2* (*Tcd2a*), hypomorphic *Nme3* (*Tcd2b*) and an isoform of *Tiam2s* (*Tcd1*) [83-86], which are pre-meiotically expressed and are therefore predicted to function intercellularly in wild type cells after meiosis I [83-86]. The identification of *Tcd*s indicates disrupted Rho-signaling pathways act to dysregulate SMOK1. However, there are still many unidentified components in this drive system including *Tcd3* and the proteins that link *Tcd*s to Rho-signaling. Furthermore, TAGAP1 and FGD2 are thought to enhance both inhibitory and activating regulators of Rho-signaling, respectively, but the directionality of SMOK1 dysregulation is not known. Interestingly, *Smok1* is present in multiple copies on the *t*-haplotype and wild type chromosome 17 [100, 101], but it is unclear why wild type copies of *Smok1* present on the *t*-haplotype do not sensitize *t*-haplotype sperm. The identification of SMOK1 targets will help understand how flagellar function is impaired leading to sperm motility defects.

Saccharomyces pombe and *Saccharomyces kambucha—wtf4*

The *wtf* meiotic drivers have been uncovered in yeast hybrids between *S. pombe* and *S. kambucha* [93-97]. The *wtf4* gene, on chromosome 3 in *S. kambucha* encodes both the poison

and antidote, due to alternative transcriptional start sites (Figure 1-4C) [93]. The longer isoform encodes the antidote and the short isoform encodes a poison. The poison (short isoform) acts intercellularly to poison spores that do not encode it, whereas the antidote (long isoform) acts intracellularly. However, while interspore bridges have been identified in distantly related *S. cerevisiae,* which may enable gene product sharing, it is unclear whether these hybrids have bridges [102]. With or without interspore bridges, the *wtf4* poison is expressed before meiosis which enables *wtf4* mRNA/protein to be present in all spores (Figure 1-4C). In contrast, the antidote is expressed after meiotic divisions and is present exclusively in cells with *S. kambucha wtf4* gene (Figure 1-4C) [93]. These findings indicate that poison induced toxicity is specific to post-meiotic cells as earlier cells (pre-meiotic and meiotic) containing the poison appear unaffected. Recent work indicates that the poison by itself forms dispersed aggregates which are toxic and kill spores, though the mechanism underlying this toxicity is unclear [103]. In cells with the antidote, the poison and antidote aggregate together near vacuoles and are no longer toxic, indicating the targeting of the complex to the vacuole is an important step (Figure 1-4C) [103].

In *S. pombe* the *wtf* gene family has expanded and diverged at the sequence level, resulting in multiple additional dual poison-antidote, and antidote only, *wtf* genes [93-96, 104]. The fact that *wtf4* can also function in *S. cerevisiae,* which is 350MY diverged from *S. kambucha*, suggests they target a common biological pathway [103]. It remains unclear how *wtf* systems act independently of one another given their sequence similarity and likely similar mechanism dependent on alternative transcriptional start sites. Interestingly*, Spok* genes in the fungus *P. anserina* also constitute both the poison and antidote [91]. Unlike *wtf4,* which relies on distinct

isoforms, a single isoform of *Spok* appears to simultaneously function as the poison and antidote, though the mechanism and regulation of these functions is unknown [92]. Future studies could investigate the sequence differences between *wtf* family members that enable them to function as distinct poison-antidote meiotic drivers.

Discussion

Meiotic drive systems continue to shape the evolutionary trajectory of genomes and species, yet remain challenging to study for multiple reasons [22, 24, 105, 106]. First, meiotic drivers reside in regions of the genome where recombination is suppressed and are therefore not amenable to traditional genetic approaches. Second, meiotic drivers are typically not associated with an easily observable phenotype. In rare cases when they are genetically-linked with readily observable phenotypes (*e.g.,* sex ratio distortion when involving the sex chromosomes or shortened tails associated with the *t*-haplotype), then they are more easily detected. Third, suppressors can evolve to silence the driver, necessitating hybrid models to place meiotic drivers in a naïve background lacking suppressors. Lastly, meiotic drivers are often lineage-specific, rapidly evolving and in duplicated regions of the genome, making their identification, annotation and characterization more challenging than conserved single-copy sequences. As a result, even within a species, independent mechanisms can govern seemingly similar drive systems, as is the case for female mouse centromeric drive [30, 31, 33, 41].

With the recent advances in DNA sequencing technologies there is the potential to detect novel meiotic drivers and new components of existing drive systems in newly sequenced genomes. Comparative sequence analyses of individuals within a species or between species, will be

important in addressing some of the challenges in detecting meiotic drivers and in improving our mechanistic understanding of their functions. For example, for asymmetric meiosis, long-read sequencing has now been able to resolve centromere sequences and architecture, providing an opportunity to track their transmission and evolution and determine the underlying sequences governing in mouse hybrid drive systems [43, 44, 107]. For symmetric meiosis, single cell RNA-sequencing of meiotic and post-meiotic testicular germ cells will more precisely define temporal gene expression patterns, which is important for which factors are expressed and intracellular versus intercellular in haploid germ cells [64]. Additionally, since some meiotic drivers are in complex regions of the genome, high quality genome assemblies with long-read sequencing technologies will help resolve these complex regions and provide an opportunity for them to be characterized via reverse genetic approaches (*e.g.*, CRISPR). Whether the meiotic drive system represents sequence variation at a single gene (*e.g., wtf4*) or in a complex genomic region (*e.g.,* centromeres) the utilization of these advanced sequencing technologies for comparative studies will enable the identification of new meiotic drivers.

New meiotic drive systems can also evolve on top of one another by integrating into pre-existing meiotic drive pathways. In maize, TR-1 repeats create neocentromeres which can suppress 180bp repeat neocentromeres (knobs) [53, 54]. Similarly, two sex chromosome drive systems in *Drosophila simulans,* Winters and Durham, share a common suppressor [108]. This complex layering of drivers, enhancers and suppressors may be a common theme of meiotic drive. Such layering further complicates their mechanistic characterization, creating systems not easily classifiable under existing models. Greater mechanistic understandings may also reclassify

existing drive systems, such as the Sd-RanGAP killer with Rsp^S being the target, may be Sd-RanGAP as a poison and Rsp^I as the antidote.

Emerging drive models with evolving complexity: The case of Slxl1 and Sly in mice.

In mouse, a sex ratio drive system between X-linked *Slxl1* and Y-linked *Sly* does not fit under existing models. Mechanistically, the ratio of *Slxl1* to *Sly* gene copy number governs the offspring sex ratio [18, 109]. Removal of all *Slxl1* gene copies results in male biased litters (60% male), whereas overexpression of *Slxl1* and the related *Slx* gene results in female biased litters (60% female) [109]. The poison-antidote model requires both components be on the same chromosome, but *Slxl1* and *Sly* are on opposite sex chromosomes. Under the target-killer model, loss of the killer, *Slxl1,* would be expected to neutralize meiotic drive, yet loss of *Slxl1* results in meiotic drive. *Slxl1* and *Sly* may represent individual poison antidote systems or factors beneficial to X-bearing and Y-bearing sperm, respectively. Under either of these models, the back and forth duplication of *Slxl1* and *Sly* would alter the offspring sex ratio to a female or male bias, respectively. Repeated back and forth duplication may be a common theme of meiotic drivers [109]. *Slxl1* and *Sly* might also be regulators of another drive system as they both interact with the Y-linked massively duplicated SSTY1 and SSTY2 [109, 110]. Given the shared signature of gene duplication and testis expression, it is tempting to speculate that *Ssty1/2* are sex ratio meiotic drivers, creating a complex *Ssty1/2-Slxl1-Sly* network of meiotic drive [9, 109].

Conclusion

The impact of meiotic drivers is not trivial. Since meiotic drivers are associated with negative fitness costs [111], suppressors capable of silencing the driver evolve and are readily selected

for. A back and forth arms race ensues as drive enhancers and suppressors continuously emerge, altering the genome. The evolution of suppressors and enhancers can create new gene functions that reconfigure existing biological pathways. Meiotic drivers are thus a powerful force continuously shaping the genetic architecture of future genomes and biological pathways.

Figures

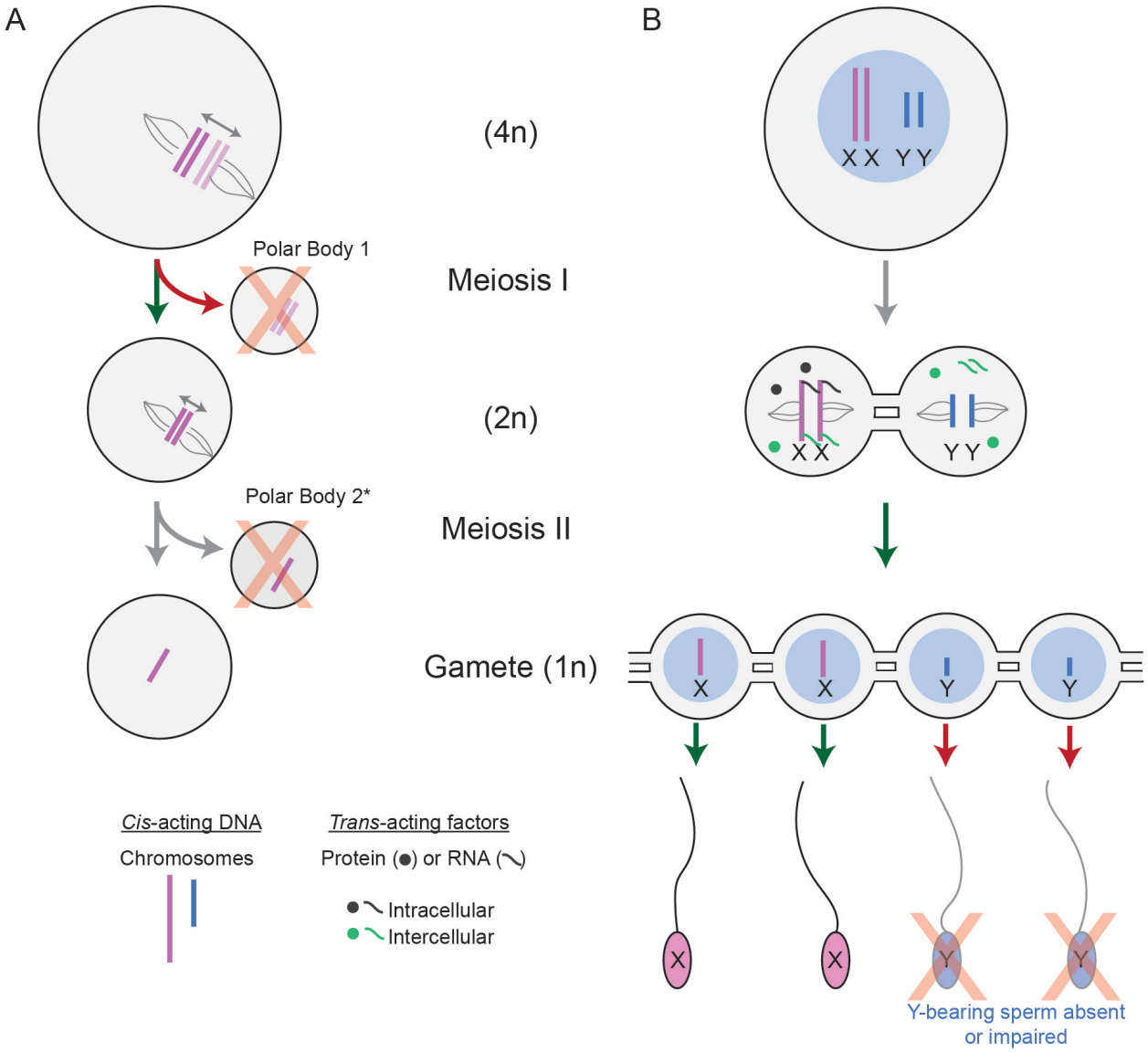

Figure 1-1.The defining features of meiotic drive in symmetric and asymmetric meiosis

A) Females undergo asymmetric meiosis—a single gamete is produced from a single round of meiosis. The driving *cis*-acting chromosomes (dark pink) biases its retention to the egg by interacting with the inward facing egg pole (green arrow). The non-driving chromosome (light pink), binds the outward facing cortical pole and is extruded to a polar body (red arrow) which is degraded (red X). * The second polar body is extruded upon fertilization. **B)** Males undergo symmetric meiosis—four gametes are produced from a single round of meiosis. Male meiotic drive systems bias fertilization by increasing the relative abundance of sperm carrying the driving chromosome (green arrow), or by decreasing the fitness of sperm with the non-driving chromosome (red arrow). Grey mRNA and protein represent X-linked *trans*-acting factors which remain in X-bearing cells (*e.g.,* intracellular). Green mRNA and protein represent X-linked *trans*-acting factors which are shared and present in Y-bearing cells (*e.g.*, intercellular).

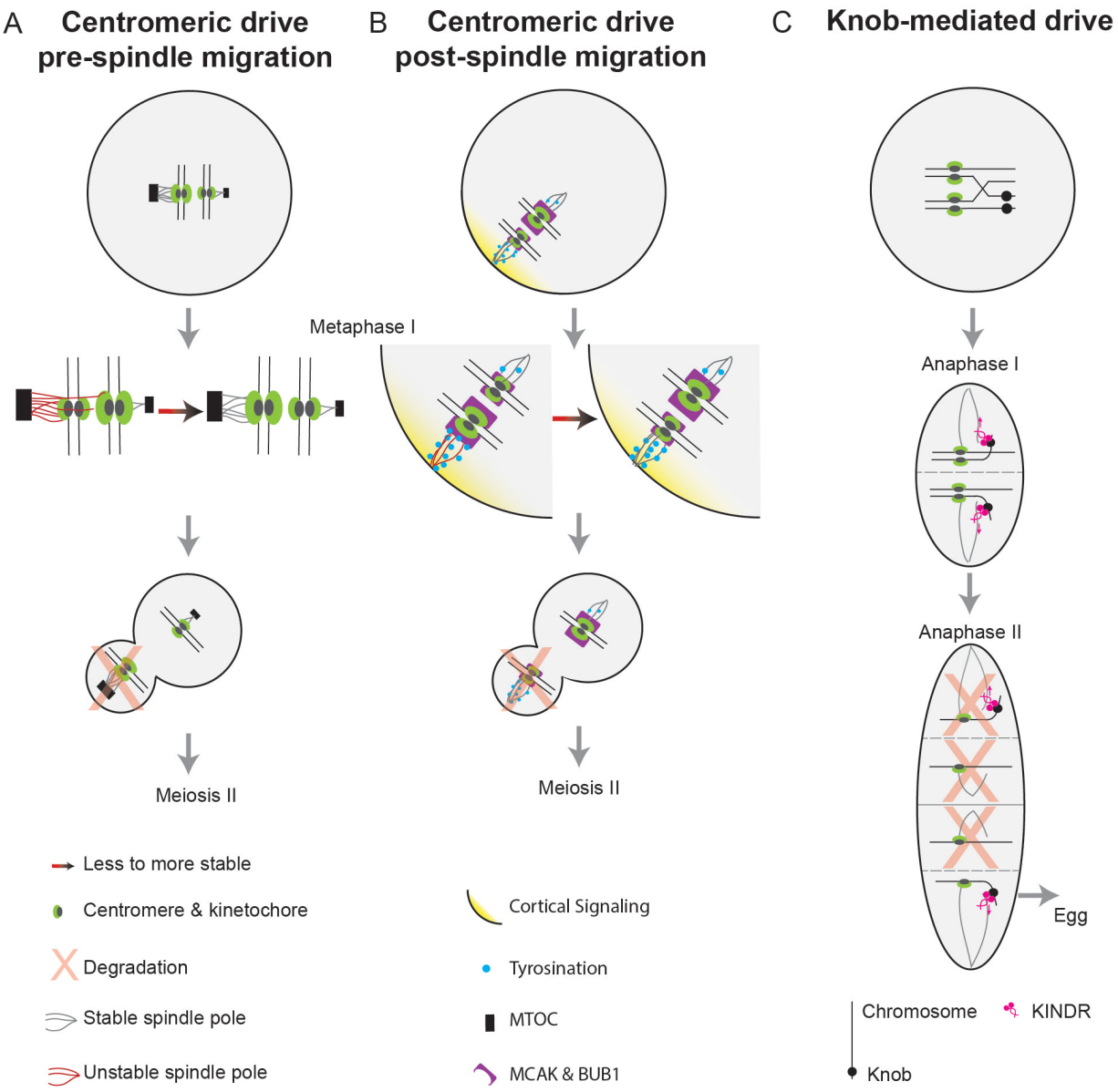

Figure 1-2.Models of Asymmetric Meiotic Drive

This figure depicts the mechanistic understanding of two examples of centromeric drive (A and B) and one example of non-centromeric drive (C). **A)** An example of female centromeric drive in hybrid mice where *cis*-acting chromosome re-orientation occurs before *trans*-acting spindle migration. In this system, larger MTOCs (black box) give rise to denser spindle poles (grey line) which preferentially interact with larger kinetochores (green oval). If this favorable interaction is not initially established (red line), then proteins involved in fixing erroneous microtubule attachments are recruited and chromosomes re-orient to the more favorable interaction (red-black arrow). Spindles migrate to the periphery and the outward facing larger kinetochore is extruded to the polar body and degraded (red X). **B)** Another example of female centromeric drive in hybrid mice where chromosomes re-orientation occurs after spindle migration. Cortical signaling (yellow gradient) leads to an enrichment of tyrosination (blue circle) on cortical spindle poles. Spindle pole tyrosination is less stable (red lines) on larger kinetochores (green) with more BUB1 kinase and MCAK (purple). If not in the more stable orientation, then proteins involved in fixing erroneous microtubule attachments cause chromosomes to re-orient to the stable orientation (red-black arrow), causing the smaller kinetochore to be extruded to the polar body (red X). **C)** Maize knob-mediated drive requires KINDR (pink kinesin) which binds knob repeats (black circles) and migrates along the spindle microtubules toward the outward spindle poles (pink arrow), including the distal cell which becomes the egg.

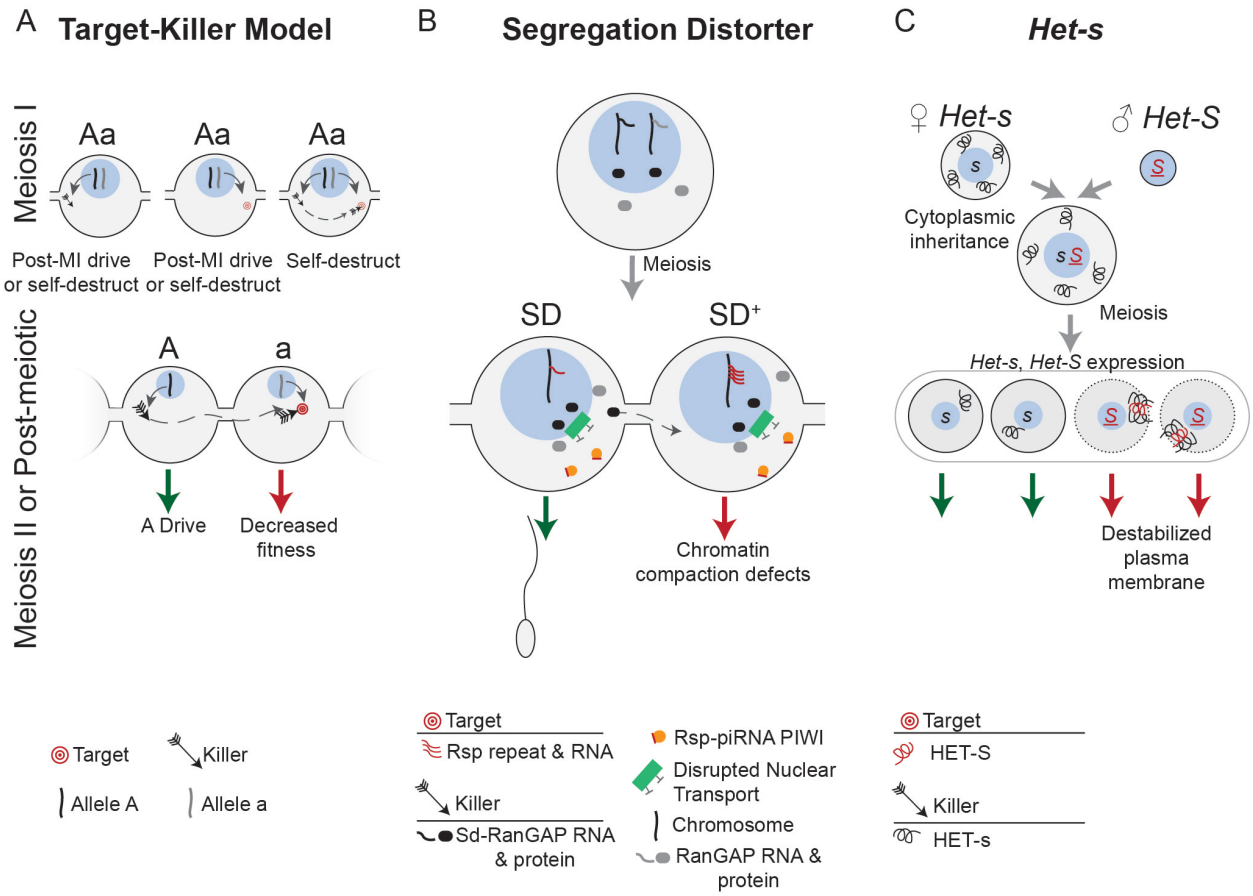

Figure 1-3.Symmetric Meiotic Drive—Target-Killer

This figure depicts the theoretical importance of intracellular versus intercellular regulation on target-killer meiotic drive systems (A), and the mechanisms underlying two target-killer meiotic drivers (B and C). **A)** The killer protein (black arrow, encoded on the "A" haplotype) targets, directly or indirectly, the target (red bullseye, encoded on the "a" haplotype). During meiosis I (MI), expression of only the killer before or during MI can result in post-MI drive, if the target is a *trans*-acting factor expressed during or after meiosis II (MII). If the target is a *cis*-acting sequence, expression of the killer before or during MI could cause the driver to self-destruct. If only a *trans*-acting target is expressed during MI, post-MI drive occurs if the killer is expressed during or after MII, assuming the target acts intracellularly. However, if the target is partitioned into all MII cells and is therefore intercellular, then expression of the killer will result in the system self-destructing. If a trans-acting killer is expressed during MI and a *cis*-acting or *trans*-acting target are accessible, then the system will self-destruction. The target and killer are present in different cells and on different haplotypes in order to not self-destruct, as would be the case if both were expressed in meiotic cells. Expression of the target or killer following homologous chromosome separation in MII prevents self-destruction and results in meiotic drive (green and red arrows). Post-meiosis II expression of the killer necessitates sharing (dashed grey arrow) through cytoplasmic bridges, the target should not be shared in order to prevent self-destruction. **B)** *Drosophila melanogaster* Segregation Distorter (SD) encodes the killer Sd-RanGAP. One model proposes that Sd-RanGAP mislocalization disrupts piRNA-based silencing (orange) of the target, the high copy number *Rsp* (red lines) resulting in chromatin compaction defects and SD drive. **C)** The female strain of *P. anserina* encodes the killer allele, *Het-s,* and HET-s protein (black curly line) is therefore present upon gamete fusion as the cytoplasm (grey surrounding blue nucleus) is maternally inherited. The male strain's Het-S allele and female Het-s are expressed following meiosis where, they complex in *Het-S* spores and integrate and destabilize the plasma membrane (red arrow), resulting in Het-s drive (green arrow). Cells are contained within an ascus (large grey oval).

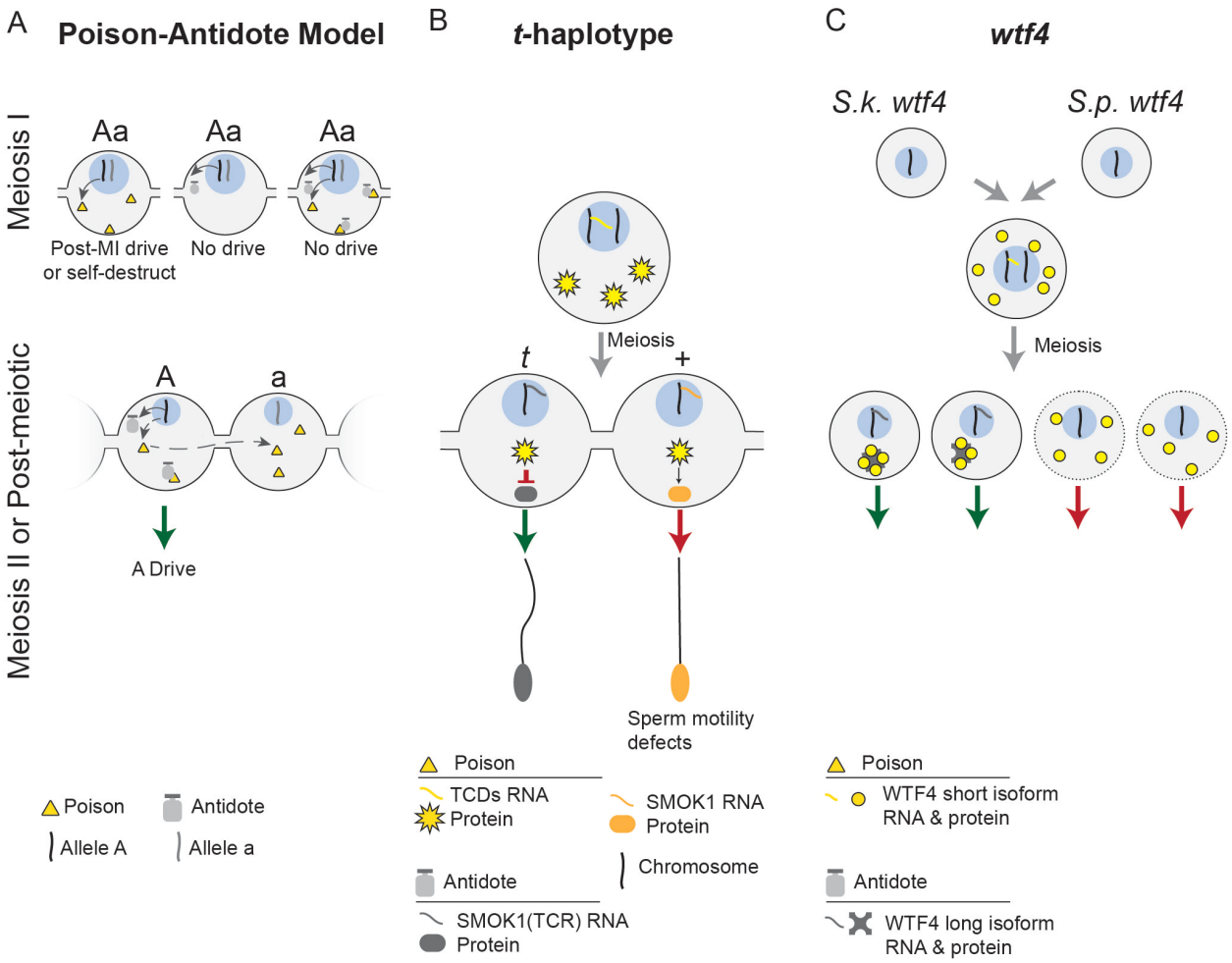

Figure 1-4.Symmetric Meiotic Drive—Poison-Antidote

This figure depicts the theoretical importance of intracellular versus intercellular regulation on poison-antidote meiotic drive systems (A), and the mechanisms underlying two poison-antidote meiotic drivers (B and C). **A)** The poison protein (yellow triangle) and antidote (grey vial) are encoded by the same haplotype ("A") in close genetic proximity. The antidote acts intracellularly ("A" haplotype) to spare driving chromosomes from the effects of the intercellular poison. Expression of the poison before or during MI can result in post-MI drive, if the poison acts specifically in MII or post-meiosis. However, if the poison acts on a biological pathway present before or during MI, expression before or during MI leads to self-destruction. Expression of the antidote before or during MI would result in it being partitioned into and consequently sparing all daughter cells, preventing drive. Expression of both the poison and antidote before homologous chromosomes separate would result in the antidote neutralizing the poison and preventing drive. Meiosis II or later expression of the poison requires that the poison is shared through cytoplasmic bridges (dashed grey arrow) to poison the other cell containing the "a" haplotype, resulting in A drive (green arrow). **B)** In the mouse *t*-haplotype, the poisons, TCDs (yellow star), are expressed before meiosis and disrupt the post-meiotically expressed SMOK1 (orange oval) resulting in flagellar dysregulation (red arrow). The antidote, SMOK1(TCR) (grey oval), is a dominant negative variant of SMOK1 and is insensitive to TCD induced dysregulation, resulting in *t*-haplotype drive (green arrow). **C)** In *Schizosaccharomyces* the *wtf4* gene encoded both the pre-meiotically expressed poison (yellow circles) and the post-meiotically expressed antidote (grey shape). These represent distinct isoforms of *wtf4*. The antidote sequesters poison into distinct subcellular regions preventing its toxicity and results in drive (green arrow).

Chapter 2

Male mice with large inversions or deletions of X-chromosome palindrome arms are fertile and express their associated genes during post-meiosis.[2]

Abstract

Large (>10 kb) palindromic sequences are enriched on mammalian sex chromosomes. In mice, these palindromes harbor gene families (≥2 gene copies) expressed exclusively in post-meiotic testicular germ cells, a time when most single-copy sex-linked genes are transcriptionally repressed. This observation led to the hypothesis that palindromic structures or having ≥2 gene copies enable post-meiotic gene expression. We tested these hypotheses by using CRISPR to precisely engineer large (10's of kb) inversions and deletions of X-chromosome palindrome arms for two regions that carry the mouse *4930567H17Rik* and *Mageb5* palindrome gene families. We found that *4930567H17Rik* and *Mageb5* gene expression is unaffected in mice carrying palindrome arm inversions and halved in mice carrying palindrome arm deletions. We assessed whether palindrome-associated genes were sensitive to reduced expression in mice carrying palindrome arm deletions. Male mice carrying palindrome arm deletions are fertile and show no defects in post-meiotic spermatogenesis. Together, these findings suggest palindromic structures on the sex chromosomes are not necessary for their associated genes to evade post-meiotic

[2] This chapter is published in *Scientific Reports* as:
Kruger, A.N.*, Ellison, Q.*, Brogley, M.A., Gerlinger, E.R., and Mueller, J.L. (2018). Male mice with large inversions or deletions of X-chromosome palindrome arms are fertile and express their associated genes during post-meiosis. Sci Rep *8*, 8985.
* Co-first authors
Author contributions listed under Author Contributions section

transcriptional repression and that these genes are not sensitive to reduced expression levels. Large sex chromosome palindromes may be important for other reasons, such as promoting gene conversion between palindrome arms.

Introduction

In humans and mice, the sex chromosomes are enriched for large (>10 kb), nearly identical (>99% nucleotide identity) segmental duplications in palindromic orientation [7, 9, 112, 113]. In mice, genes within large X-chromosome palindromes are expressed predominantly or exclusively in post-meiotic testicular germ cells [7]. This specific expression pattern is surprising, because most single-copy X-linked genes are transcriptionally repressed post-meiosis [4, 114-116]. The mechanism by which palindrome-associated genes escape transcriptional repression is unknown. Two hypotheses have been suggested to explain this distinct expression pattern. First, palindromes may form secondary structures (e.g. palindrome arms pairing to form a hairpin) enabling their associated genes to evade transcriptional repression [7]. Intrachromosomal synapsis of palindrome arm pairing could facilitate the evasion of post-meiotic gene repression, which itself is a consequence of asynapsis-triggered meiotic sex chromosome inactivation [117-119]. Second, X-palindromic genes may be sensitive to reduced expression levels and thus require ≥2 gene copies [7]. Consistent with this, the mouse X chromosome also carries non-palindromic multicopy genes that are expressed specifically in post-meiotic cells [7]. To test the two hypotheses, individual palindrome arms must be genetically manipulated, *in vivo*.

To rigorously test whether palindrome structure or gene copy number are required for post-meiotic expression, we genetically dissected two mouse X-palindromes. We utilized CRISPR to

generate large-scale (10's of kb) inversions and deletions in mice of two X-palindrome arms harboring the *4930567H17Rik* and *Mageb5* (*Melanoma antigen gene family member b5*) gene families. We chose these two X-palindromes because they possess the canonical features of palindromes across mammals; they have >99% percent nucleotide identity between the two arms, the arms are >10 kb in length, and they harbor a gene family expressed specifically in post-meiotic testicular germ cells. We also selected these two gene families because they have nucleotide variants that differ between the two gene copies, enabling detection of palindrome arm-specific expression of each gene copy. We found that for the *4930567H17Rik* and *Mageb5* palindromic gene families, palindrome structure is not necessary for regulating their associated post-meiotic gene expression, since mice containing palindrome arm inversions exhibit wild-type expression. We observed that deletion of a single palindrome arm, for both the *4930567H17Rik* and *Mageb5* gene families, reduces gene expression levels by half. Reduced expression levels did not lead to male infertility or spermatogenic defects in either case. This suggests that palindromes enrichment on the sex chromosomes is important for other reasons and that there are alternative, unknown mechanisms for palindrome-associated genes to evade post-meiotic repression.

Results

The mouse X chromosome harbors eight singleton palindromes.

Large palindromes on mammalian sex chromosomes are typically found as isolated pairs of palindrome arms (singleton palindromes) or in complex arrays of palindromes. We investigated singleton palindromes, because they are more commonly found across mammalian sex chromosomes and can be genetically manipulated *in vivo* more precisely. Of the eight singleton

palindromes on the mouse X chromosome (Table 2-1 and Figure 2-1A), we selected two harboring the *4930567H17Rik* and *Mageb5* gene families, because they share canonical features of sex chromosome palindromes: >10 kb, >99% nucleotide identity between palindrome arms, harbor genes expressed specifically in testicular germ cells, and have a spacer sequence between the palindrome arms (Table 2-1 and Figure 2-1B). Additionally, the palindrome carrying the *4930567H17Rik* gene family has the longest palindrome arm (65 kb), for a singleton palindrome, which will serve as a proof of principle for the manipulation of shorter palindrome arms.

We validated the exclusive expression of the *4930567H17Rik* and *Mageb5* gene families in post-meiotic round spermatids by reanalyzing previously published RNA-seq datasets from a tissue panel, juvenile testis (Figure 2-1C) and sorted testicular germ cells (Figure 2-5). To determine if both gene copies of *4930567H17Rik* and *Mageb5* are expressed, we utilized individual nucleotide differences between gene copies. Sequencing of RT-PCR products for both *4930567H17Rik* and *Mageb5* show that both gene copies are expressed (Figure 2-1D). Having confirmed that both gene copies are expressed exclusively in post-meiotic round spermatids, we proceeded to delete or invert individual palindrome arms to assess the importance of palindrome structure and gene copy number.

Generation of mice carrying precise inversions and deletions of individual X-palindrome arms via CRISPR.

We utilized CRISPR/Cas9 technology to precisely invert or delete large X-palindrome arms in mice. Pronuclear injection of mouse zygotes with dual single guide RNAs (sgRNAs), targeting unique flanking regions of each palindrome arm, and use of a single stranded oligonucleotide

donor enabled us to generate large (29 kb and 65 kb) inversions and deletions of individual arms for the *4930567H17Rik* and *Mageb5* X-palindromes (Figure 2-2A). The single stranded oligonucleotide donors were used to promote inversions and deletions. We screened founder mouse lines with combinations of primers flanking the sgRNA cut sites in order to detect and distinguish inversions and deletions (Figure 2-2A, B). We validated inversion and deletion junctions by PCR followed by Sanger sequencing (Figure 2-2C). After ~300 pronuclear injections, we obtained 2 and 3 independent mouse lines carrying deletions of a single palindrome arm for the *4930567H17Rik* and *Mageb5* gene families, respectively. Similarly, after ~300 pronuclear injections we obtained 4 and 2 independent mouse lines carrying inversions of a single palindrome arm for the *4930567H17Rik* and *Mageb5* gene families, respectively. The independently obtained inversion and deletion junctions differed from each other by only a few nucleotides at the junctions. We also confirmed the deletions via Sanger sequencing of RT-PCR products to show that only a single sequence family variant was expressed in each mouse line (Figure 2-1D). Eight independent mouse lines, backcrossed onto a C57BL/6J genetic background, were selected for further study, two lines carrying deletions and two lines carrying inversions for each of the two X-palindromic regions. Throughout this study, the genotypes for the eight deletion and inversion carrying lines are designated *4930567H17RiK*^{InvArm}, *4930567H17Rik*^{DelArm}, *Mageb5*^{InvArm}, and *Mageb5*^{DelArm}, followed by a '1' or '2' to denote individual mouse lines. Our dual sgRNAs combined with single stranded oligonucleotides approach was successful in generating 29 kb and 65kb inversions and deletions of single palindrome arms.

Disruption of palindrome structure, via inverting a single palindrome arm, does not affect the gene expression levels of the palindrome associated gene family.

With the generation of mice carrying precise inversions of two different X-palindrome arms that disrupt palindrome structure, we tested whether palindrome structure is necessary for post-meiotic gene expression. If palindrome structure is necessary for post-meiotic gene expression, then we expected to abolish gene expression of *4930567H17Rik* and *Mageb5* in *4930567H17RiK*$^{InvArm/Y}$ and *Mageb5*$^{InvArm/Y}$ mice, respectively. We compared the testis gene expression levels of *4930567H17Rik* and *Mageb5* gene families via quantitative RT-PCR (RT-qPCR). Expression was normalized to *Trim42* and compared to wild-type controls. *4930567H17RiK*$^{InvArm/Y}$ and *Mageb5*$^{InvArm/Y}$ mice, in two independent mouse lines, express their associated genes at levels similar to wild-type mice (Figure 2-3A). Consistent with their similar gene expression levels, *4930567H17RiK*$^{InvArm/Y}$ and *Mageb5*$^{InvArm/Y}$ mice are fertile and do no exhibit detectable spermatogenic defects. Assuming the post-meiotic-specific gene expression of *4930567H17Rik* and *Mageb5* is maintained in mice carrying palindrome arm inversions, our data demonstrate that palindrome structure is not required for gene expression of *4930567H17Rik* and *Mageb5*.

Deleting a single palindrome arm reduces the gene expression level of the palindrome-associated gene family by half.

Using mice carrying single palindrome arm deletions, we reduced the gene copy number of the palindrome-associated *4930567H17Rik* and *Mageb5* genes by half (from 2 gene copies to 1). We expected *4930567H17Rik* and *Mageb5* gene expression levels would be reduced by half in *4930567H17Rik*$^{DelArm/Y}$ and *Mageb5*$^{DelArm/Y}$ mice. We compared the testis gene expression levels

of *4930567H17Rik* and *Mageb5* gene families via quantitative RT-PCR (RT-qPCR). Expression was normalized to *Trim42* and compared to wild-type controls. We found that *4930567H17Rik*$^{DelArm/Y}$ and *Mageb5*$^{DelArm/Y}$ mice, in two independent mouse lines, expressed their associated genes at approximately half the levels of wild-type males (Figure 2-3B). The reduction of gene expression by half, in mice carrying palindrome arm deletions, is consistent with reducing gene copy number from 2 to 1.

Male mice carrying deletions of individual palindrome arms do not exhibit defects in fecundity, testis histology, or number of round spermatids.

The reduction of gene expression by half allows us to test whether male mice are sensitive to reduced gene expression of the *4930567H17Rik* and *Mageb5* gene families. We performed a systematic characterization of fecundity and post-meiotic spermatogenic development of *4930567H17Rik*$^{DelArm/Y}$ and *Mageb5*$^{DelArm/Y}$ mice. We found that *4930567H17Rik*$^{DelArm/Y}$ and *Mageb5*$^{DelArm/Y}$ mice are fertile and produce litter sizes and relative testis weights similar to wild-type controls (Figure 2-4A, B). To detect potential defects in post-meiotic spermatid development, we examined histological sections of testis from *4930567H17Rik*$^{DelArm/Y}$ and *Mageb5*$^{DelArm/Y}$ mice. We did not observe defects in spermatid morphology, formation of the acrosome, or spermatid elongation (Figure 2-6). To assess whether the number of round spermatids were affected in *4930567H17Rik*$^{DelArm/Y}$ and *Mageb5*$^{DelArm/Y}$ mice, we quantified the number of round spermatids per testis as the ratio of round spermatids/spermatocytes (control) via FACs (Figure 2-7). The ratio of round spermatids/spermatocytes of *4930567H17Rik*$^{DelArm/Y}$ and *Mageb5*$^{DelArm/Y}$ mice was similar to wild-type males (Figure 2-4C). Altogether,

4930567H17Rik$^{DelArm/Y}$ and *Mageb5*$^{DelArm/Y}$ mice do not exhibit detectable defects in fecundity or post-meiotic spermatid development.

Discussion

Our findings suggest that palindrome structure is not necessary for regulating post-meiotic gene expression levels for the *4930567H17Rik* and *Mageb5* gene families. Our findings also show that a reduced gene expression level of the *4930567H17Rik* and *Mageb5* gene families, via deletion of a single palindrome arm, does not result in spermatogenic defects or male infertility. It will be important to compare our studies with complete knockouts of the *4930567H17Rik* and *Mageb5* gene families. If either gene family is necessary for spermatogenesis, then it would support our findings that palindrome structure or copy number are not necessary for spermatogenesis.

Our findings suggest there are alternative mechanisms for X-palindromic genes to be expressed on the otherwise transcriptionally repressed X chromosome. A small number of X-linked single-copy genes are expressed in round spermatids [115, 120], indicating that multiple gene copies are not a strict requirement for post-meiotic gene expression from the sex chromosomes. Specific enhancers and transcription factors may have evolved to overcome the transcriptional repression associated with post-meiotic sex chromosomes. Two transcription factors that may facilitate post-meiotic sex-linked gene expression are Heat Shock Transcription Factor 1 (HSF1), which localizes to sex chromatin [121] and HSF2, which preferentially binds chromatin of Y-palindromic genes [122]. Consistent with this, the testis is known to have specialized transcription regulation strategies in post-meiotic testicular germ cells [123] that appear to also apply to palindromic and multicopy X- and Y-linked genes.

This work leaves open the question as to why palindromes are heavily enriched on both the mammalian X and Y chromosomes. It is possible that X- and Y-chromosome palindromes are necessary for the long-term evolutionary stability of the genes they harbor in order to rapidly purge deleterious mutations via gene conversion [14]. Alternatively, the presence of two or more palindromic gene copies provides a larger substrate for new beneficial mutations to arise and become fixed, via gene conversion [124]. For both purging or fixing new mutations in palindrome arms, it will be important to assess arm-to-arm gene conversion rates.

Materials and Methods

Generation of 4930567H17Rik and Mageb5 palindrome arm inversions and deletions

To generate mice carrying palindrome arm inversions and deletions we used CRISPR with dual single guide RNAs (sgRNAs). sgRNAs were designed to unique sequences flanking the targeted palindrome arm, as close to the edge of the arm as possible (Table 2-2). Since sgRNA cutting efficiency varies between sgRNAs, we tested their activity via pronuclear injection of an sgRNA/Cas9 expression plasmid, pSpCas9(BB)-2A-GFP (pX458) [125] in mouse zygotes. The surviving mouse zygotes were allowed to develop into 64-128 cell blastocysts and the cutting efficiency of each sgRNA was determined by PCR of the cut sites (Table 2-2) and Sanger sequencing of purified PCR products to identify edits at the target sites.

After active sgRNAs were identified for both sides of each targeted palindrome arm, two pX458M plasmids encoding the sgRNAs and Cas9 together with a single-stranded oligonucleotide were injected into the pronucleus of (C57BL/6JXSJL) F1 mouse zygotes.

Palindrome arm inversions for *4930567H17Rik* and *Mageb5* and the palindrome arm deletion for *4930567H17Rik* we added single-stranded oligonucleotides with sequence homology flanking the junction boundaries, as listed in Table 2-2, to promote the events. For the *Mageb5* palindrome arm deletion, we only used dual sgRNAs. The zygotes were generated from mating C57BL/6J females to (C57BL/6JXSJL) F1 males so that all targeted X chromosomes were C57BL/6J. Blastocysts from the pronuclear injection were implanted into pseudopregnant females. Genomic DNA from resulting pups was screened by PCR and Sanger sequencing of the inversion and deletion junctions. At least two independent mouse lines were obtained for inversions and deletions of the *4930567H17Rik* and *Mageb5* palindrome arms. Male and female mice were able to transmit both the *4930567H17Rik* and *Mageb5* deletions and inversions through the germline. Thus, their overall health was unaffected by the CRISPR-mediated chromosome engineering.

Mice and testis sample collection

Females heterozygous for an inversion or deletion of a single palindrome arm were repeatedly backcrossed to C57BL/6J. Backcrossing was performed up to seven generations, for two independent lines per genotype, to minimize any CRISPR-mediated off-target effects. The heterozygous females mating scheme resulted in wild-type and deletion/inversion male littermates which were directly compared in all experiments. Use of wild-type littermates as controls minimized the effects of genetic background and age. If wild-type littermates were not available, then we used age-matched controls from the same breeding line. To assess fecundity (average litter size per male), we mated mutant males to CD1 females. Testes were collected from 2-6 month old males for all experiments and weighed, along with total body, in order to

determine relative testis weight. The alleles for the first mouse lines of each type were named *4930567H17Rik*^{InvArm1}, *4930567H17Rik*^{DelArm1}, *Mageb5*^{InvArm1}, *Mageb5*^{DelArm1} with respective registered symbols In(X4930567H17Rik)1Jbmu, Del(X4930567H17Rik)1Jbmu, In(XMageb5)1Jbmu and Del(XMageb5)1Jbmu. All experiments performed on mice were approved by the University of Michigan Committee on Use and Care of Animals, and all experiments followed the National Institutes of Health Guidelines of the Care and Use of Experimental Animals.

Preparation of adult testis cDNA and quantitative real-time PCR (qRT-PCR)

Intron-spanning primers (Table 2-2), when possible, were used to perform RT-qPCR on adult testis cDNA preparations. One testis per mouse was used to isolate RNA using Trizol (Invitrogen) following the manufacturers recommendations. Five µg of total RNA was DNase treated with TurboDNase (Ambion) and reversed transcribed using Superscript II (Invitrogen) and oligonucleotide (dT) primers following the manufacturers protocol. qRT-PCR was performed in triplicate using Power SYBR Green master mix (Thermo Fisher Scientific) on a 7500 Real-time PCR thermalcycler (Applied Biosystems). Reactions were performed in 25 µl volumes, with 200nM of each primer, 40 cycles of 95°C for 15 seconds followed by 60°C for 1 minute, and completed with a melt curve analysis. All PCR products produced a single peak based upon the melt curve analysis, indicating a single, specific, product is amplified in each reaction. We performed three technical replicates, per animal, for each qRT-PCR reaction. All comparisons of gene expression used the same standard reference control gene, *Trim42* (*Tripartite motif-containing 42*), because it is expressed specifically in the same post-meiotic testicular cells and at similar levels as *4930567H17Rik* and *Mageb5*. Normalized gene

expression (ΔC_T) was calculated by subtracting *Trim42* crossing thresholds (C_T) values from *4930567H17Rik* or *Mageb5* C_T values, for each biological replicate. Control biological replicates (wild-type littermates from the same transgenic line) ΔC_T values were averaged. $\Delta\Delta C_T$ values were determined by subtracting the average ΔC_T of control samples from the ΔC_T values of mice carrying either a deletion or inversion. Fold changes in *4930567H17Rik* and *Mageb5* gene expression were determined via the $2^{-\Delta\Delta CT}$ method [126]. Statistical tests of differential gene expression were performed by comparing mean gene expression via unpaired, one-tailed, moderated t-tests.

Testis Histology

Testes were fixed overnight in Bouin's solution, paraffin embedded, sectioned to 5 μm, and stained with Periodic acid Schiff (PAS) and hematoxylin. Sections were visualized under a light microscope and specific germ cell populations were identified by their location within a tubule, nuclear size, and the nuclear staining pattern of chromatin [127].

FACs-based estimates of round spermatid frequencies

We largely followed a previously published protocol [128] to isolate round spermatids (1n) and spermatocytes (4n). Briefly, we disassociated cells from a single testis by enzymatic treatment with Collagenase type I, DNase I (Worthington Biochemical Corporation), and Trypsin (Life Technologies). The cell suspension was passed through cell strainers (100 μm and 40 μm) and incubated with Hoechst 33342 (Life Technologies) to determine DNA content and propidium iodide (Acros Organics) to evaluate cell viability. Cell sorting was performed on a FACSAria II cell sorter (BD Biosciences). The purity of each sort was determined via fluorescence

microscopy visual inspection of 100 cells morphology and nuclear staining with DAPI for round spermatids and with gH2AX antibody staining for pacyhtene spermatocytes. The purity of round spermatids was typically >85%, which is consistent with previous studies [128].

RNA-seq analyses

RNA-seq analyses were conducted by analyzing previously published datasets. Specifically, mouse tissue panel data were analyzed from SRP016501 [129], ovary data from SRP017959 [130], juvenile testis data from SRP018695 [131] and sorted testicular germ cell populations from SRP065082 [132] and SRP018124 [133]. Alignments were performed using Tophat [134] with the mm10 mouse reference genome, a refFlat file with RefSeq gene annotations and --max-multihits set to 240; otherwise standard default parameters were used. We used Cufflinks [134], using the refFlat gene annotation file, to estimate expression levels as fragments per kilobase per millions of mapped fragments (FPKM).

Dot plots

Self-symmetry triangular dot plots that show repeats within a sequenced region were generated from a custom Perl script that can be found at http://pagelab.wi.mit.edu/material-request.html.

Acknowledgements

We thank Sundeep Kalantry and Miriam Meisler for comments on the manuscript, Dirk de Rooij, Thomas Wilson and Michael Pihalja for technical advice, Thomas Saunders and the University of Michigan Transgenic Animal Model Core for pronuclear injections to generate the *4930567H17Rik* and *Mageb5* palindrome arm deletion and inversion mouse lines, University of Michigan Flow Cytometry Shared Resource Laboratory for FACs, DNA Sequencing Core for Sanger Sequencing, and Cancer Center Tissue Core for generating testis histological sections.

These studies were supported by National Institutes of Health grants R00HD064753 to JLM, T32GM007544 to ANK and T32HD079342 to QE, a National Science Foundation Graduate Research Fellowship DGE 1256260 to ANK and a Cell and Molecular Biology Graduate Program Fellowship to QE.

Author Contributions

Q.E. and J.L.M. designed the study; Q.E., A.N.K., M.A.B. and E.R.G. conducted the experiments; A.N.K., Q.E. and
J.L.M. analyzed and interpreted the results; A.N.K. and J.L.M. wrote the paper.

Figures

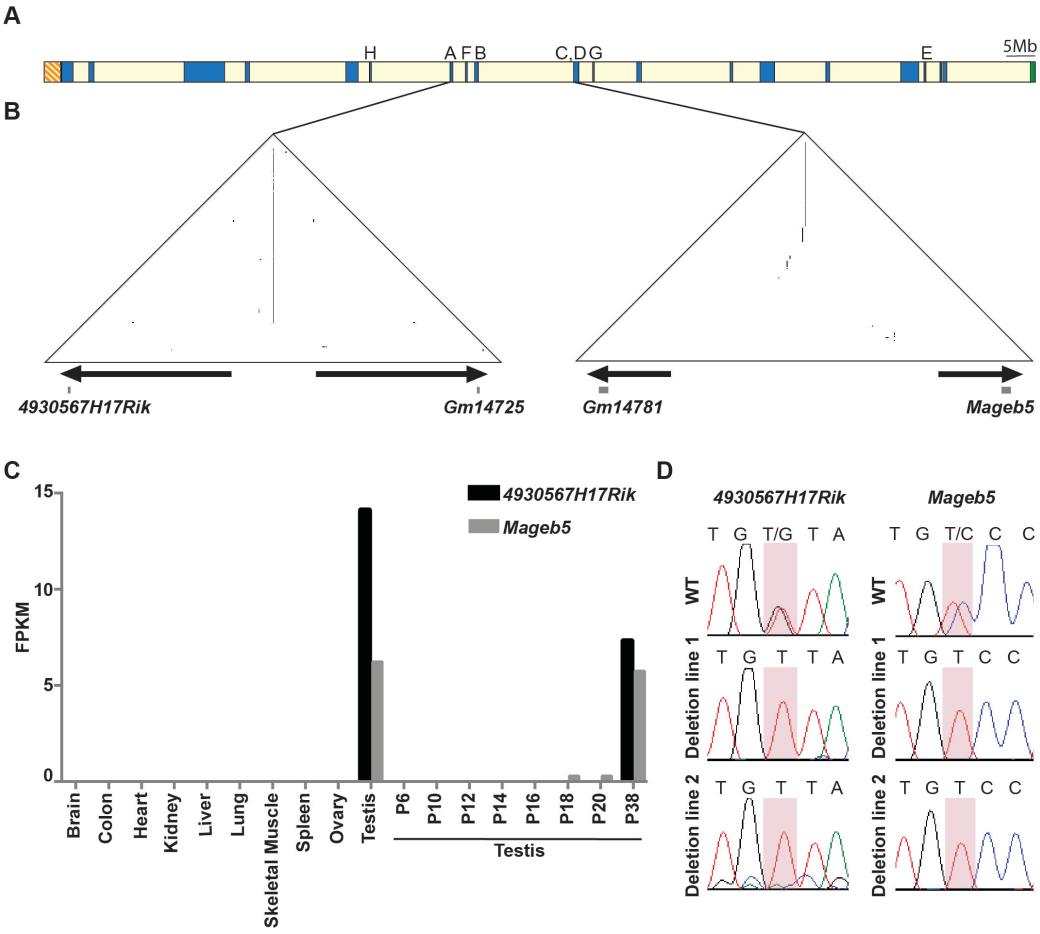

Figure 2-1. Singleton palindromes on the mouse X chromosome

A) The location of the eight singleton palindromic regions on the mouse X chromosome are labeled by arm size, the sequence features of which can be found in Table 2-1. **B**) Self-symmetry triangular dot plots of the two singleton X-palindromes to be studied, carrying the *4930567H17Rik* and *Mageb5* gene families, respectively. Each dot plot represents the palindromic X chromosome sequence (*4930567H17Rik* = chrX:70385921-70553920 and *Mageb5*= chrX:91624421-91790420) plotted against itself with a sliding window of 100 nucleotides (step size=1 nucleotide). When the window of 100 nucleotides is identical to the sequence it is compared to, a dot is plotted. Segmental duplications in an inverted orientation are visualized as vertical lines. A visual representation of the palindrome arms (arrows) and the gene copies (squares) are plotted at the base of the triangular plots across the 168 kb *4930567H17Rik* and 166 kb *Mageb5* palindromic regions. **C**) Expression levels of *4930567H17Rik* and *Mageb5* genes in adult tissues and juvenile testis, shown as FPKMs (number of fragments per kilobase per million mapped fragments). **D**) Sanger sequencing of RT-PCR products displaying the nucleotide differences that distinguish the two palindromic gene copies. In *4930567H17Rik*$^{DelArm/Y}$ and *Mageb5*$^{DelArm/Y}$ mice, expression is detected only from the remaining copy. WT = wild-type.

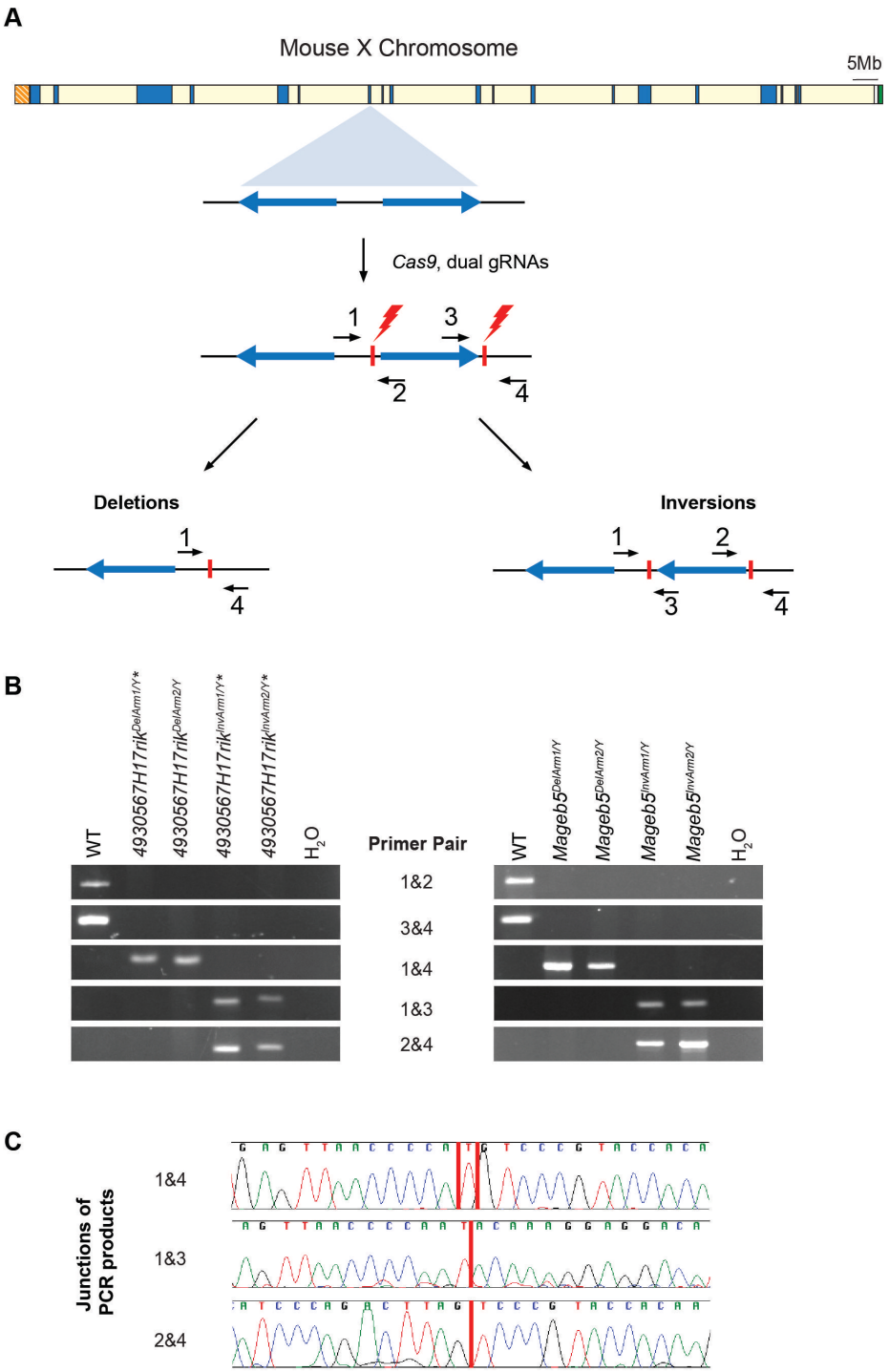

Figure 2-2. CRISPR strategy to generate large inversions and deletions of individual palindrome arms

A) Schematic of the mouse X chromosome with a diagram of a singleton palindrome shown below. Palindrome arms are shown as blue arrows, sgRNA sites as red vertical lines and primers as black arrows. **B)** PCR genotyping of DNA from the two independent mouse lines for each deletion and inversion of *4930567H17Rik* and *Mageb5* palindrome arms. Numbered primers from panel A used to amplify deletion (1&4) and inversion (1&3, 2&4) junctions (Table 2-2). Full-length agarose gels are in Figure 2-5. WT = wild-type. **C)** Representative example of Sanger sequencing chromatograms of the deletion and inversion junctions for *4930567H17Rik* palindrome arm rearrangements. Junction sites are shown with a vertical red line. The mm10 coordinates for the sequence removed in the *4930567H17Rik*$^{DelArm1/Y}$ line is ChrX:70389542-70457358 and coordinates for the sequence inverted in the *4930567H17RiK*$^{InvArm1/Y}$ are ChrX:70389544-70457357.

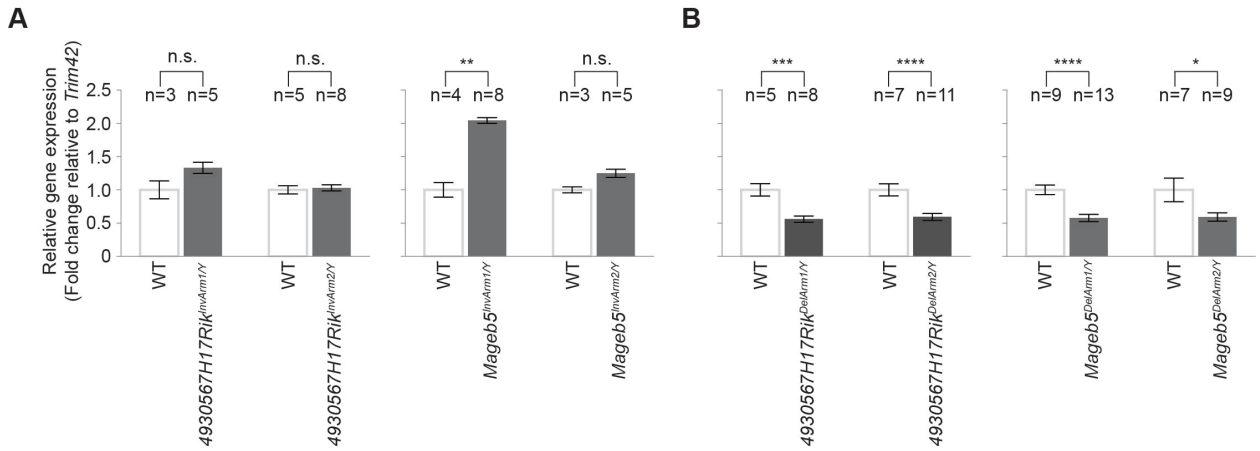

Figure 2-3. CRISPR strategy to generate large inversions and deletions of individual palindrome arms

A) *4930567H17Rik* and *Mageb5* gene expression levels from testes of male mice carrying palindrome arm inversions as compared to wild-type controls. **B)** *4930567H17Rik* and *Mageb5* gene expression levels from testes of male mice carrying palindrome arm deletions as compared to wild-type controls. For **A** and **B**, the gene expression values are shown as fold changes normalized to wild-type (WT=1) and to the standard reference gene *Trim42* for two independent mouse lines, per genotype (inversion or deletion of *Mageb5* or *4930567H17Rik* palindrome arms). Error bars represent the standard error of the mean across the biological replicates. The number of biological replicates (n) examined per line is shown above each bar graph. Unpaired two-tailed t-tests, with a Welch correction, were performed to compare mean gene expression (n.s. = not significant, * = P<0.05, ** = P<0.01, *** = P<0.001, **** = P<0.0001).

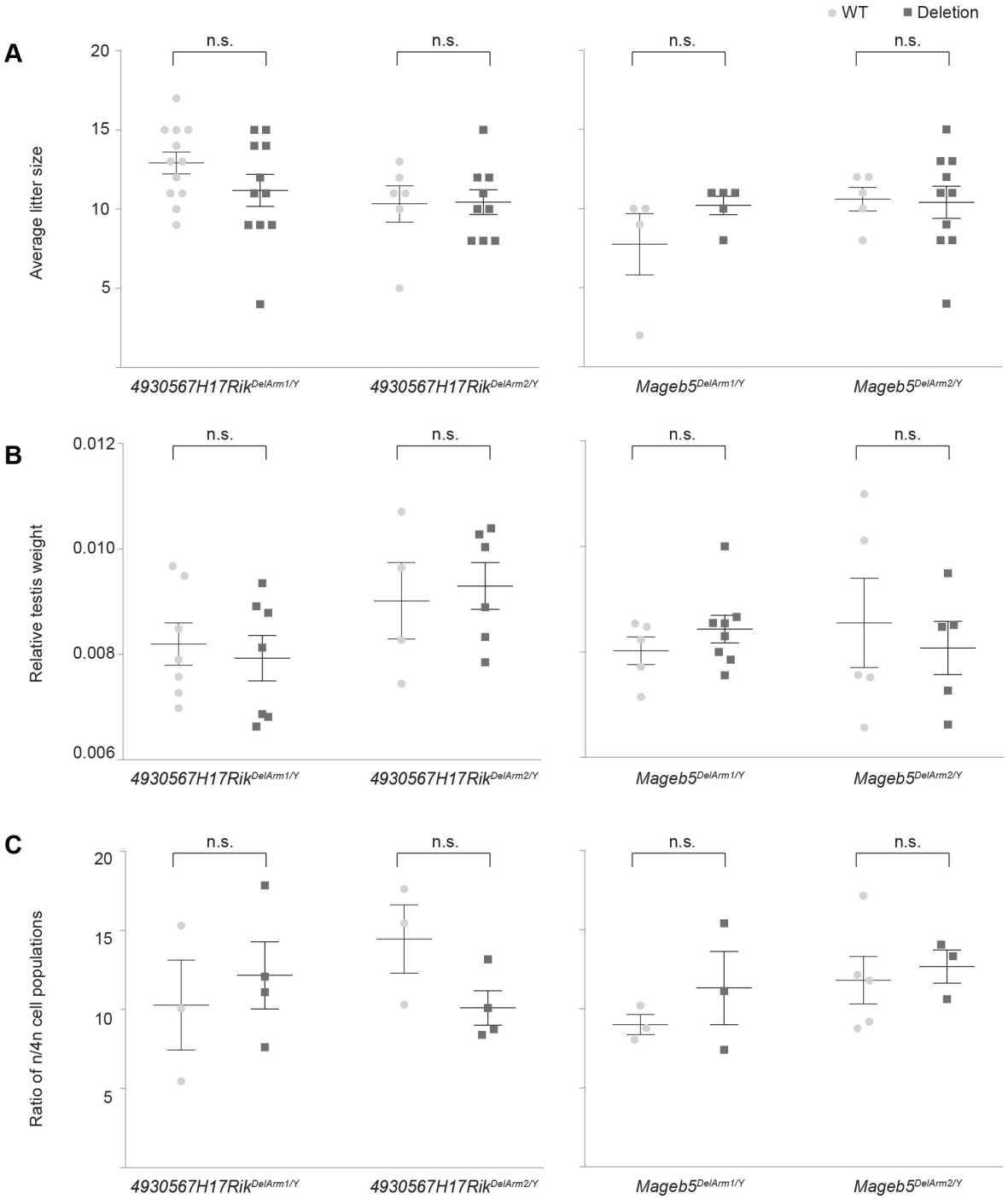

Figure 2-4. Male mice carrying 4930567H17Rik and Mageb5 palindrome arm deletions are fertile and do not display defects in spermatogenic cell population frequencies

A) Multiple males from each *4930567H17Rik*$^{DelArm/Y}$ and *Mageb5*$^{DelArm/Y}$ line and control males (wild-type littermates) were mated to multiple CD1 females to assess fertility and fecundity. **B)** Total testis weight (g) from *4930567H17Rik*$^{DelArm/Y}$ and *Mageb5*$^{DelArm/Y}$ lines were normalized to total body weight (g). **C)** The frequency of post-meiotic round spermatids was assessed by normalizing the percentage of round spermatids (1n) to spermatocytes (4n). The spermatocyte population serves as a control and should be unaffected, because they do not express *4930567H17Rik* and *Mageb5*. Error bars represent the standard error of the mean of biological replicates. Statistical significance was determined using an unpaired T-test assuming the same standard deviation between populations and correction for multiple comparisons using Holm-Sidak correction.

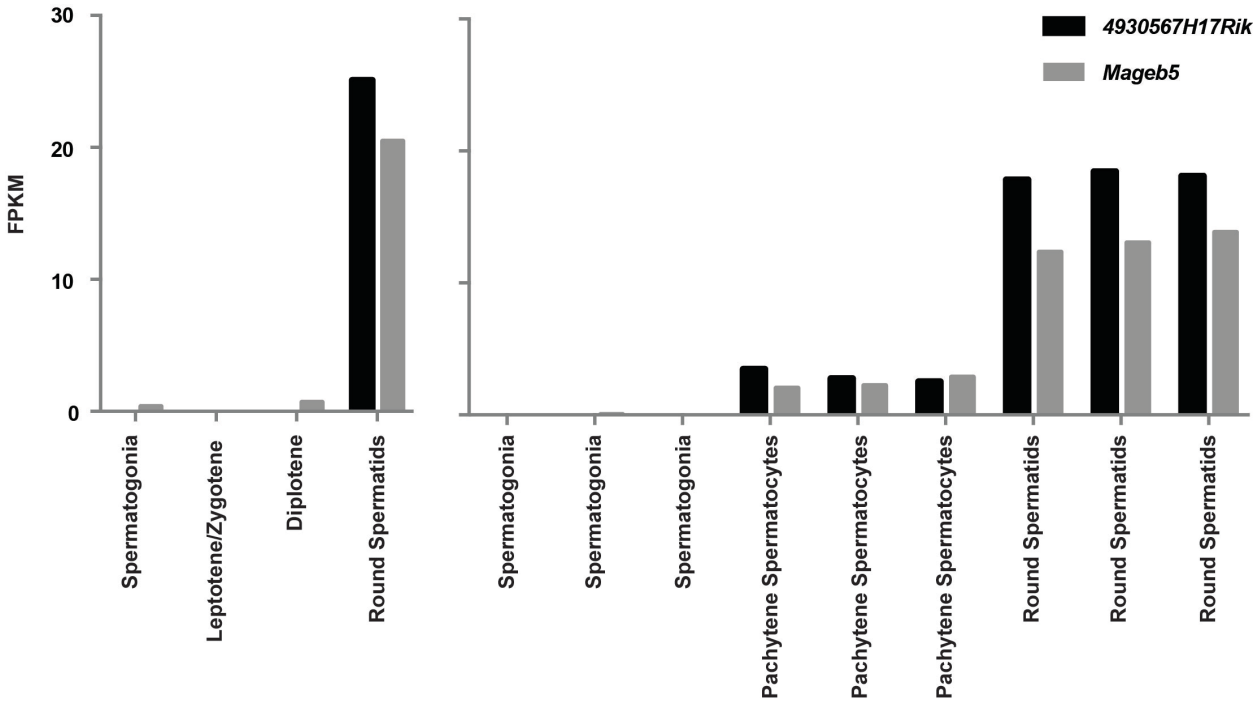

Figure 2-5. Expression levels of 4930567H17Rik and Mageb5 genes in sorted spermatogenic populations from independent studies

Gene expression is shown as FPKMs (number of fragments per kilobase per million mapped fragments). The left panel shows data from Larson et al., 2016, Genetics, and the right panel shows three biological replicates from Soumillon et al., 2013, Cell Reports.

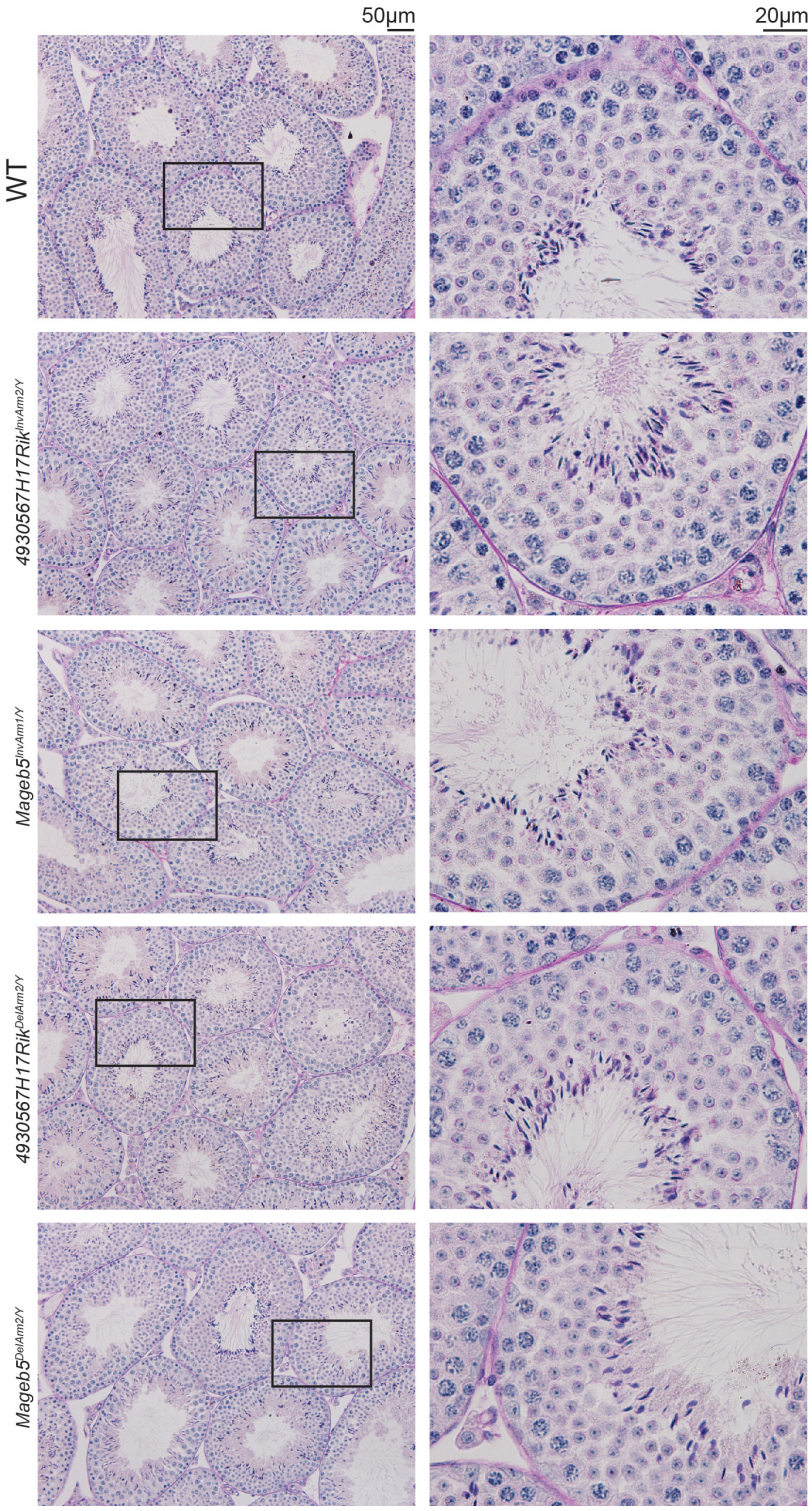

Figure 2-6. Male mice carrying inversions or deletions of a single palindrome arm, for the 49305667H17Rik or Mageb5 X-palindromes do not exhibit detectable spermatogenic defects as based upon histological sections

Male mice carrying inversions or deletions of a single palindrome arm, for the 49305667H17Rik or Mageb5 X-palindromes do not exhibit detectable spermatogenic defects as based upon histological sections. Histological sections were stained with hematoxylin and periodic acid-Schiff (He-PAS). Low magnification images are shown to the left and higher magnification images of a representative, and boxed, seminiferous tubule are shown to the right. WT = wild-type.

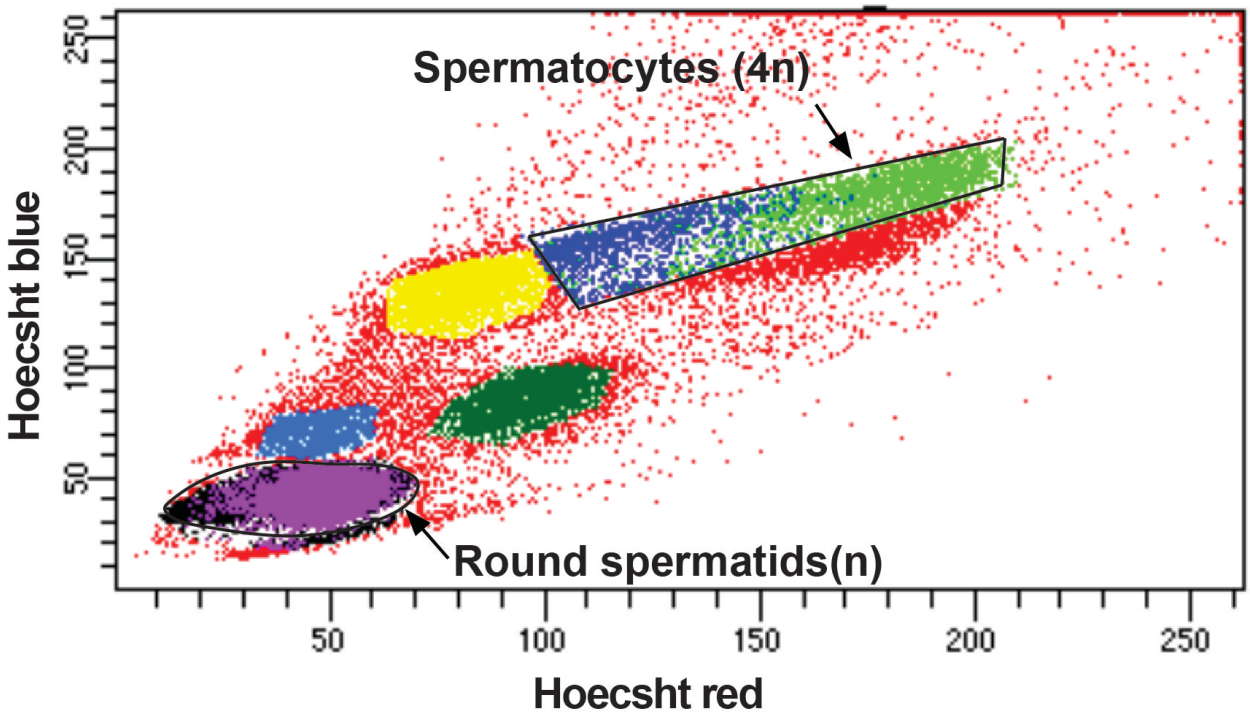

Figure 2-7. Representative FACS plot of spermatogenic cell

Round spermatids (1n) and spermatocytes (4n) populations that were sorted are contained within the black outlines.

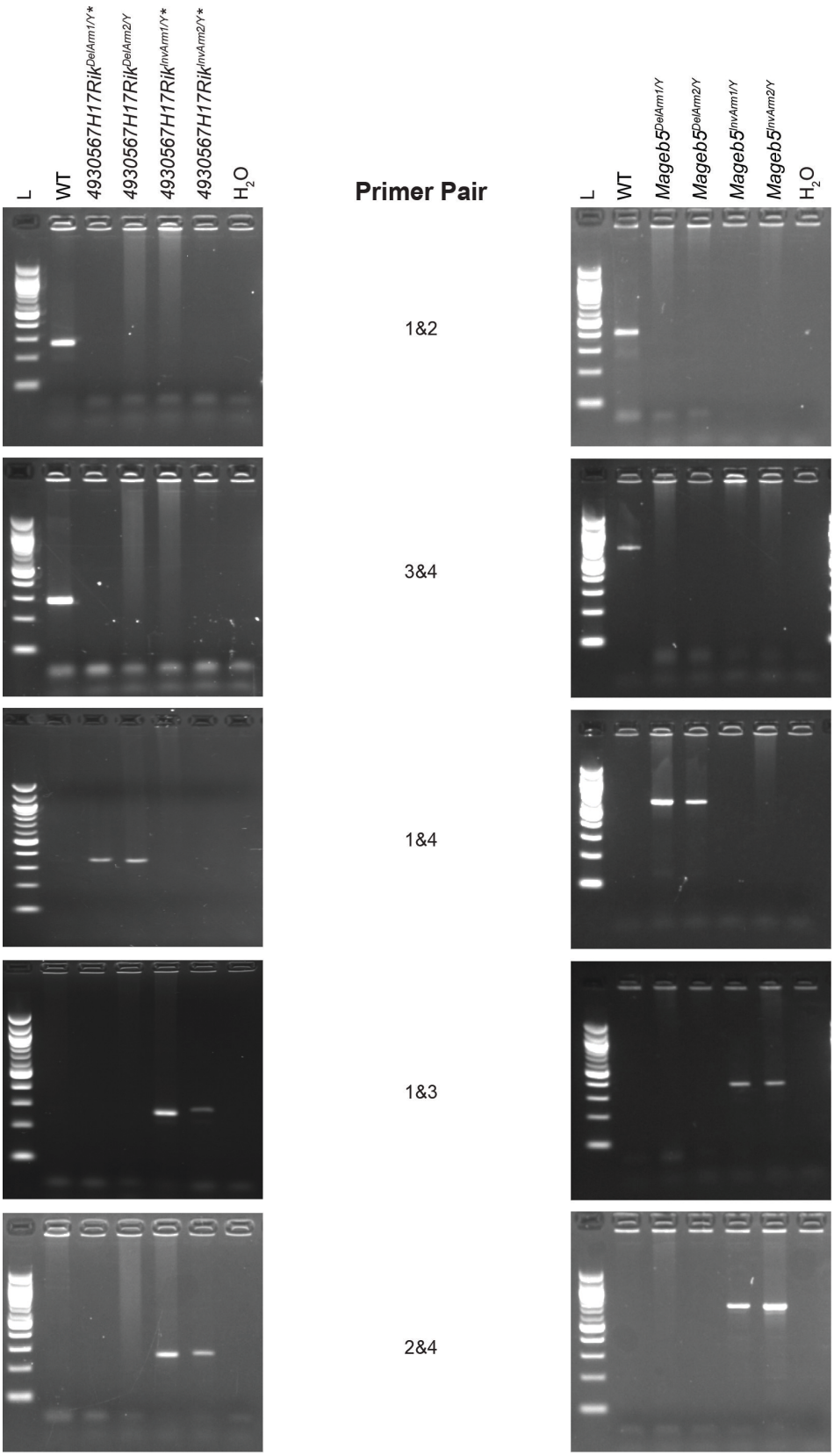

Figure 2-8. Full length agarose gels, with ladders (L), of PCR genotyping from Figure 2-2

Tables

Table 2-1. Sequence features of mouse X chromosome singleton palindromes

Palindrome	Genes*	Arm Size (kb)+	Spacer size (kb)	Percent Identity+
A	*4930567H17Rik*	64.7	29.1	99.26
B	*Gm5640*	47.1	11.7	99.61
C	*Gm5071*	34.6	44.9	99.88
D	*Mageb5*	30.0	98.8	99.26
E	*3010001F23Rik*	28.5	47.8	99.49
F	*Xlr5a*	27.0	3.7	99.59
G	*Zxda*	21.4	67.8	99.56
H	*Gm773*	13.3	25.7	99.36

***** In cases where two gene family members have different names, only one was selected (e.g. *Mageb5* was selected for gene family that has *Mageb5* and *Gm14781*).

+ Palindrome arm size and percent identities between arms were identified from the "Segmental Dups" track of the UCSC genome browser mm10 mouse genome assembly.

Table 2-2. List of sgRNA sequences and oligos used in this study (5' to 3')

sgRNAs:	
4930567H17Rik 5'	CCCAGACTTAGTGCATT
4930567H17Rik 3'	TGGTACGGGACTGACAA
Mageb5 5'	AAATACTCAACATGCAATGA
Mageb5 3'	AAAGTTTGATATCGCCTTGG
Single-stranded oligo donors:	
*4930567H17Rik*_Deletion	AGTACGTGAACAGCATCCAGGGGCCCATGGGACAAGTCTGGGAGCAGTCACT GAGTTAACCAAGGGAGATTTCTCAGGCAACACACCCCTATCCTAAGCGTTCTA AAGCATCCTAACCTT
*4930567H17Rik*_Inversion	CATGGGACAAGTCTGGGAGCAGTCACTGAGTTAACCCCAATCAAAGGAGGAC ATGCTGGATTACTTGGCATCTTTTATTGTGGTACTTCCTCAGTCTGTACTCAGG ATATTATCATTTCTACTAAGTGAACCAGAGC
*Mageb5*_Inversion	TACCTTATTGGTATGTGTGAGTACAGCTGAGCCACTTCATTATTTTAATGCTCT AAGTAGACAGAGTTTTCTGGGTATTCTGTTCTAGCACCATCATGGGGGCATTA TATTCCCCTTCTTGCAGGAATCTAGTTATT
RT/ qRT-PCR primers:	
4930567H17Rik F	GGGCCTCTGAGACCACAT
4930567H17Rik R	TCTGCATGGGTCGTATGA
Mageb5 F	GGGAGAATCATCCACTTCTGA
Mageb5 R	TGGATTTTCTTGGCAGGTTC
Trim42 F	GAAGCATCGTCACCTCCTCT
Trim42 R	CTTCTCGCATAGGCTGTGGT
Mageb5 SFV F	CCATGCAAACATTGCCTAGA
Mageb5 SFV R	CTCCCTGGGTACACTTGCAT
Genotyping Primers:	
4930567H17Rik_1	TGCTGTTTTCTGGATTGCACA
4930567H17Rik_2	ACAGTTTTGGTTGTTGAGGGA
4930567H17Rik_3	ACGGCTCTGGTTCACTTAGT
4930567H17Rik_4	TAGGAACCACTTGCATGTCG
Mageb5_1	GTTTGCAGAGTTGTGGACTGATAC
Mageb5_2	ATCATTTTCCTTGTAGAGAACACAGC
Mageb5_3	TAAATACTAGTCTCTTCTCAAGATGTCC
Mageb5_4	TGCATTGATCAAAAGGGAGA

Chapter 3

A neofunctionalized X-linked ampliconic gene family is essential for male fertility and equal sex ratio in mice[3]

Summary

The mammalian sex chromosomes harbor an abundance of newly acquired ampliconic genes, although their functions require elucidation [7-9, 113, 135-139]. Here we demonstrate that the X-linked *Slx* and *Slxl1* ampliconic gene families represent mouse-specific neofunctionalized copies of a meiotic synaptonemal complex protein, *Sycp3*. In contrast to the meiotic role of *Sycp3*, CRISPR-loxP-mediated multi-megabase deletions of the *Slx* (5Mb) and *Slxl1* (2.3Mb) ampliconic regions result in post-meiotic defects, abnormal sperm and male infertility. Males carrying *Slxl1* deletions sire more male offspring whereas males carrying *Slx* and *Slxl1* duplications sire more female offspring, which directly correlates with *Slxl1* gene dosage and gene expression levels. SLX and SLXL1 proteins interact with spindlin protein family members (SPIN1 and SSTY1/2) and males carrying *Slxl1* deletions downregulate a sex chromatin modifier, *Scml2*, leading us to speculate that *Slx* and *Slxl1* function in chromatin regulation. Our

[3] This chapter is published in *Current Biology* as:
Kruger, A.N., Brogley, M.A., Huizinga, J.L., Kidd, J.M., de Rooij, D.G., Hu, Y.C., and Mueller, J.L. (2019). A Neofunctionalized X-Linked Ampliconic Gene Family Is Essential for Male Fertility and Equal Sex Ratio in Mice. Curr Biol *29*, 3699-3706 e3695.
Author contributions listed under Authors Contributions section

study demonstrates how newly-acquired X-linked genes can rapidly evolve new and essential functions and how gene amplification can increase sex chromosome transmission.

Results and Discussion

The megabase size and complexity of ampliconic (large (>10kb) and nearly-identical (>99% nucleotide identity) segmental duplications) regions have made it difficult to assess their evolutionary history and associated genes functions. Here, we examined the evolution and function of the *Slx* and *Slxl1* (*Sycp3*-like X-linked and *Slx*-like 1) ampliconic gene families in mice. The *Slx* and *Slxl1* gene families share sequence similarity with autosomal *Synaptonemal complex protein-3 (Sycp3*), but the evolutionary history of *Slx* and *Slxl1* remains unclear [21, 140]. Double knockdown studies of *Slx/Slxl1* exhibit defects in post-meiotic spermatogenesis, male fertility and meiotic drive [18, 20]. However, the lack of complete deletion mutants has hindered functional studies, because *Slx/Slxl1* knockdowns are incomplete, may have off-target effects, are on a mixed genetic background, and do not allow one to assess the independent functions of *Slx* versus *Slxl1*. To more thoroughly characterize the functions of *Slx* and *Slxl1*, we generated precise, complete, and independent deletions of the megabase-sized *Slx* and *Slxl1* ampliconic regions on an inbred genetic background.

We first investigated the evolutionary history of *Slx* and *Slxl1*, by retracing *Slx* and *Slxl1* gene families origination from *Sycp3*. Our sequence analyses indicate that in the mouse-rat ancestor, a single copy of *Sycp3* transposed via a copy and paste mechanism to an X-linked region syntenic to mouse *Slxl1*. *Slxl1* is thus the first family member to evolve, as no additional copies of *Slxl1, Slx* or *Sly* are detectable on rat autosomal or Y chromosomal sequences (Figure 3-1A, Figure 3-5A). In rats, *Slxl1* remains single-copy and appears non-functional, based upon low to no gene expression across rat tissues (Figure 3-5B, C). In mice, *Slxl1* maintains the intron-exon structure of *Sycp3* (Figure 3-6A) and a *Slxl1*-related gene family member, *Slx,* was acquired on an

additional region of the mouse X chromosome (Figure 3-1A). *Slx* and *Slxl1* underwent repeated segmental duplications resulting in ~5Mb (*Slx*) and ~2.3Mb (*Slxl1*) ampliconic regions, comprising 4% of the mouse X chromosome (Figure 3-1A, Figure 3-7A) [7]. Mouse SLX and SLXL1 protein sequence is highly diverged from SYCP3 (<40% amino acid identity) (Figure 3-6B) and from rat SLXL1 (<39% amino acid identity) (Figure 3-5D), as compared to the median of all mouse-rat orthologs (95% amino acid identity) [141]. The high level of divergence suggests SLX/SLXL1 evolved new functions. Our findings establish the evolutionary acquisition and trajectory of the *Slx, Slxl1* and *Sly* gene family, which was previously unclear.

The rapid sequence divergence of *Slx* and *Slxl1* from *Sycp3* appears to reflect neofunctionalization, based on their gene expression patterns and protein localization. SYCP3, a component of the meiotic synaptonemal complex, is expressed in male and female meiotic germ cells and localizes to the nucleus (Figure 3-1B, C) [142]. In contrast, SLX and SLXL1 are expressed exclusively post-meiosis in testicular germ cells (Figure 3-1B, Figure S3-7B) and are present within the cytoplasm (Figure 3-1C), supporting previous studies [143]. The cytoplasmic localization of SLX and SLXL1 is consistent with their loss of the putative nuclear localization signal and DNA-binding domain of SYCP3 (Figure S3-7B) [143-145]. Our findings suggest *Slx* and *Slxl1* are neofunctionalized copies of *Sycp3*.

To explore the independent functions of *Slx* and *Slxl1*, we used CRISPR and Cre/loxP (Figure 3-2B) to generate precise and complete multi-megabase deletions of *Slx* ($Slx^{-/Y}$) and *Slxl1* ($Slxl1^{-/Y}$). We generated individual deletions as they may have independent functions with 61% protein identity and having rapidly diverged from each other (dN/dS=0.947) (Figure 3-2A-C, Figure 3-

5D, 3-8A, B). *Slx*$^{-/Y}$ and *Slxl1*$^{-/Y}$ mice exhibit wildtype fertility, fecundity, testis weights, sperm counts, and no observable spermatogenic defects as observed via histology, which is in contrast to previous studies observing male fertility phenotypes in *Slx* knockdown mice (Figure 3-2D, Figure 3-8C, D)[20].

To test for genetic redundancy between *Slx* and *Slxl1*, we generated double mutants (*Slx*$^{-/Y}$, *Slxl1*$^{-/Y}$), via recombination of the independent deletions that are complete null mutants at the RNA and protein levels (Figure 3-1C, 3-2C, Figure 3-8A, B). In contrast to the independent deletions, double deletion mice (*Slx*$^{-/Y}$, *Slxl1*$^{-/Y}$) are infertile and produce <1% the wildtype number of cauda epididymal sperm, which when present are morphologically severely abnormal (Figure 3-2D, F). Our double deletion mice resemble previous knockdown studies, but the complete loss of *Slx* and *Slxl1* in *Slx*$^{-/Y}$, *Slxl1*$^{-/Y}$ mice now allow us to precisely identify that defects in post-meiotic germ cells occur during the transition from round spermatids to elongated spermatids at stage 7/8 (Figure 3-2E, Figure 3-8F) [20]. The timing of elongation defects is consistent with our stage specific determination of SLX/SLXL1 protein presence in wildtype males (Figure 3-1C, Figure 3-8F). To assess whether *Slx*$^{-/Y}$, *Slxl1*$^{-/Y}$ mice produce competent meiotic products (round spermatids), we performed round spermatid injections (ROSI). Oocytes injected with round spermatids from WT or *Slx*$^{-/Y}$, *Slxl1*$^{-/Y}$ males develop to blastocysts at the same frequency (Figure 3-8G), indicating that *Slx*$^{-/Y}$, *Slxl1*$^{-/Y}$ round spermatids successfully progress through meiosis, supporting *Slx* and *Slxl1* being functionally distinct from meiotic *Sycp3* [146, 147]. To help explain why *Slx*$^{-/Y}$, *Slxl1*$^{-/Y}$ exhibit defects in spermatid elongation, we performed mRNA-seq on round spermatids from *Slx*$^{-/Y}$, *Slxl1*$^{-/Y}$ and wild-type males and identified 990 misregulated genes (adjusted $P<0.01$), which in combination likely perturb round spermatid elongation (Data

S1). These results demonstrate that *Slx* and *Slxl1* acquired new functions in post-meiotic spermatids and function redundantly with each other [147].

While our results confirm that *Slx* and *Slxl1* are essential for male fertility, they do not explain their massive gene amplification (Figure 3-5B, 3-7A). *Slx* and *Slxl1*'s massive gene amplification has been proposed to be a result of their involvement in meiotic drive (the non-Mendelian inheritance of chromosomes), however the importance of gene dosage has never been formally tested [9, 18]. If increases in gene dosage, via gene amplification, serve to increase chromosome transmission (meiotic drive), then complete deletions ($Slxl1^{-/Y}$ or $Slx^{-/Y}$) or duplications ($Slx^{dup/Y}$ or $Slxl1^{dup/Y}$ or $Slx^{dup/Y}$, $Slxl1^{dup/Y}$) (Figure 3A, B) of these regions should decrease or increase X chromosome transmission, respectively. $Slxl1^{-/Y}$, but not $Slx^{-/Y}$, sire more male offspring (58.5% male, 141/241 pups) (two tailed Fisher's Exact test, $P < 0.05$) as compared to wildtype males (48.5% male, 94/194 pups; Figure 3-3C). Conversely, $Slx^{dup/Y}$, $Slxl1^{dup/Y}$ sire more female offspring (58.2% female, 181/311 pups; Figure 3-3C) as compared to WT (two tailed Fisher's Exact test, $P = 0.1672$) and is statistically significant when compared to $Slxl1^{-/Y}$ (two tailed Fisher's Exact test, $P < 0.0001$). We suspect differences between observing sex ratio distortion in $Slx^{Dup/Y}$, $Slxl1^{Dup/Y}$ mice, but not $Slxl1^{Dup/Y}$ mice, is due to unequal crossing over decreasing *Slxl1* copy number in the $Slxl1^{Dup/Y}$ line. Previous knockdown studies were unable to decipher *Slxl1*'s specific role and the impact of gene dosage in meiotic drive [20]. We suspect the distinct functions of *Slx* and *Slxl1* in meiotic drive are due to diverged residues (they share 61% amino acid identity) or gene expression levels, and the redundant functions in fertility are due to their conserved residues (Figure 3-6B). Our findings support *Slxl1*s involvement in meiotic drive and via a gene dosage-dependent mechanism.

Slxl1 has been proposed to be in meiotic conflict, resulting in drive with a related Y-linked gene family *Sly* (*Sycp3*-like Y-linked), where *Sly* represses *Slx* and *Slxl1* gene expression [18, 19]. Our finding that *Slxl1* gene dosage contributes to meiotic drive (Figure 3-3C) led us to test if mice with sex ratio distortion exhibit corresponding gene expression changes in *Sly, Slxl1*, or both. We performed mRNA-seq on round spermatids and found that increases in *Slxl1* gene dosage have corresponding increases in *Slxl1* expression, while *Sly* expression remains relatively unchanged (Figure 3-3D). Our findings suggest the ratio of *Slxl1* to *Sly* gene expression levels mediates meiotic drive (Figure 3-3D); however, the ratio does not affect the number of X versus Y-bearing sperm from *Slxl1*$^{-/Y}$ mice (Figure 3-3E). Meiotic drive likely impacts the relative fitness of X- versus Y-bearing sperm via changes in SLXL1 to SLY protein abundance and interactions with protein partners.

We next identified SLX- and SLXL1-interacting proteins that may contribute to meiotic drive. We performed endogenous SLX/SLXL1 co-immunoprecipitation and mass spectrometry on testis lysates from wildtype, *Slx*$^{-/Y}$, *Slxl1*$^{-/Y}$ and *Slx*$^{-/Y}$, *Slxl1*$^{-/Y}$ mice. Candidates were prioritized by their reproducibility across multiple wildtype samples and absence in *Slx*$^{-/Y}$, *Slxl1*$^{-/Y}$ samples. We identified spindlin family members SPIN1, SSTY1, SSTY2 (SSTY1/2) and 26S proteasome components PSMC1 and PSMD4 (Figure 3-4A, Table 3-1). We did not immunoprecipitate SLY, suggesting SLXL1 and SLY conflict does not occur through direct protein interactions. Instead, SLX, SLXL1 and SLY may compete for spindlin family members, as SSTY1/2 have been shown to interact with SLX, SLXL1 and SLY [110]. SLX and SLXL1 are present in all haploid spermatids (Figure 3-1C) and therefore could compete with SLY for SPIN1 and SSTY1/2 by

diffusing across the cytoplasmic bridges connecting haploid spermatids (Figure 3-4C). SPIN1 is a chromatin reader and post-transcriptional regulator of mRNA stability [148, 149]. SPIN1 binds H3K4me3-R8me2a via its Spin/Ssty domains, which are shared with SSTY1/2 [149]. We hypothesize that changes in SLXL1 to SLY abundance could alter SPIN1 distribution and may have transcriptomic consequences that impact the downstream fitness of X- versus Y-bearing sperm. PSMC1 and PSMD4 may be non-specific interactions, as our antibody has non-specific localization to the acrosome (present in *Slx*$^{-/Y}$, *Slxl1*$^{-/Y}$) where proteases are known to reside (Figure 3-8E).

Based on SLXL1 and SLY protein interaction with spindlin family members SPIN1 and SSTY1/2 we speculated that misregulated X- or Y-linked genes may cause X- versus Y-sperm fitness differences. Comparison of round spermatid mRNA-seq data from wildtype versus *Slxl1*$^{-/Y}$ males identified five X-linked (not including *Slxl1* gene family members), two Y-linked and 50 autosomal genes that are significantly misregulated (adjusted $P<0.01$)(Data S1). One of the seven is an alternative splice form of *Scml2* that is significantly downregulated only in *Slxl1*$^{-/Y}$ males (Figure 3-4B, Data S1). SCML2 is a germline-specific polycomb group protein that regulates sex chromosome-wide silencing in meiotic and post-meiotic cells via chromatin modifications [150]. Together, the interactions of SLXL1 with SPIN1 and SSTY1/2 and the downregulation of *Scml2*, lead us to speculate that changes in round spermatid chromatin may mediate meiotic drive.

The neofunctionalization and amplification of *Slx* and *Slxl1* evolved in the past ~20 MY of mouse-lineage evolution, creating a gene family that functions in a post-meiotic manner that is

essential for male fertility (Figure 3-4C). Our findings build upon previous studies, providing new insights into the evolution, neofunctionalization and the independent contributions of *Slx* versus *Slxl1* [18, 20]. Additionally, we demonstrate the impact gene dosage has on gene expression and conflict between *Slxl1* and *Sly*. We propose that the acquisition of *Slxl1* in the rat-mouse ancestor conferred a selective advantage to increase X chromosome transmission (Figure 3-4C). In response, *Sly* evolved on the Y chromosome specifically in the mouse-lineage to equalize the sex ratio. The rapid changes in gene dosage, gene expression levels and protein sequence chronicle the continued bouts of *Slx*/*Slxl1* versus *Sly* genetic conflict within the mouse-lineage (Figure 3-4C). In the present day C57BL/6J mouse strain, *Slxl1* is likely a primary mediator of meiotic drive, because the frequency of female offspring correlates with increases ($Slx^{dup/Y}$, $Slxl1^{dup/Y}$) and decreases ($Slxl1^{-/Y}$) in *Slxl1* gene dosage (Figure 3-3C, D). These evolutionary signatures inform our proposed model in which SLXL1 and SLY compete for interactions with spindlin family members SPIN1 and SSTY1/2 in a dose-dependent manner (Figure 3-4C). We speculate the interaction of SLX/SLXL1 with the conserved and ubiquitously expressed SPIN1 mediates the male fertility and SLX/SLXL1 interaction with the newly-acquired and ampliconic Y-linked gene family SSTY1/2 mediates meiotic drive (Figure 3-4C) [9, 151]. Consistent with this idea, the chromatin reader SSTY1/2 localizes to X and Y chromatin, where it can have impacts on the localization and regulation of transcription [110].

Mammalian sex chromosomes harbor a plethora of newly acquired ampliconic genes expressed predominantly in the testis [7-9, 113, 135, 136]. Is X-Y co-amplification of newly acquired genes a universal phenomenon continually reshaping sex chromosome evolution? In mice, *Ssty1/2 and Sstx* are X-Y co-amplified gene families that pre-date *Slx*, *Slxl1* and *Sly [9, 21]*. *Ssty1/2* and *Sstx*

may represent a former or current system of genetic conflict. Given SLX, SLXL1 and SLY proteins interact with SSTY1/2, it is tempting to speculate that conflict between gene families on the X and Y chromosome can continuously re-emerge and converge upon pre-existing pathways. The sex chromosomes are a known battleground for genes in conflict and competition between co-amplified X- and Y-linked genes could provide the genetic basis for speciation and hybrid male sterility; both processes known to be associated with the X chromosome [152-154]. Indeed, in other mammals there are hints of entirely new co-amplified X-Y gene families [155]. More complete assemblies of X and Y chromosomes will determine the extent of X-Y gene co-amplification across mammals. We conclude that prime candidates of X-Y genetic conflict can be readily identified in future studies by the presence of three defining signatures: new acquisition, X-Y co-amplification, and rapid sequence evolution.

Acknowledgments

We acknowledge Cincinnati Children's Hospital Medical Center Transgenic Animal and Genome Editing Core for mutant mouse production, Celvie Yuan and Yang Yu for their assistance with ROSI experiments, the University of Michigan Flow Cytometry Shared Resource Laboratory for FACS, DNA Sequencing Core for Sanger and Next Generation Sequencing, Venkatesha Basrur at the Proteomics Resource facility for mass spectrometry and Cancer Center Tissue Core for generating testis histological sections. We thank D. Ginsburg for sharing *EIIa*-Cre mice. We thank M. Arlt, S. Kalantry, J. Moran, C. Swanepoel and Y. Yamashita for their comments. **Funding:** This work was supported by National Institutes of Health grants HD064753 and HD094736 to JLM, T32GM007544 to ANK and a National Science Foundation Graduate Research Fellowship DGE 1256260 to ANK.

Author Contributions A.N.K. and J.L.M. planned the project. A.N.K., M.A.B. and J.L.H. performed experiments. D.G.D. performed histological characterization. J.M.K. performed copy number estimates. A.N.K. and J.L.M. wrote the manuscript.

Declaration of Interests

The authors declare no competing interests.

Materials and Methods

Lead Contact and Materials Availability

Further information and requests for resources and reagents should be directed to and will be fulfilled by the Lead Contact, Jacob L. Mueller (jacobmu@umich.edu). The SLX/SLXL1, Rabbit polyclonal antibody we generated is available from our lab. Mice will be available from our lab until they become available from the Mutant Mouse Resource and Research Center Repository.

Experimental model and subject details

Transgenic mice used in this study were generated from injected zygotes (see *Generation of transgenic lines*) derived from the cross of F1 (DBA2xC57B/6N) and C57B/6N mice, ordered from Envigo. Heterozygous transgenic female mice were mated to C57BL/6J male mice ordered from Jackson Laboratory (Bar Harbor, ME) to backcross. Breeding was conducted with one male and one or two females, all mice were older than 6 weeks of age. Resulting pups were weaned at 21dpp, separated by sex and no more than 5 pups per cage (Allentown, 11.5in x 7.5in x 5in). All experiments were conducted with adult males (2-6 months of age) transgenic males were compared to wildtype littermates or age matched wildtype controls. Cages were kept on ventilated racks (Allentown) at 72°F, 30-70% humidity, on 12hr: 12hr light:dark cycle. Cages

are monitored daily and changed at least every two weeks in a room that is specific-pathogen free, monitored by sentinel mice. Mice were provided water and fed Lab Diet 5008 food *ad libitum.* Adult mice were sacrificed by CO_2 asphyxiation followed by cervical dislocation and pups were euthanized using decapitation in compliance with the ULAM standard procedures of euthanasia. The Institutional Animal Care and Use Committee at the University of Michigan Medical School (PRO00007498) approved all procedures involving mice.

Gene expression of mouse and rat X/Y co-amplified genes

RNA-seq analyses were conducted by analyzing previously published datasets. Specifically, mouse tissue panel data were analyzed from SRP016501 [129], fetal ovary data from SRP058992 [156], ovary data from SRP017959 [157], and sorted testicular germ cell populations from SRP113417 [158]. Rat tissue panel data was used from SRP016501 [129] and rat sorted testicular germ cell populations from SRP026340 [159]. Alignments were performed using Tophat with the mm10 mouse reference genome, a refFlat file with RefSeq gene annotations and --max-multihits set to 240; otherwise standard default parameters were used. We used Cufflinks, using the refFlat RefSeq gene annotation file, to estimate expression levels as fragments per kilobase per millions of mapped fragments (FPKM).

Round spermatid FACS isolation and library generation

We largely followed a previously published protocol to isolate round spermatids (1n) [128]. Briefly, we disassociated cells from a pair of testes by enzymatic treatment with Collagenase type I (Worthington Biochemical Corporation), DNase I (Worthington Biochemical Corporation), and Trypsin (Life Technologies). The cell suspension was passed through cell

strainers (100µm and 40µm) and incubated with Hoechst 33342 (Setareh Biotech) to determine DNA content and propidium iodide (Acros Organics) to evaluate cell viability. Cell sorting was performed on a Synergy Head Cell Sorter cell sorter (Sony). The purity of each sort was determined via fluorescence microscopy visual inspection of 100 cells morphology and nuclear staining with DAPI for round spermatids. The purity of round spermatids was typically >85%, which is consistent with previous studies [128].

TRIzol LS (Thermo Fisher Scientific) was used to extract total RNA. RNA was DNAse treated to remove any genomic DNA contamination using RNeasy Mini Kit and RNase-Free DNase Set (QIAGEN). Libraries were generated using samples with >7 RIN scores and >5ng of total RNA. Stranded mRNAseq libraries were generated using the NEBNext Ultra II Directional RNA Library Prep Kit (NEB) and Agencourt AMPure XP beads (Beckman Coulter) following the manufacturers protocol. We generated at least two biological replicate round spermatid mRNA-seq libraries per genotype. All libraries were sequenced on a single Illumina NovaSeq lane (~50 million sequenced fragments per library) and in NCBI SRA: PRJNA545829. Alignments were performed with Kallisto and DESeq2 using the RefSeq index with bootstrapping set to 100 [160, 161].

Generation of transgenic lines

To generate mice with multi-megabase deletions of the *Slx* and *Slxl1* ampliconic region, loxP sites were sequentially integrated upstream and downstream of either the *Slx* or *Slxl1* ampliconic region via CRISPR. sgRNA targeting unique sequence flanking the ampliconic region was selected based on scores from either the CRISPR Design Tool (http://www.genome-engineering.org/) or CRISPOR (http://crispor.tefor.net) [162]. sgRNA and Cas9 mRNA were synthesized *in vitro*, using the MEGAshorscript T7 kit (ThermoFisher) and mMESSAGE

mMACHINE T7 ULTRA kit (ThermoFisher), respectively, followed by MEGAclear Kit (ThermoFisher) for clean-up. sgRNA, Cas9 mRNA, and single stranded oligo donor carrying the loxP sequence (IDT; Table 3-2) were mixed for microinjection at concentration of 50, 100, and 100 ng/ul, respectively. Cytoplasmic microinjection was performed on zygotes derived from the cross of F1 (DBA2xC57BL/6N) and C57BL/6N mice, using a piezo-driven microinjection technique [163]. Floxed mice were mated against C57B/6J *Ella*-Cre mice resulting in mice carrying either a *Slx* or *Slxl1* deletion or duplication (Fig. S10). Two independent deletion and duplication lines were generated for each *Slx* and *Slxl1* ampliconic region. No differences were observed between independent lines and data was therefore compiled. All deletion or duplication carrying males were derived from heterozygous female mice that had been backcrossed to C57BL/6J males for at least four generations. Mice were genotyped by extracting DNA out of a tail biopsy using Viagen DirectPCR lysis reagent using primers that flank loxP sites (Table 3-2).

Testis Histology

Testes were collected from 2-6 months old mice. The tunica albuginea was nicked and the testes were fixed with Bouins Fixative overnight at 4ºC. Testes were then washed through a series of ethanol washes (25%, 50%, 75% EtOH) before being stored in 75% EtOH at 25ºC. Testes were paraffin embedded and 5µm sections were made that were stained with Periodic acid Schiff (PAS) and hematoxylin. Sections were studied using a light microscope and staged [164]. Specific types of germ cells were identified based upon their location, nuclear size and nuclear staining pattern [164].

Immunohistochemistry

Immunohistochemistry was performed on 5µm paraffin embedded sections. Sections were deparaffinized and rehydrated prior to antigen presentation. Antigen presentation was performed by boiling slides in 0.01M Citrate Buffer pH 6 for 10 minutes. Sections were blocked for 1hr at room temperature using 3% BSA and 0.05% Triton X-100 in PBS and subsequently probed with primary and secondary antibodies.

Our SLX/SLXL1 antibody was generated against a CVSFSEEWQRFARS-KLH conjugated peptide. Genemed Synthesis Inc. synthesized and injected the peptide into rabbits and affinity purified the antibody. Antibody specificity was assessed by probing whole testis lysates from wildtype (C57BL/6J), *Slx*$^{-/Y}$ and *Slxl1*$^{-/Y}$ mice with both pre-immune serum and purified antibodies on western blots. The following commercially available antibodies were used: SCP3 (Abcam, ab97672), Peroxidase AffiniPure (Jackson ImmunoResearch, 711-035-152), FITC AffiniPure (Jackson ImmunoResearch, 711-095-152), Rhodamine RedX AffiniPure (Jackson ImmunoResearch, 715-295-151).

RT-PCR

Total RNA was extracted using Trizol (Life Technologies) according to manufacturer's instructions. Ten µg of total RNA was DNase treated using Turbo DNAse (Life Technologies) and reverse transcribed using Superscript II (Invitrogen) using oligo(dT) primers following manufactures instructions. Intron-spanning primers were used to perform RT-PCR on adult testis cDNA preparations for *Slx, Slxl1* and a round spermatid specific gene *Trim42* (Table 3-2).

Assaying Fertility

The fecundity of males was assessed by mating at least three males 2-6 months of age of a given genotype to 2-6 month old C57B/6J females and monitoring females for copulatory plugs. The fertility of all lines was compared to that of C57B/6J males (wildtype). Offspring sex ratios data was compiled by sex genotyping offspring from the aforementioned crosses as well as pups resulting from males bred with CD1 females. Sperm counts were conducted on sperm isolated from the cauda epididymis. Briefly, the cauda epididymis was isolated and nicked three times to allow sperm to swim out. The nicked epididymis was then rotated for 1hr at 37ºC in Toyoda Yokoyama Hosi media (TYH). Sperm were fixed in 4%PFA and counted using a hemocytometer. For each genotype, at least three male mice were counted with three technical replicates performed for each mouse and averaged. Testes were collected from 2-6 month old males for all experiments and weighed, along with total body, in order to determine relative testis weight.

X-Y Chromosome Paint

Cauda epididymal sperm were collected and fixed onto slides using 3:1 methanol: acetic acid. Slides were stored at -20ºC. Slides were immersed twice in 2x SSC for three minutes followed by a series of ethanol washes (70%, 90%, 100% ethanol) for two minutes each. Slides were incubated at room temperature for 30 minutes in 5mM DTT, 1% Triton X-100, 50mM Tris. Slides were again washed with 2x SSC and the ethanol series. Slides were incubated in 70% formamide, 2x SSC at 78ºC for five minutes and then washed in ethanol series for one minute each. Mouse X and Y paint probes from MetaSystems Probes were mixed and denatured at 80ºC for ten minutes before placing on slide. Slides were incubated overnight at 37ºC in a humid chamber. Slides were washed in 50% formamide, 2x SSC three times at 45ºC for five minutes,

2x SSC once at 45ºC for five minutes and rinsed in Photo-Flo 200 (Kodak). Slides were mounted with VECTASHIELD with DAPI (Vector Laboratories).

Co-Immunoprecipitation and Mass Spectrometry

SLX/SLXL1 co-immunoprecipitation was performed on whole testis lysate using our SLX/SLXL1 antibody conjugated to protein A Dynabeads (Life Technologies). Briefly, testes from wildtype, *Slx*$^{-/Y}$, *Slxl1*$^{-/Y}$ and *Slx*$^{-/Y}$, *Slxl1*$^{-/Y}$ males were lysed (150 mM KCl, 0.05% NP-40, 0.5 mM DTT, and protease inhibitors (EDTA-free Complete PI) and centrifuged at full speed in a tabletop centrifuge at 4C. The top lipid layer was discarded and the remaining supernatant was transferred to a new tube and incubated with SLX/SLXL1 antibody. Protein A dynabeads were rinsed 3 times with lysis buffer before adding the lysate/antibody solution and incubated at 4ºC for at least 1hr. Beads were subsequently washed 2X with lysis buffer and 1X with lysis buffer containing no detergent and 1X with PBS containing protease inhibitors. A small aliquot of beads was removed for western blot analysis. The remaining beads were stored at -20ºC after removing all liquid. Prior to trypsin digestion, beads were resuspended in 50ul of 0.1M ammonium bicarbonate buffer (pH~8). Cysteines were reduced by adding 50ul of 10 mM DTT and incubated at 45°C for 30 min. To alkylate cysteines, the samples incubated at room temperature, protected from light, with 65 mM 2-Chloroacetamide. Proteins were digested overnight with 1ug sequencing grade modified trypsin at 37°C with constant shaking in a Thermomixer. Digestion was stopped by acidification and peptides were desalted using SepPak C18 cartridges using manufacturer's protocol (Waters). Samples were dried using a vacufuge. Samples were dissolved in 8ul of 0.1% formic acid, 2% acetonitrile solution and then 2ul of the peptide solution was resolved on a nano-capillary reverse phase column (Acclaim PepMap C18,

2 micron, 50 cm, ThermoScientific) using a 0.1% formic acid, 2% acetonitrile (Buffer A) and 0.1% formic acid, 95% acetonitrile (Buffer B) gradient at 300 nl/min over a period of 180 min (2-22% buffer B in 110 min, 22-40% in 25 min, 40-90% in 5 min followed by holding at 90% buffer B for 5 min and requilibration with Buffer A for 25 min). Eluent was directly introduced into Orbitrap Fusion tribrid mass spectrometer (Thermo Scientific, San Jose CA) using an EasySpray source. MS1 scans were acquired at 120K resolution (AGC target=$1x10^6$; max IT=50 ms). Data-dependent collision induced dissociation MS/MS spectra were acquired using Top speed method (3 seconds) following each MS1 scan (NCE ~32%; AGC target $1x10^5$; max IT 45 ms).

Proteins were identified by searching the MS/MS data against *Mus Musculus* (UniProt; 60627 entries) using Proteome Discoverer (v2.1, Thermo Scientific). Search parameters included MS1 mass tolerance of 10 ppm and fragment tolerance of 0.2 Da; two missed cleavages were allowed; carbamidimethylation of cysteine was considered fixed modification and oxidation of methionine, deamidation of aspergine and glutamine were considered as potential modifications. False discovery rate (FDR) was determined using Percolator and proteins/peptides with a FDR of ≤1% were retained for further analysis.

Candidate interacting proteins were filtered based upon high confidence (<1% FDR), reproducible presence across multiple wildtype samples (PSM >5) and reproducible absence across all $Slx^{-/Y}$, $Slx11^{-/Y}$ samples. Three biological replicates-wildtype and $Slx^{-/Y}$, $Slx11^{-/Y}$, two biological replicates $Slx^{-/Y}$ and $Slx11^{-/Y}$ were performed. The mass spectrometry proteomics data

have been deposited to the ProteomeXchange Consortium via the PRIDE [165] partner repository with the dataset identifier PXD014276.

Estimation of amplicon copy number

For estimating the number of *Slxl1* copies in the rat genome, read depth analysis was performed using the mrsFAST [166] aligner and the fastCN pipeline [167]. Reads were mapped against the rn6 reference genome in which sequences identified by RepeatMasker, Tandom Repeat Finder, and 50-mers with an occurrence greater than 50 were masked. Read depth was normalized to account for GC content, averaged in windows containing 3,000 unmasked positions, and converted to copy-number based on the observed depth in autosomal regions not previously identified as copy-number variable [168]. Analysis was performed using male and female genomic data obtained from SRP029216 [169].

Comparisons of exon-intron structure

Complete RefSeq mRNA sequences were obtained for mouse *Sycp3* (NM_011517), *Slx* (NM_001136476), *Slxl1* (NM_029181), and *Sly* (NM_201530). Pairwise comparisons for each of the four genes were performed via Exalign [170] to determine conservation on exon-intron structure.

Dot-plots

Self-symmetry triangular dot plots that show repeats within a sequenced region were generated from a custom Perl script that can be found at http://pagelab.wi.mit.edu/materials-request.

Round spermatid Injections (ROSI)

Round spermatids were collected and enriched from the testes of 2-6 month old WT and *Slx* $^{-/Y}$,*Slx11* $^{-/Y}$ males, as described previously [171]. Briefly, testes were placed in red blood cell lysis solution (Miltenyi Biotec) to remove Tunica albuginea. Seminiferous tubules were transferred to GL-PBS (0.01% PVP in Dulbecco's PBS containing glucose and pyruvate from GIBCO), cut into small pieces and pipetted gently to release spermatogenic cells. The cell suspension was filtered through a 50-um nylon mesh, centrifuged at 200xg for 5 min at 4ºC, and resuspended in GL-PBS containing 0.4 mg/ml pronase E (SERVA). The cell suspension was centrifuged again at 400xg for 5 min at 4ºC to precipitate most elongating spermatids and spermatozoa. The remaining suspension containing most round spermatids was washed twice at 200xg for 5 min at 4ºC and stored in 7.5% glycerol, 7.5% FBS, 0.01% PVP in GL-PBS at -80C.

Unfertilized eggs were harvested from 5-weeks-old superovulated C57BL6/DBA2 F1 females. Round spermatids were thawed and washed twice with 7.5% FBS in GL-PBS at 400xg for 5 min at 4ºC. More than 90% cells were alive after thawing, as determined by the trypan blue extrusion test. On the injection dish, eggs and round spermatids were placed in a droplet of the M2 medium (Sigma) and a droplet of GL-PBS, respectively. Using a needle with 6um inner diameter and 15 um outer diameter for piezo-driven microinjection, individual round spermatids were drawn into the needle to break the plasma membrane, and the nucleus was injected into the cytoplasm of the egg. Following round spermatid injection, eggs were activated in the M16 medium (Sigma) containing 5 mM $SrCl_2$ and 5 mM EGTA for 20 min at 37 ºC [172]. Eggs were then washed and cultured in KSOM media for development.

Quantification and Statistical Analysis

Two-tailed Fisher's Exact tests were used to calculate statistical significance between wildtype and transgenic groups in offspring sex ratio (Figure 3) and X versus Y sperm counts (Figure 3) as the outcomes are binary. The number of pups or sperm screened are noted in the figure and figure legend, respectively. To determine statistical significance for average litter size, sperm counts and testis weights between wildtype and transgenic groups, a two-tailed T-test was performed. The number of mice used is denoted in the figure legends. All error bars denote standard deviation.

Data and Code Availability

Sequencing data is available on NCBI SRA: PRJNA545829. Mass spectrometry data is available on the PRIDE database: PXD014276.

Figures

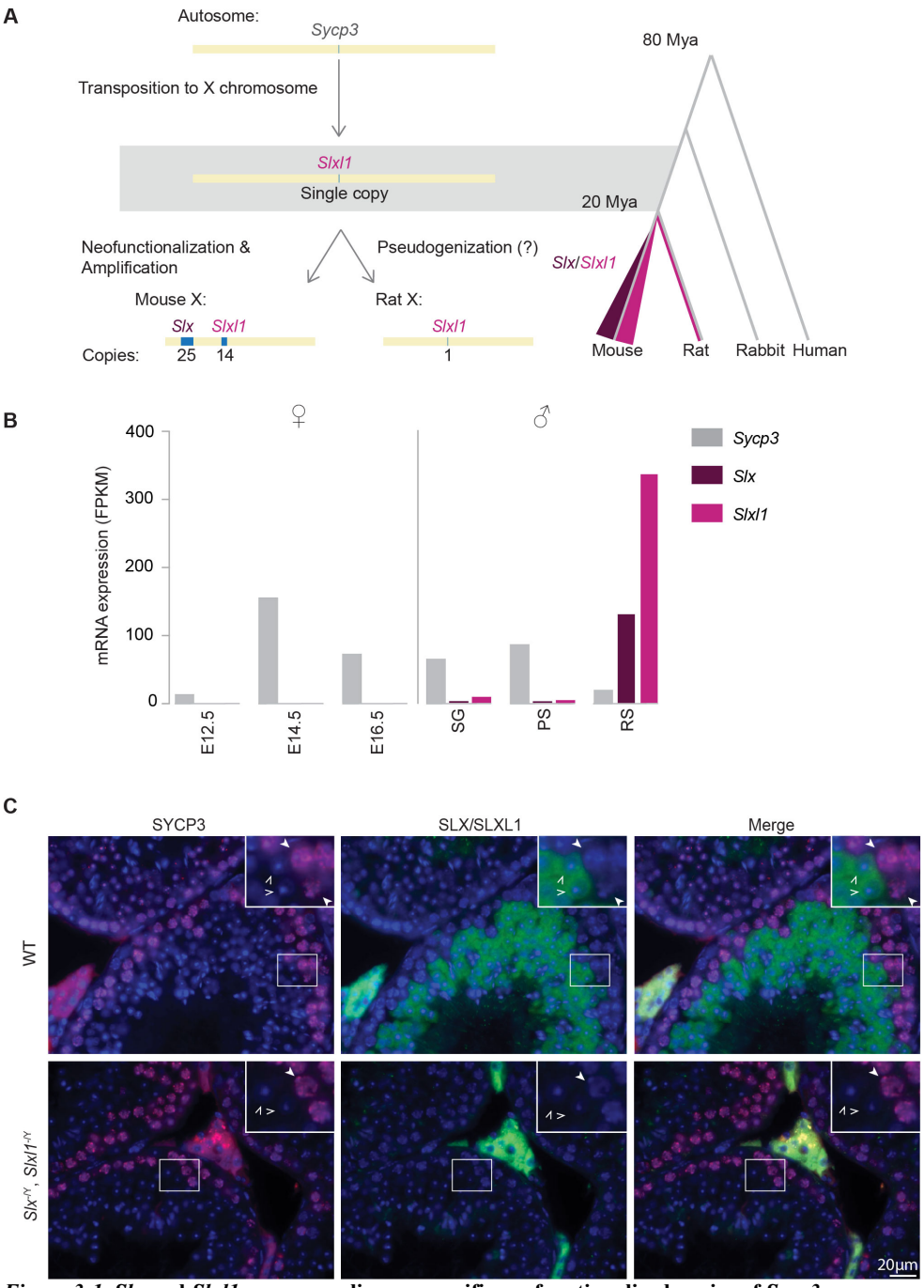

Figure 3-1. Slx* and *Slxl1* are mouse-lineage specific neofunctionalized copies of *Sycp3

A) *Sycp3* transposed to the X chromosome in the mouse-rat ancestor. Following mouse and rat speciation, *Slx* was acquired and both *Slx*/*Slxl1* were segmentally duplicated within the mouse-lineage. *Sycp3* (light grey), *Slx* (purple), *Slxl1* (pink). **B)** mRNA-seq analysis on publically available data sets [156, 158]. In female mice, *Sycp3* expression is detected embryonically at E14.5 and in male mice, *Sycp3* expression is detected in spermatogonia (SG) and pachytene spermatocytes (PS). *Slx* and *Slxl1* are expressed exclusively in the male germline, post-meiotically, in round spermatids (RS). **C)** Immunofluorescence of SYCP3 (red) and SLX/SLXL1 (green) on DAPI stained testis histological sections from wildtype mice and mice lacking SLX/SLXL1 ($Slx^{-/Y}$, $Slxl1^{-/Y}$). RS (open arrow) and PS (closed arrow). Staining between tubules (Leydig cells) is non-specific. See also Figure 3-5, 3-6 and 3-7.

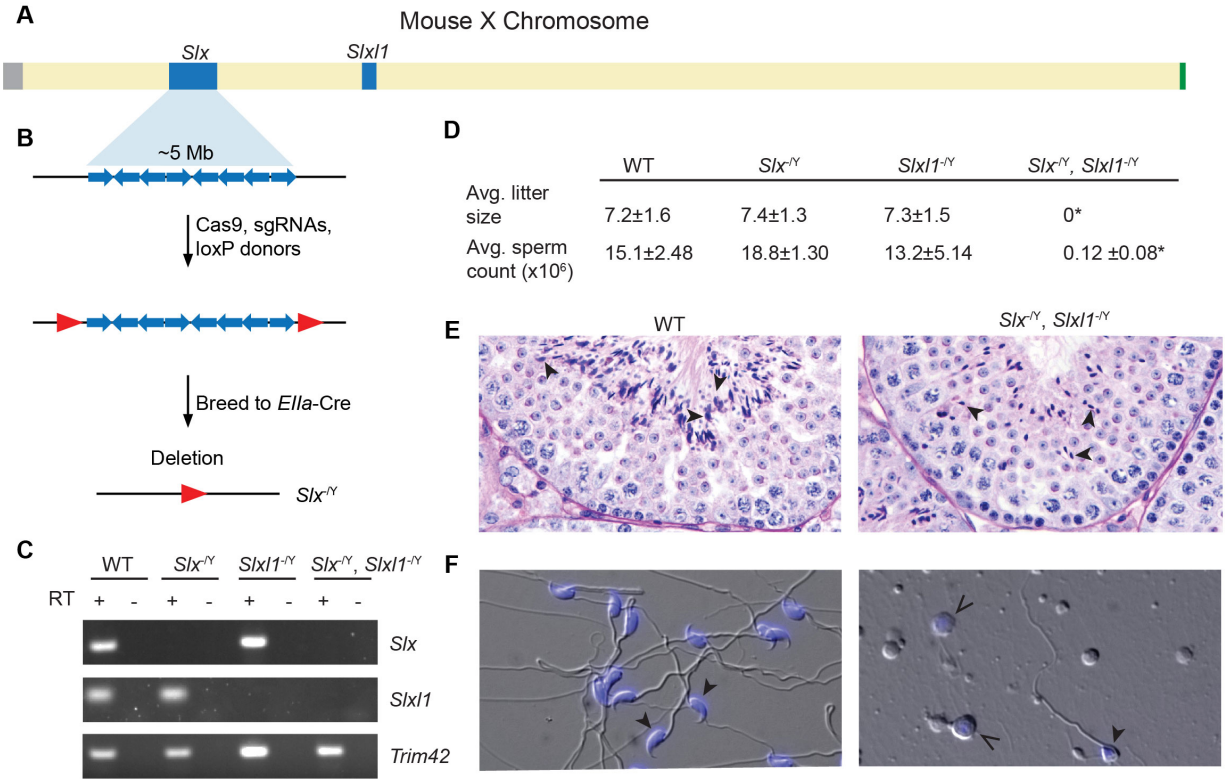

Figure 3-2. *Slx* and *Slxl1* are essential for male fertility and exhibit post-meiotic spermatogenesis specific defects

A) Schematic representation of the mouse X chromosome. Ampliconic regions are shown in blue, centromere in grey and pseudoautosomal region (PAR) in green. **B)** Schematic representation of Slx ampliconic region consisting of segmental duplications (blue arrows), red arrows denote loxP sites. Mice carrying loxP sites flanking the ampliconic region were mated to Ella-Cre carrying mice. *Slxl1*$^{-/Y}$ mice were generated in a complementary manner. **C)** RT-PCR (+) and no RT controls (-) performed on RNA isolated from adult testis. Trim42 is a testis specific gene that was used as a control. All primers are intron-spanning. **D)** Average litter size and cauda epididymal sperm count including standard deviation. Average litter size was determined by mating three males from each genotype against five females each for a total of 15 litters. Sperm were counted from at least three males. Two tailed t-tests were used to compare to WT, * p-value <0.0001 **E)** Periodic-acid Schiff stained testis histology from WT and *Slx*$^{-/Y}$, *Slxl1*$^{-/Y}$ males. Stage 7 tubules, elongated spermatids (see black arrowheads) exhibit abnormal morphology in *Slx*$^{-/Y}$, *Slxl1*$^{-/Y}$ testis. **F)** Cauda epididymal sperm from a WT and *Slx*$^{-/Y}$, *Slxl1*$^{-/Y}$ male, DIC and DAPI (closed arrows). Open arrows indicate cells that resemble round spermatids based upon DAPI stain present in *Slx*$^{-/Y}$, *Slxl1*$^{-/Y}$. See also Figure 3-8.

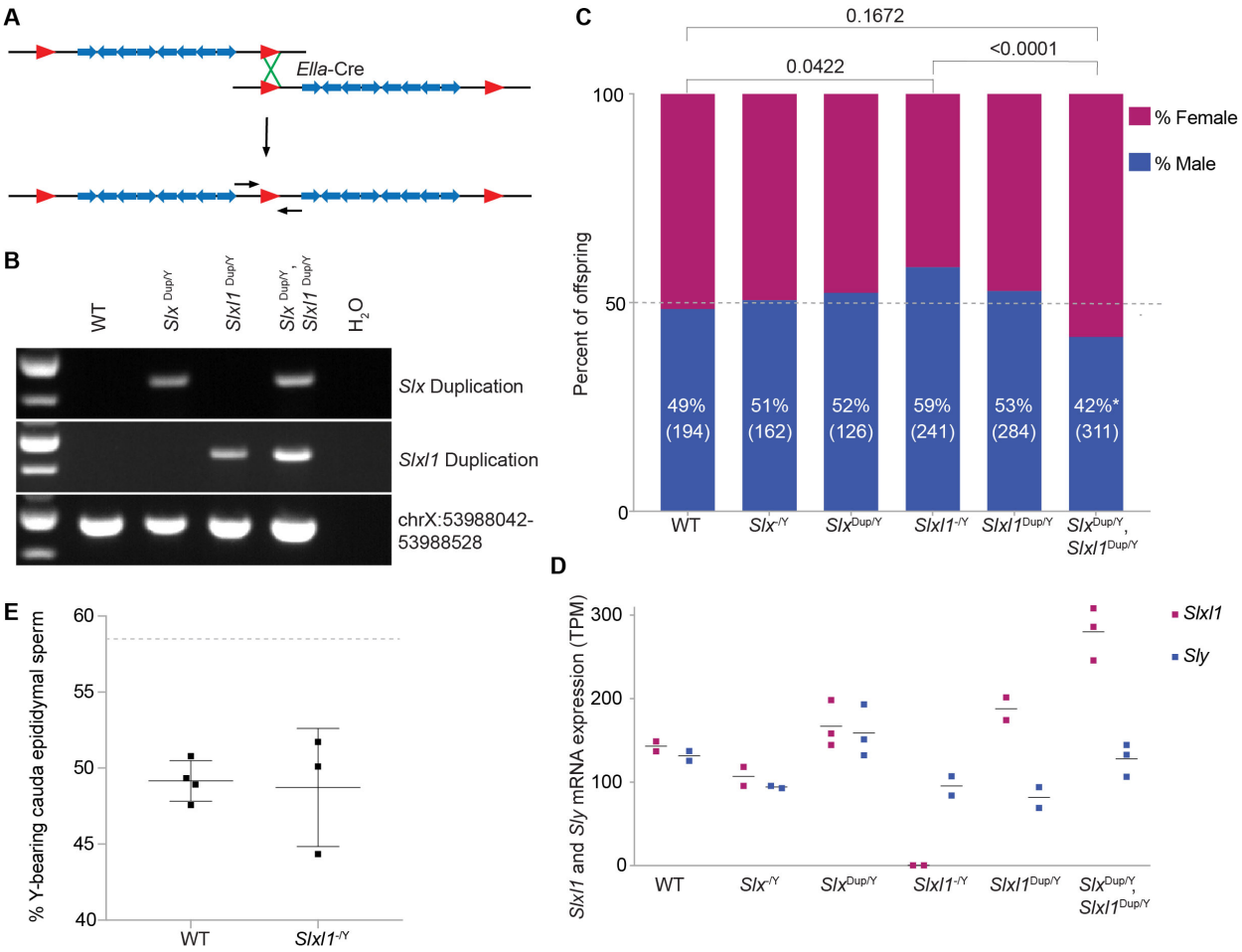

Figure 3-3. Changes in *Slxl1* gene dosage results in sex ratio distortion of offspring and *Slxl1* gene expression levels

A) Schematic representation of a floxed (red triangles) ampliconic region with segmental duplications (blue arrows). Duplications were generated by expression of *Ella*-Cre and pups were genotyped using PCR primers spanning the duplication junction (small black arrows). **B)** Representative genotyping of wildtype (WT), *Slx* duplication (*Slx* $^{dup/Y}$), *Slxl1* duplication (*Slxl1* $^{dup/Y}$) and *Slx*/*Slxl1* (*Slx* $^{dup/Y}$,*Slxl1* $^{dup/Y}$) duplication mice. ChrX:53988042-53988528 is unique sequence, which controls for retaining the intervening sequence present between the *Slx* and *Slxl1* ampliconic regions. **C)** Males of each genotype were mated against wildtype females and progeny were sex genotyped. The percent of male offspring is shown as a percentage along with the number of pups screened in parentheses. P-values were calculated using a two-tailed Fisher's Exact test, compared to experimental WT data (bars on top) and theoretical 50:50 data with an equivalent population size ($p<0.05$, asterisk near male percentage). **D)** mRNA-seq was performed on isolated round spermatids. The horizontal line represents average expression across biological replicates (bullets) for *Slxl1* and *Sly*. TPM, Transcripts per million. **E)** X and Y chromosome paint was performed on sperm collected from the cauda epididymis of wildtype and *Slxl1*$^{-/Y}$ males. Each bullet represents the percentage of Y-bearing sperm from one male, with overall mean and standard deviation. Dotted line denotes expected percentage of Y-bearing sperm if ratio of X- to Y- bearing sperm reflected observed *Slxl1*$^{-/Y}$ sired offspring sex ratio. Differences between wildtype and *Slxl1*$^{-/Y}$ are not significant, Fisher's exact test two-tailed.

A

SLX/SLXL1 IP Mass Spec PSMs

Gene	WT	*Slx* $^{-/Y}$	*Slxl1* $^{-/Y}$	*Slx* $^{-/Y}$, *Slxl1* $^{-/Y}$
SLX*	121	0	93	0
SLXL1	87	73	0	0
SPIN1	15	13	10	0
SSTY2	11	4	7	0
PSMC1	7	5	3	0
SSTY1	6	0	3	0
PSMD4	6	4	4	0

B

	Adjusted p-values					
Scml2	0.99	0.99	0.001	0.86	0.99	0.90
WT vs.	*Slx*$^{-/Y}$	*Slx*$^{Dup/Y}$	*Slxl1*$^{-/Y}$	*Slxl1*$^{Dup/Y}$	*Slx*$^{Dup/Y}$, *Slxl1*$^{Dup/Y}$	*Slx*$^{-/Y}$, *Slxl1*$^{-/Y}$

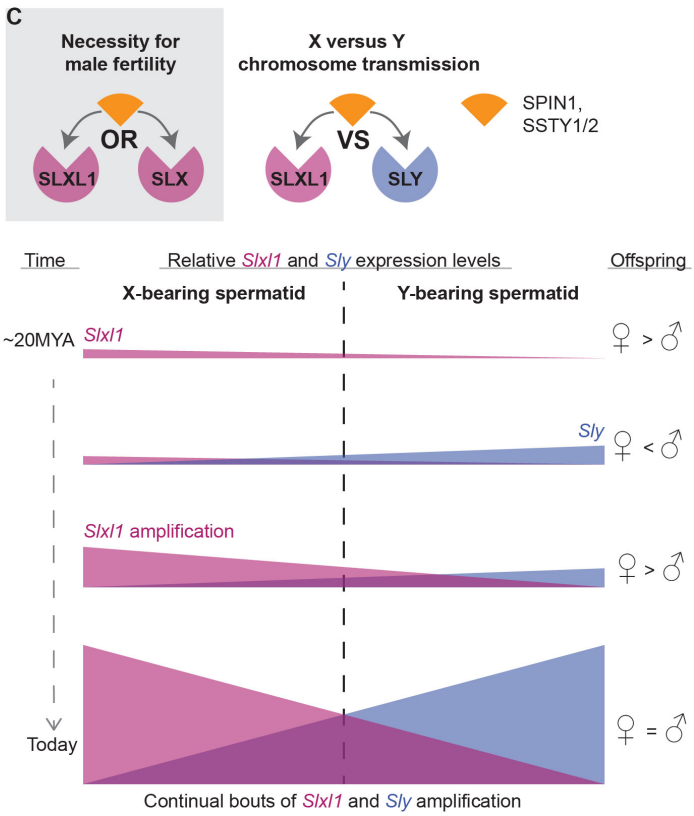

Figure 3-4. SLX/SLXL1 interact with spindlin family members and regulate chromatin

A) Mass spectrometry results from SLX/SLXL1 immunoprecipitations on wildtype, *Slx*$^{-/Y}$, *Slxl1*$^{-/Y}$, and *Slx*$^{-/Y}$, *Slxl1*$^{-/Y}$ whole testis lysates. PSMs (peptide-to-spectrum matches) were quantified to determine relative protein abundance. Candidates were filtered by high confidence (<1% FDR) and reproducibility. (*, additional SLX accessions were removed for simplicity, see Table 3-1 for biological replicates) **B)** Expression level adjusted p-values for *Scml2* isoform NM_001290652 when comparing wildtype versus deletion or duplication genotype round spermatid mRNA-seq samples. **C)** Our model in which SLX or SLXL1 interactions with spindlin family members, SPIN1 and SSTY1/2, is essential for fertility and how SLXL1 and SLY competition for spindlin family members, SPIN1 and SSTY1/2, influences chromosome transmission through the sharing of proteins and transcripts across cytoplasmic bridges. Changes in the relative expression of *Slxl1* to *Sly* result in corresponding changes in the fitness of X and Y sperm that influence offspring sex ratio.

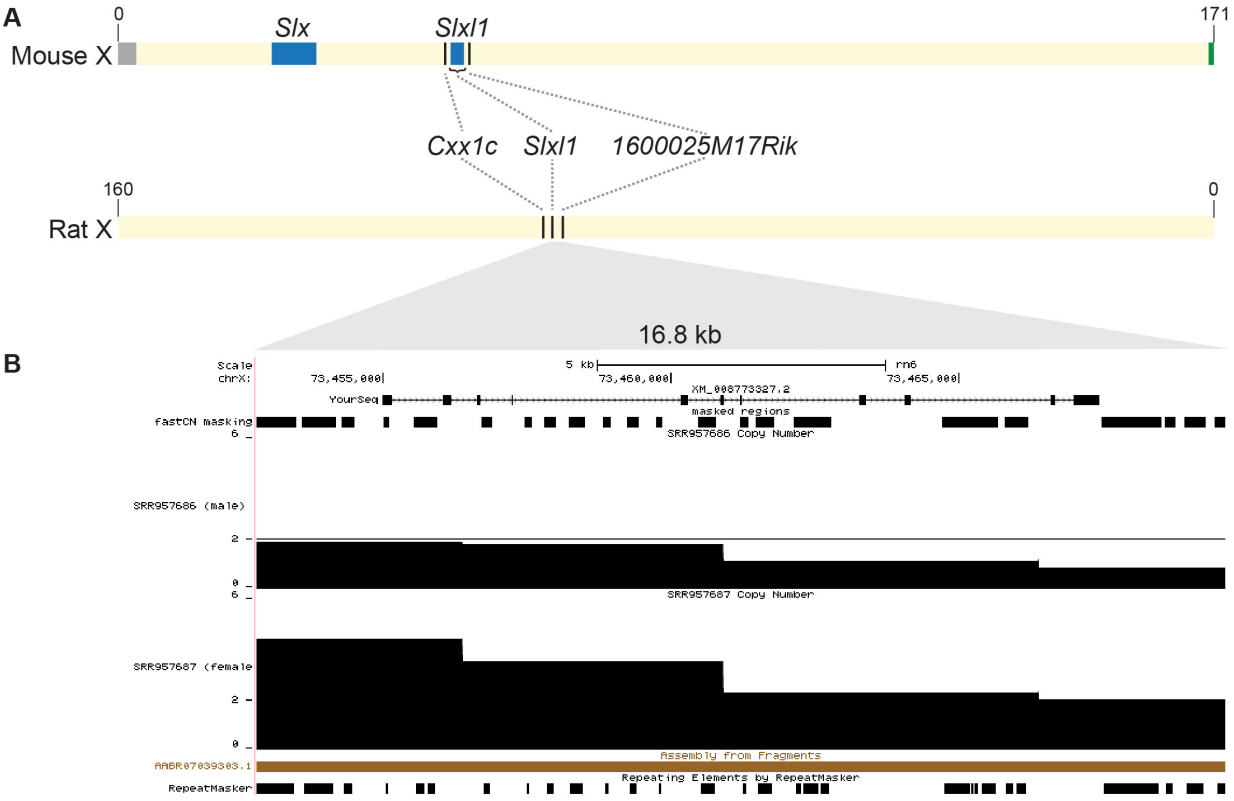

C

	FPKM (Fragments per kilobase per million mapped reads)												
Gene	**Brain**	**Colon**	**Heart**	**Kidney**	**Liver**	**Lung**	**Muscle**	**Spleen**	**Testis**	**Sertoli**	**SG**	**SC**	**RS**
Slxl1 (XM_008773327.2)	0	0	0.02	0	0.43	0	0.04	0	0.64	0	1.3	0.13	0.08
Acrv (NM_021747.1)	0	0	0	0	0	0.02	0.03	0	75.34	0	0	16.97	29.50

D

	Synonymous (dS) and Non-synonymous (dN) substitution rates					
Gene Comparison	**S**	**N**	**dS**	**dN**	**dN/dS**	**AA identity**
Rat SLXL1 vs. Mouse SLXL1	102.4	365.6	0.299	0.255	0.853	37%
Rat SLXL1 vs. Mouse SLX	138.2	479.8	0.282	0.252	0.894	39%
Mouse SLX vs. Mouse SLXL1	91.3	376.7	0.190	0.180	0.947	61%

Figure 3-5. The rat X chromosome carries a single-copy gene that is orthologous to the rapidly evolving mouse *Slx*/*Slxl1*/*Sly* genes, in a region syntenic with mouse *Slxl1*, and is not expressed in spermatids

A) The best tBLASTN alignment match of mouse SLX, SLXL1 and SLY to the rat genome is to an X-linked region that is syntenic (based upon flanking orthologous genes) with the Slxl1 region in mice. **B)** A predicted X-linked gene, XM_008773327.2, maps to this syntenic region on the rat X chromosome (chrX:73,452,814-73,469,623), shares sequence similarity with mouse SLX/SLXL1/SLY. The Slxl1 syntenic region in rat appears to be present in a single-copy as based upon read depth analyses of male versus female genomic sequence [169]. **C)** Analysis of previously published mRNA-seq data from a rat tissue panel and sorted testicular germ cells [129, 159]. FPKM is shown for the predicted XM_008773327.2 gene, which does not exhibit spermatid-specific expression, in contrast to the spermatid-specific gene expression of acrosomal protein Acrv1. XM_008773327.2 does appear to be expressed at low levels in spermatogonia. SG = Spermatogonia. SC = Spermatocytes. RT = Round spermatids. **D)** Pairwise comparisons of sequence evolution rates between the three genes, based upon their protein and mRNA alignments. S= # of synonymous sites. N= # on non-synonymous sites. dS = synonymous substitution rate. dN= non-synonymous substitution rate. Percent identity was determined using BLATp. SLXL1 (rat), SLX (mouse), and SLXL1 (mouse). Rat SLX/SLXL1 is based upon the predicted protein XP_008771549 from CDS XM_008773327. Canonical SLX (NP_001103439) and SLXL1 (NP_001346637) protein sequences were used for alignments.

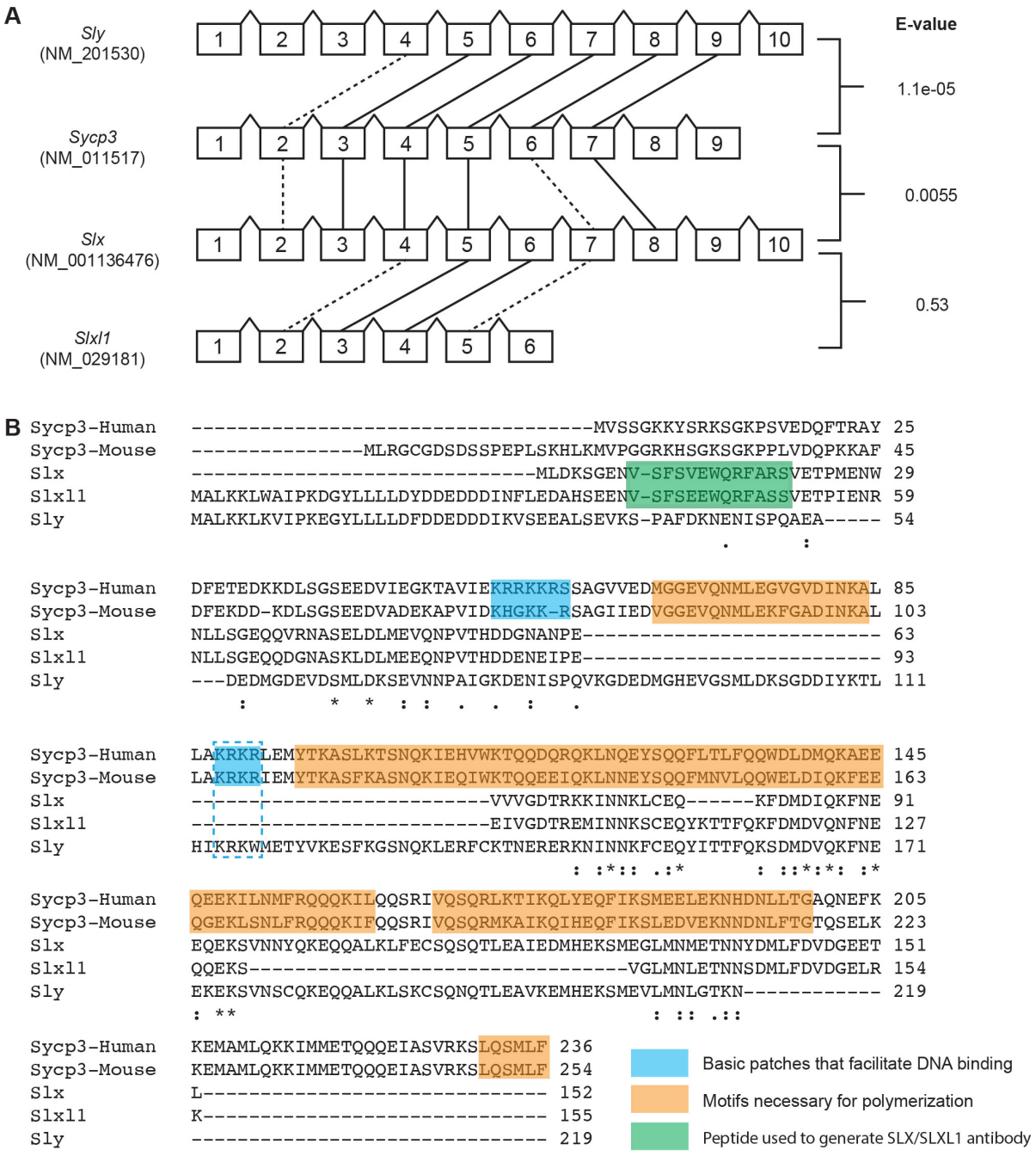

Figure 3-6. Slx, Slxl1, and Sly have conserved exonic structures with Sycp3, but lack the polymerization domain and nuclear localization signal

A) Exonic alignments and E-values were determined by Exalign [170]. Genbank accessions used for each alignment are shown underneath the gene names. Solid lines show exons that share sequence similarity via BLAST, have exactly (or nearly) the same exon length and are in the same reading frame. Dashed lines show exons sharing sequence similarity via BLAST and in the same reading frame. **B)** Clustal alignment of human and mouse SYCP3, SLX, SLXL1 and SLY. Basic regions that have been shown to facilitate DNA binding are highlighted in blue. These regions are largely conserved between human and mouse SYCP3 but are missing or diverged in SLX, SLXL1 and SLY [144]. Regions necessary for SYCP3 polymerization are highlighted in orange and display conservation between human and mouse SYCP3, but are absent or highly diverged in SLX, SLXL1 and SLY [173]. The putative nuclear localization domain of SYCP3 is outlined in blue and is absent in SLX and SLXL1 [7]. The region outlined in green represents the peptide used to generate the antibody against SLX and SLXL1 that is used in this study.

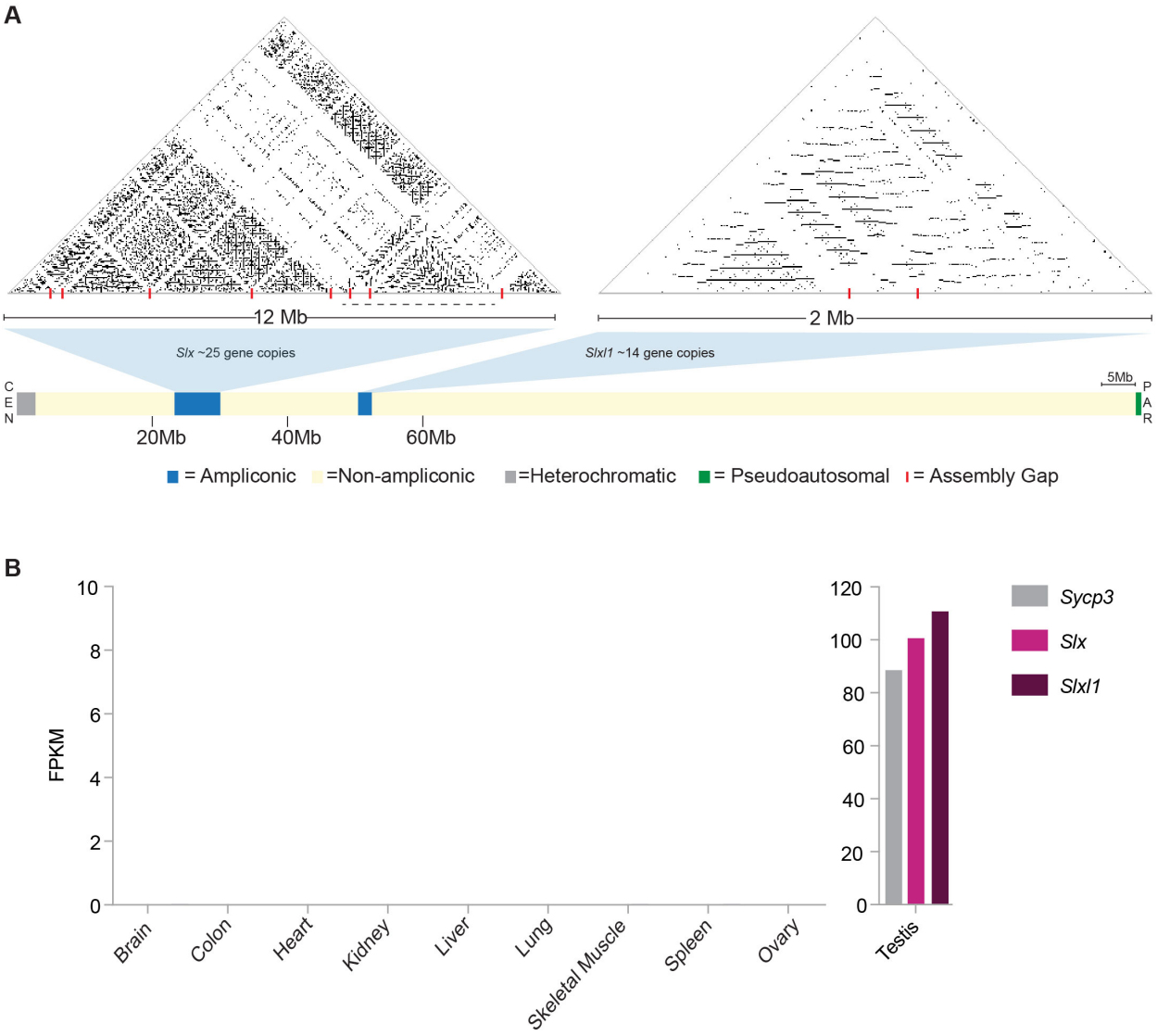

Figure 3-7. Slx and Slxl1 gene families are harbored in multi-megabase-sized ampliconic regions of the mouse X chromosome are expressed exclusively in the adult testis

A) Self-symmetry triangular dot plots are shown with the underlying sequence compared to itself. Each dot represents a perfect match of 200 nucleotides, which when strung together as a horizontal line shows tandemly-oriented amplicons and as a vertical line shows palindromic-oriented amplicons, each with >99.5% nucleotide sequence identity between amplicons. Gene copy number estimates are based upon a previous publication [145]. The mm10 coordinates of the chromosomal regions shown are chrX:24000000-36000000 for Slx and chrX:54000000-56000000 for Slxl1. Each region is incompletely assembled in the mm10 reference genome sequence, as evidenced by the multiple physical gaps shown as red lines. Within the Slx genomic region there is a large contig, underscored with a dotted line, which is incorrectly placed in the reference sequence and likely belongs at the proximal end of the chromosome where an amplicon array with highly similar sequence identity maps. **B)** Slx, Slxl1 and Sycp3 gene expression is detected exclusively in the adult testis. mRNAseq analysis performed on publically available datasets [129, 145].

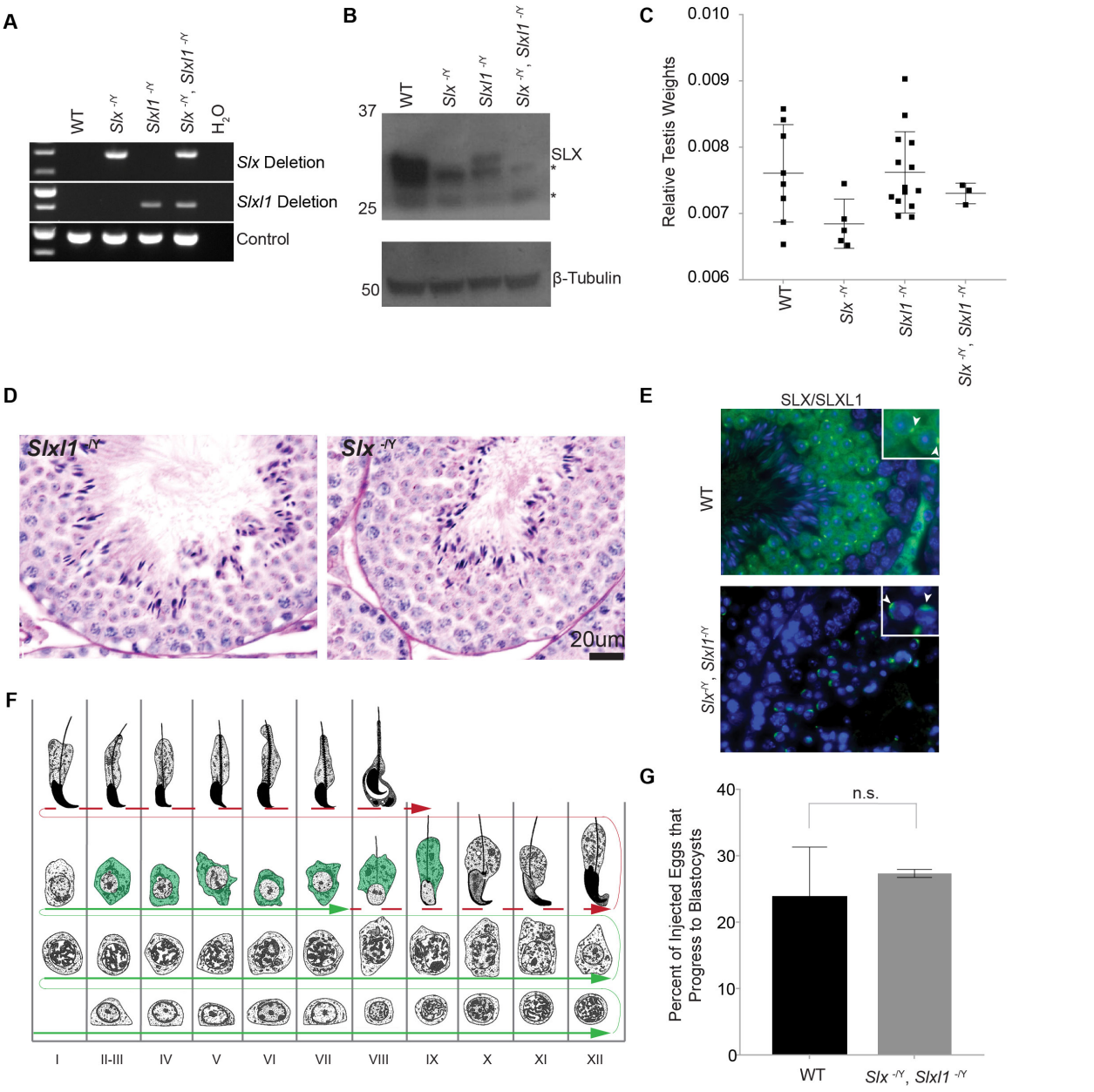

Figure 3-8. Validation and characterization of the precise and complete 5Mb and 2.3Mb deletions of the *Slx* and *Slxl1* ampliconic regions, respectively

A) Genotyping of wildtype (WT), *Slx*$^{-/Y}$, *Slxl1*$^{-/Y}$ or *Slx*$^{-/Y}$, *Slxl1*$^{-/Y}$ males for deletion of the *Slx* or *Slxl1* region, and a control region between the *Slx* and *Slxl1* ampliconic region (chrX:53988042-53988528. **B)** Western blot from wildtype, *Slx*$^{-/Y}$, *Slxl1*$^{-/Y}$ and *Slx*$^{-/Y}$, *Slxl1*$^{-/Y}$ whole testis lysate probing for SLX/SLXL1, using the antibody we generated, and β-tubulin. Detection of SLXL1 on a western blot is difficult, but works well in immunofluorescence and immunoprecipitation/mass spectrometry applications. * = non-specific bands. **C)** Relative testis weight of individual males (an individual bullet) normalized to total body weight (g/g), error bars denote standard deviation. T-test p-value *<0.05 as compared to WT. **D)** Periodic-acid Schiff testis histology from WT and Slx-/Y and Slxl1-/Y males. **E)** Immunofluorescence of SLX/SLXL1 (green) on DAPI stained testis histological sections from wild-type mice and mice lacking SLX/SLXL1 (*Slx*$^{-/Y}$, *Slxl1*$^{-/Y}$), where non-specific acrosome staining is detected (closed arrow). **F)** By histological characterization, spermatogenesis in Slx-/Y, Slxl1-/Y males develop without observable defects (green arrow) until stage 7/8 round spermatids. Development is then perturbed (red dashed arrow) (Figure 2E, F), correlating with the presence of SLX/SLXL1 protein (green cytoplasmic color). Image adapted from [174]. **G)** Round spermatid injection (ROSI) was performed using round spermatids from two WT and Slx-/Y, Slxl1-/Y males and injected into oocytes monitored for progression to the blastocyst stage (T-test, standard deviation).

Tables

Table 3-1. SLX/SLXL1 candidate interacting proteins identified across biological replicates

Bio. Rep. 1

Gene	Accession	Wildtype	*Slx* -/Y	*Slxl1* -/Y	*Slx* -/Y, *Slxl1* -/Y
Slx	Q5M8P2	97	0	96	0
Slxl1	A6X8J1	92	82	0	0
Slx	A6X8I0	89	0	84	0
Slx	Q4KL05	73	0	64	0
Slx	L7MUF1	69	0	59	0
Slx	D3Z7C4	8	0	5	0
Spin1	Q61142	15	17	11	0
Ssty2	J3QM67	10	3	5	0

Bio. Rep. 2

Gene	Accession	Wildtype	*Slx* -/Y	*Slxl1* -/Y	*Slx* -/Y, *Slxl1* -/Y
Slx	A6X8I0	121	0	93	0
Slx	B1B0R1	119	0	96	0
Slx	Q5M8P2	114	0	89	0
Slx	Q4KL05	100	0	81	0
Slx	L7MUF1	97	0	74	0
Slx	Q497S0	87	0	69	0
Slx	D3Z4U6	24	0	15	0
Slx	D3Z7C4	18	0	8	0
Slxl1	A6X8J1	87	73	0	0
Spin1	Q61142	15	13	10	0
Ssty2	Q5FWB5	11	4	7	0
Psmc1	P62192	7	5	3	0
Ssty1	A0A0A6YXW2	6	0	3	0
Psmd4	O35226-2	6	4	4	0

Bio. Rep. 3

Gene	Accession	Wildtype	*Slx* -/Y, *Slxl1* -/Y
Slxl1	A6X8J1	155	0
Slx	Q4KL05	116	0
Slx	L7MUF1	109	0
Slx	B1B0R1	107	0
Slx	A6X8I0	101	0
Cand1	Q6ZQ38	19	0
Eno1	P17182	16	0
Aldh2	P47738	15	0
Idh1	O88844	13	0
Fam117b	Q3U3E2	10	0
Ssty2	J3QM67	10	0
Ssty1	A0A0A6YXW2	9	0
Akr1b1	P45376	9	0
Nasp	B1AU75	9	0
Spin1	Q61142	7	0
Pfn1	P62962	7	0

Psmc1	P62192	6	0
Psmd4	O35226-2	6	0

Table 3-2. Supplemental Experimental Procedures

Oligos for Genotyping

Name	Sequence
Slx 5' F	AGACAACAGTCTAATCTCCAGTGC
Slx 5' R	AGAACTGCTGAATTCCATGGTC
Slx 3' F	GATTTACTGCAATAACATGGCAC
Slx 3' R	CAATGAATTACCTGGTCTGGAG
Slxl1 5' F	AGCAGGCTCCTTCATAGTGATC
Slxl1 5' R	TGGACAGGGAACAGACACTTAGTC
Slxl1 3' F	CTTGCTTTAACCCACATTCATC
Slxl1 3' R	TGAACTGATGACCCTTTAGAGC
Ube1XY_F	TGGATGGTGTGGCCAATG
Ube1XY_R	CACCTGCACGTTGCCCTT
E2A-Cre F	GCGGTCTGGCAGTAAAAACTATC
E2A-Cre R	GTGAAACAGCATTGCTGTCACTT
E2A-Cre ctrl F	CTAGGCCACAGAATTGAAAGATCT
E2A-Cre ctrl R	GTAGGTGGAAATTCTAGCATCATCC

Oligos for RT-PCR

Trim42 F	GAAGCATCGTCACCTCCTCT
Trim42 R	CTTCTCGCATAGGCTGTGGT
Slx_RT_F	AGTGATAATCGGCTCTGCTCA
Slx_RT_R	GCGGCATATTCTCATGTTTGC
Slxl1_RTqPCR_F	CCTGAAGAAATCGTTGGAGATA
Slxl1_RTqPCR_R	CCATATCAAACTTCTGAAATGTA

Oligos used to generate transgenic lines

Slx_5'donor	GTGATGCATTCTGTGACTAGCAACTGTGCAGGAGTCCATTATTTTGATAGTTGATGGATAA GCTTATAACTTCGTATAATGTATGCTATACGAAGTTATCCCTGGTGATGGCTGTGATGTGT GTTGTTGCTTGAGAATCTTTAAAAATTCAGGGTCCAT
Slx_3'donor	AGGGTCTCTCTGGCATAGATGCCCCTCAGCCCTTCTCTGTAGGCCTCGCAAACAAAGTAA TGTACATAACTTCGTATAATGTATGCTATACGAAGTTATGCTTGGAATCCATACTGCTACA GCCTAGGTCACTGACCAAGCCCCATTCAGGAGGCTTTT
Slxl1_5'donor	CAACAGATTGGTTCGCCTTCAGCTTCGTCTGCCTAAGAGAAAGATCAGAGGTAGGCTAGG ATCCATAACTTCGTATATAATGTATGCTATACGAAGTTATCGATCTGAGGTGGCGCTCACC TCAAAGCAGAATTT
Slxl1_3'donor	AACAGTTTTACCCAACAGTTTCTTTCCATTAGTACTGCTAAAAGTTCTTTAAATCCTCTTAT CGATAACTTCGTATAATGTTATGCTATACGAAGTTATCTTAAGTCTCCGCTGGTTTAAGAC AAGCATGCTGGAGCAGATCACATCCAGATTGATCTGGAAG
Slx/5' gRNA	TTGATAGTTGATGGATACCC
Slx/3' gRNA	CCTCGCAAACAAAGTAAGCT
Slxl1 5'gRNA	TGAGGTGAGCGCCACCTCAG
Slxl1 3'gRNA	CTTAAACCAGCGGAGACAAG

Chapter 4

Discussion and Future Directions

My studies explore the importance of palindrome structure and the functions of genes harbored within palindromes on the mouse X chromosome. First, genetic manipulations of two singleton palindromes (*Mageb5* and *4930567H17Rik*) reveals that these genes are not dosage sensitive and that palindromic orientation is not necessary for their post-meiotic expression or male fertility. Studies on the *Slx* and *Slxl1* large palindrome arrays reveal these genes are partially redundant and essential for male fertility and that *Slxl1* has a dose-dependent role influencing offspring sex ratio. Altogether, this work highlights the structural and functional diversity of palindrome-associated genes in the context of spermatogenesis, lays the groundwork for future explorations into these four palindrome-associated genes, and serves as an outline to study and characterize additional palindrome structure and gene biology.

Singleton Palindromes

Structure

With only a single duplication, singleton palindromes are more amenable to questions regarding the structural significance that palindrome arrays. However, given the lack of phenotypes associated single-copy deletions and inversions (tandem orientation), the structural significance of singleton palindromes remains unclear. Singleton palindromes might serve a role under certain environmental conditions or instead be reflective of a previous role that they no longer

serve but are retained due to the stability of palindromic duplications. Segmental duplications in tandem orientation are subject to non-allelic homologous recombination, which could contract the region down to a single copy. While palindromic duplications can result in isodicentric chromosomes, the presence of two centromeres complicates chromosome segregation and would likely prevent isodicentric chromosomes from being maintained in a population. Therefore, singleton palindromes are more stable over evolutionary time as compared to tandem duplications. The presence of two gene copies is also beneficial against inactivating mutations and it is known that singleton palindromes maintain a high level of sequence identity by gene conversion events, which homogenize variants between the duplications [14, 15, 175]. Whether gene conversion rates are dependent on the palindromic orientation versus tandem orientation of duplications remains unknown. Steric hindrance could prevent tandem duplications from pairing as efficiently. Singleton palindrome duplications are separated by an intervening sequence (spacer). In mouse, spacers range in size (3.7-99.8kb), but a majority are greater than 25 kb [176]. This large physical separation may be sufficient to enable tandem duplications to pair without steric hindrance, but has yet to be tested. This question cannot be evaluated from an evolutionary perspective, given the lack of singleton tandem duplications on the sex chromosomes. Instead, an *in vivo* sequencing based approach could be used to answer whether or not palindromic orientation facilitates higher rates of gene conversation. *Mageb5*^{InvArm} and *4930567H17Rik*^{InvArm} mice, contain tandem duplications with naturally existing sequence family variants (SFV) that distinguish the duplications. By sequencing, SFVs could be monitored for gene conversion events *in vivo*.

How palindrome-associated genes evade post-meiotic silencing remains unclear. Chromosome pairing during meiosis is thought be important for meiotic and post-meiotic expression [114, 117, 119]. The mammalian X and Y chromosomes only pair in the small pseudoautosomal region during meiosis and X- and Y-linked genes are transcriptionally repressed through a process known as meiotic sex chromosome inactivation (MSCI) [177]. While single copy genes on the sex chromosomes generally remain silenced in post-meiotic cells, palindrome-associated genes are expressed [7]. If palindrome arms underwent intra-chromosomal pairing, this does not explain the post-meiotic expression of palindrome-associated genes as *Mageb5*^{DelArm} and *4930567H17Rik*^{DelArm} mice still express their genes post-meiotically [176]. These findings suggest that post-meiotic palindromic gene expression is independent of structure and instead may be dependent on alterations in the chromatin state as well as specific transcription factors. Of note, RNF8 and SCML2 have been implicated in the regulation of post-meiotic sex-linked gene expression, through their regulation of H2AK119ub and H3K27ac [150, 178, 179]. Candidate transcription factors include Heat Shock Transcription Factor 1 and 2 (HSF1 and HSF2) [121, 122]. Based on CHIP-seq, HSF1 localizes to X and Y palindrome array genes, and HSF2 localizes to Y palindrome array genes [121, 122]. Examination of singleton palindromes for HSF1 and HSF2 binding motifs may support HSF1 and HSF2 regulation of singleton palindromes [180]. Alternatively, distinct transcription factors may regulate individual singleton palindrome genes potentially identifiable by motif analysis and reverse-ChIP approaches.

Gene Functions

Complete knockouts of *Mageb5* and *4930567H17Rik* can be generated through CRISPR/Cas9 targeting of the coding sequence to determine if these genes are essential for fertility. By

targeting protein-coding sequence in wildtype mice, the palindromic structure can be conserved and reduce the chance of any confounding effects such as the removal of regulatory regions contained within singleton palindromes.

Mageb5 is a member of a large family of genes characterized by the presence of a MAGE homology domain (MHD), testis expression and often ectopic expression in cancer [181]. Some MAGE proteins interact with E3 RING ubiquitin ligases and regulate the ubiquitination of protein targets [182]. Loss of Mage-a family members (*Magea 1-3, 5, 6, 8)* causes disruptions to the apoptotic pathway within the testis [181]. In mouse, *Mageb5* shares >65% sequence identity with other X-linked family members and may have a non-redundant function, but MAGEB5 interaction partners have not been identified [182].

4930567H17Rik is annotated as a single exon, long non-coding gene. However, 4930567H17Rik appears to have a functional open reading frame and both copies of the gene are expressed [7]. The lack of protein domains makes it difficult to predict its biological function.

Though the presence of two gene copies is beneficial against inactivating mutations, it is unclear why singleton palindromes initially arose. Even if singleton-palindrome genes (*Mageb5, 4930567H17Rik,* etc.) are found to be essential, this fails to explain their duplicated state as many essential X- and Y- linked genes are present as a single copy (e.g. X-linked *Ar* and Y-linked *Sry*). In the *Slxl1* and *Sly* palindrome arrays, copy number and corresponding gene expression levels are thought to underlie X-Y conflict (meiotic drive) [109]. Are singleton palindromes remnants of a previous X-Y conflict or are they duplicated in response to X-Y

conflict? If conflict is neutralized the selective pressures to maintain high copy numbers is relaxed and non-allelic homologous recombination could contract palindrome arrays into singleton palindromes. This is a difficult idea to test, but high confidence assemblies of sex chromosomes in related species may provide clues. Alternatively, the significance of singleton palindromes can also be explored by identifying a *Mus* sub-species with a unique singleton palindrome, one that is single-copy, or absent, in the reference genome. If singleton palindromes are involved in meiotic drive, it is possible that by introducing them into a naïve system, in this case the reference genome strain C57BL/6J, which has not evolved repressors, meiotic drive could be reinstated. Similar approaches have been used in both yeast and female centromeric drive in mice through the creation of hybrids [28, 30-33, 93, 95-97]. This would build support for the idea that singleton palindromes are involved in sex chromosome meiotic drive and provide a model to study the molecular functions of the protein in the absence of a complex regulatory network of drive suppressors and enhancers.

Palindrome Arrays

Infertility phenotype

Slx and *Slxl1* are partially redundant and essential for male fertility [109]. Defects in spermatogenic development in $Slx^{-/Y}$, $Slxl1^{-/Y}$ males coincide with *Slx* and *Slxl1* expression in post-meiotic round spermatids. However, it is unknown what cellular defect causes infertility [109]. For example, 990 genes are misregulated in $Slx^{-/Y}$, $Slxl1^{-/Y}$ round spermatids, but whether dysregulation of those genes is causal or the byproduct of upstream defects is unknown. Round spermatids undergo extensive nuclear repackaging and cytoplasmic alterations defined morphologically by round spermatid sub-stages (S1-12) [183]. FACS sorting can isolate round

spermatids, but it does not enable sub-stage resolution. Single-cell sequencing has enabled round spermatids sub-stages S1-S8 to be transcriptionally defined [183]. Single cell sequencing of round spermatids from *Slx*$^{-/Y}$, *Slxl1*$^{-/Y}$ males could be performed to identify the sub-stage where *Slx*$^{-/Y}$, *Slxl1*$^{-/Y}$ males transcriptionally deviate from wildtype males. Given the morphological abnormalities identified at stage 7, I would anticipate single-cell sequencing to reveal gross gene dysregulation at or before the corresponding round spermatid sub-stage (S7) in *Slx*$^{-/Y}$, *Slxl1*$^{-/Y}$ males [109, 183]. Single cell sequencing may reveal earlier defects, which ultimately manifest morphologically at a later stage. These insights would enable a more targeted approach to investigate the mechanism of *Slx*$^{-/Y}$, *Slxl1*$^{-/Y}$ male infertility through the identification of the earliest dysregulated genes. These dysregulated genes might be targets of chromatin readers SPIN1, SSTY1 and SSTY2, which are though to interact with SLX and SLXL1.

Meiotic Drive

I proposed an evolutionary model for *Slxl1* versus *Sly* meiotic drive, highlighting the importance of *Slxl1* to *Sly* copy number [109]. In existing models of male meiotic drive (target-killer and poison-antidote), the molecular components of a drive system can be a DNA sequence, RNA and/or protein. While sex ratio can be modulated by increasing or decreasing the copy number of the *Slxl1* DNA sequence, *Slx/Slxl1* knockdown and *Slxl1* knockout studies implicate mRNA and/or protein as the molecular component important to *Slxl1* versus *Sly* meiotic drive [18, 109]. Notably, male biased litters are dependent on alterations in the *Slxl1* mRNA/protein (knockdown and knockout), irrespective of the presence of the *Slxl1* repeat unit (present in knockdown, absent in knockout models) [20, 109]. Similarly, female biased litters occur upon loss of *Sly* mRNA/protein, irrespective to the presence of the *Sly* repeat unit [19]. Notably, *Slxl1* versus *Sly*

meiotic drive does not fit under the target-killer or poison-antidote models. In the subsequent paragraphs, I outline five questions based upon the existing model of *Slxl1* versus *Sly* meiotic drive which serve to help elucidate the mechanism of *Slxl1* versus *Sly* meiotic drive.

What are the molecular and biological differences between X- and Y-bearing sperm?

Given that *Slxl1*$^{-/Y}$ males produce equal numbers of X- and Y-bearing sperm, molecular and phenotypic differences between X- and Y-bearing sperm must underlie *Slxl1* versus *Sly* meiotic drive [109]. X- and Y-bearing sperm may exhibit differences in their motility that can be assessed through a swim-up assay followed by X versus Y DNA-FISH. There may also be differences in the ability of X- versus Y-bearing sperm to navigate to an egg. Sperm that successfully swim to the cumulus cells surrounding the egg can be obtained and the relative ratio of X- and Y-bearing cells can be determined by DNA-FISH. If the cumulus cells are surrounded by equal numbers of X- and Y-bearing sperm, then X- and Y-bearing sperm may exhibit differences in their ability to penetrate the zona pellucida. Differences in sperm interactions with the zona pellucida can be further assessed via *in vitro* fertilization experiments.

Does Slxl1 versus Sly meiotic drive act intracellularly or intercellularly?

While SLXL1 protein is present in X- and Y-bearing round spermatids, it is unclear whether SLXL1 and SLY function specifically within the cell they are encoded by (intracellular, *e.g.*, *Slxl1* functioning in X-bearing) or if they act specifically in cells bearing the opposing sex chromosome (intercellular, *e.g.*, *Slxl1* functioning in Y-bearing). Both the target-killer and poison-antidote models of male meiotic drive necessitate the sharing of mRNA/protein through cytoplasmic bridges (intercellular). The poison-antidote model also necessitates that certain

molecules are not shared (intracellular). By understanding where SLXL1 functions, we can begin to understand the mechanism of *Slxl1* versus *Sly* meiotic drive. If *Slxl1* mRNA/protein acted intracellularly to benefit the cell it was encoded by, it would be expected that X-bearing spermatids with higher copy number of *Slxl1* would be preferentially segregated (Figure 4-1A). Alternatively, if *Slxl1* acted intercellularly to impair Y-bearing cells, Y-bearing cells receiving more *Slxl1* mRNA/protein would experience a greater impact on fitness and the fitness of X-bearing cells would remain the same regardless of *Slxl1* copy number (Figure 4-1A). *Slxl1* copy number can vary within an individual male via non-allelic homologous recombination (Figure 4-1A), however measuring such copy number changes in individual sperm is challenging. Instead, I describe three sets of experiments to assess whether SLXL1 function intracellularly or intercellularly.

Experiment #1: A sperm competition assay can be used to explore if *Slxl1* acts intercellularly or intracellularly (Figure 4-1A, B). Specifically, equal amounts of sperm from a $Slxl1^{-/Y}$ male and a $Slx^{dup/Y}$, $Slxl1^{dup/Y}$ male would be mixed and used to perform in vitro fertilization (IVF) (Figure 4-1B). Like natural matings, sex ratio distortion is detectable by IVF [184]. Resulting blastocysts would be screened by PCR to identify female blastocysts (XX) and to distinguish between fertilization by sperm with a $Slxl1^{-}$ or Slx^{dup}, $Slxl1^{dup}$ X chromosome. The expectation is that if *Slxl1* acts intracellularly, female blastocysts would be preferentially fertilized by sperm with Slx^{dup}, $Slxl1^{dup}$ X chromosomes (Figure 4-1B). In contrast, if *Slxl1* acts intercellularly female blastocysts would be fertilized by sperm with a Slx^{dup}, $Slxl1^{dup}$ or a $Slxl1^{-}$ X chromosome equally (Figure 4-1B). Ideally, analogous studies would be conducted with sperm with differing *Sly*

copies, but existing *Sly* mouse models are not amenable to the PCR-based screening approaches needed to distinguish Y-chromosomes with differing *Sly* copy number.

Experiment #2: To further test the intracellular versus intercellular function of *Sly* involves generating a mouse expressing *Sly* from the X chromosome. If *Sly* acts intercellularly in X-bearing round spermatids, expression from the X chromosome should exacerbate sex ratio distortion.

Experiment #3: To assess the intracellular vs intercellular functions would involve ablating round spermatid cytoplasmic bridges to prevent gene product sharing and assessing the resulting offspring sex ratio from different male genotypes (ex. wildtype or $Slx^{dup/Y}$, $Slxl1^{dup/Y}$). TEX14 is necessary for cytoplasmic bridges and post-meiotic conditional knockouts could be generated using a *Prm1*- or *Stra8*-Cre LoxP based strategy [185]. If SLXL1 functions intracellularly, the ablation of cytoplasmic bridges should have no impact on sex ratio distortion in $Slx^{dup/Y}$, $Slxl1^{dup/Y}$ males. This approach may have unintended effects leading to inviability of spermatids, because the sharing of some X- and Y-linked gene products may be necessary.

Does intra-germline competition exist between an individual males X-bearing sperm?

While *Slxl1* and *Sly* were massively segmentally duplicated, it remains unclear whether increases in gene dosage was selected for solely at the population level or if competition between an individual male's X-bearing sperm contributed to the expansion of *Slxl1*. In addition to providing insight on the intracellular vs intercellular functions of SLXL1, the sperm competition assays can also provide insights on this question. Specifically, understanding whether or not competition

between X-bearing sperm from a single male contributed to *Slxl1* copy number expansion over evolutionary time, and similarly competition between Y-bearing sperm contributing to *Sly* copy number expansion (Figure 4-1A, C). If *Slxl1* functions intracellularly, X-bearing sperm within a given male would be competing based upon their *Slxl1* copy number which could vary as a result of non-allelic homologous recombination (*Slxl1*$^{\text{high copy}}$ versus *Slxl1*$^{\text{low copy}}$ sperm competition) (Figure 4-1A, C). In contrast, if *Slxl1* functions in Y-bearing sperm, selection would not occur between X-bearing sperm as X-bearing sperm (*Slxl1*$^{\text{high copy}}$ and *Slxl1*$^{\text{low copy}}$) benefit collectively from the reduced fitness of Y-bearing sperm (X vs Y sperm competition) (Figure 4-1 A, C). Within the population, males with higher *Slxl1* copy number (*Slxl1* $^{\textit{Extremely high copy}}$) could exhibit a more severe female to male offspring sex ratio than wildtype or even moderate distorters (Figure 4-1C). Because these males contribute an excess of females to the population, *Slxl1* $^{\textit{Extremely high copy}}$ increases in allele frequency within the population (Figure 4-1C). Therefore, regardless if *Slxl1* functions intracellularly or intercellularly, competition between males (population level) would contribute to *Slxl1* copy number expansion. *Slxl1* functioning intracellularly would therefore provide an additional level of selection within the germline between *Slxl1*$^{\text{high copy}}$ and *Slxl1*$^{\text{low copy}}$ alleles (X vs X competition).

What biological pathways are impacted in X- and Y-bearing sperm to cause meiotic drive?

Further insights into the molecular mechanisms can be gained by exploring the functions and contributions of SLXL1 and SLY interacting proteins. It is important to validate the identified candidate proteins: SPIN1, SSTY2, PSMC1, SSTY1 and PSMD4 (Table 3-4A) [109]. The spindlin proteins, SPIN1 and SSTY1/2, are currently the top interaction candidates. The 26S proteasome is present in the acrosome, a structure with non-specific SLX/SLXL1 antibody

staining, suggesting that 26S proteasome components PSMC1 and PSMD4 are nonspecific [109, 186]. SSTY1/2 have been shown previously to interact with SLY, SLX and SLXL1 [110]. Since SLX/SLXL1 co-IP/MS experiments did not identify SLY as an interactor, it is anticipated that SLXL1 and SLY compete for the same binding sites of SSTY1/2 rather than form a large protein complex [109]. Validation of these interactions could be performed using a yeast 2-hybrid approach. A yeast-2 hybrid approach would also help to determine if SLXL1 and SLY compete for SSTY1, SSTY2 and SPIN1. Utilizing Takara's (Clontech) two-plasmid system (pBridge and pGADT7 AD), the pBridge vector can express a competitor protein under an inducible promoter. For example, *Slxl1* can be fused into the DNA binding domain (*Slxl1-BD)* and *Ssty1* fused to the activating domain (*Ssty1-AD).* If SLXL1 and SSTY1 interact, the DNA binding domain and activating domain will unite and the assay will screen positive (*e.g., lacZ* signal). If SLY competes for interactions with SSTY1, then inducing expression of SLY would be expected to cause a reduction in *lacZ* signal.

Functionally, SPIN1, SSTY1 and SSTY2 are implicated in chromatin regulation. SPIN1 binds H3K4me3-R8me2a and SSTY1/2 localize to the sex chromosomes [110, 149]. By immunofluorescence, SSTY1/2 are also present in the cytoplasm of round spermatids, perhaps interacting with cytoplasmic SLX and SLXL1 [110]. Competition between cytoplasmic SLX/SLXL1 and nuclear SLY for these chromatin regulators could result in transcriptional changes. Specifically, gene duplications would alter the stoichiometry (SLXL1 versus SLY) and consequently the localization of the chromatin regulators, SSTY1/2 and SPIN1. Misregulation of X- and Y-linked genes would be expected if transcriptomic changes underlie meiotic drive. An isoform of X-linked *Scml2* is significantly downregulated in $Slxl1^{-/Y}$ round spermatids. As *Scml2*

is thought to play a critical role in the reactivation of the sex chromosomes following MSCI, it would be anticipated that a reduction in *Scml2* would cause downregulation of other X- and Y-linked genes [150, 178, 179]. Yet, *Scml2* was the only sex-linked gene found to be misregulated in *Slxl1*$^{-/Y}$ round spermatids other than *Slxl1* itself [109]. These observations indicate *Scml2* reduction may not functionally contribute to the meiotic drive phenotype. This isoform of *Scml2* may have distinct functions. Alternatively, autosomal genes which function intracellularly may be differentially altered in X- and Y-bearing round spermatids and underlie the meiotic drive phenotype. FACS sorting based upon DNA content could isolate X- and Y-bearing round spermatids populations for RNA-sequencing and provide insights into autosomal transcriptional alterations that may contribute to the meiotic drive phenotype.

Is Slxl1 versus Sly meiotic drive an independent meiotic drive system or has it been incorporated into an ancestral meiotic drive system?

It is interesting that two X-Y co-amplified gene families, *Slx/Slxl1/Sly* and *Ssty1/Ssty2/Sstx*, appear to interact at the protein level. Perhaps *Ssty1* and *Ssty2* are components of an older meiotic drive system which *Slxl1* and *Sly* have integrated into [21, 109]. Due to the interspersed nature of Y chromosome palindrome array genes, a knockout approach analogous to the one taken with *Slx* and *Slxl1* cannot be performed. Instead, knockdown models of *Ssty1* and *Ssty2* would be needed to explore the roles of these genes in fertility and meiotic drive. If *Ssty1/2* knockdown mice exhibit sex ratio distortion, it would suggest that *Slxl1, Sly, Ssty1* and *Ssty2* are all components of a more complex meiotic drive system. As such, it would be anticipated that altering *Ssty1/2* gene expression could modulate the meiotic drive phenotype in different backgrounds (*Slxl1*$^{-/Y}$ or *Slx*^{dup}, *Slxl1*^{dup}). Future studies could then explore what genes are the

primary mediators of drive and which are enhancers or suppressors. Given that *Ssty1/2* were duplicated before *Slxl1* and *Sly, Ssty1/2* are likely to be the primary mediator of drive with *Slxl1* and *Sly* evolving as regulators.

It remains unclear whether the infertility phenotypes ($Slx^{-/Y}$, $Slxl1^{-/Y}$; MSY deletions encompassing *Sly, Ssty1, Ssty2* and *Laidy*) are truly reflective of an essential function or if they are the outcome of a sperm-killing based meiotic drive system which has teetered to an extreme, killing all sperm regardless of genotype. While challenging, reconstructing *Slxl1* versus *Sly* drive in a mouse lacking the entire gene family could provide insight. The expectation is that if the infertility phenotype arises from *Slxl1* versus *Sly* meiotic drive, removal of the entire family should result in wildtype fertility. Under the current model, *Slx* copy number expansion is peculiar as *Slx* does not appear to play a role in meiotic drive. If *Slxl1* and *Slx* play an essential function outside of drive, which could explain the infertility phenotype in $Slx^{-/Y}$, $Slxl1^{-/Y}$, selection for *Slx* copy number expansion may serve to ensure that essential process occurs while SLXL1 is sequestered away functioning in meiotic drive.

Conclusion

More generally, this thesis speaks to the broader question of male germ cell equivalency. Though, the prevailing view is that cytoplasmic bridges enable X- versus Y-bearing round spermatids and sperm to be phenotypically equivalent, a lack of equivalency has been shown to exist for a handful of proteins, and this lack of equivalency is fundamental to the evolution of a meiotic drive system like *Slxl1* versus *Sly* [60, 62, 63, 187]. A more comprehensive understanding of X- versus Y-round spermatid RNA and protein composition may reveal

important mechanisms governing proper post-meiotic development as well as substrates involved in meiotic drive.

For nearly a century, the X and Y chromosome have been implicated in the striking observation that when two related species mate, the heterogametic sex (XY or ZW) tends to be absent, rare or infertile, known as Haldane's rule [188]. More recently, the term "large-X effect" was coined to describe the disproportionately large role X chromosome genes play in infertility and speciation [189-192]. Supported by the finding that *Slx* and *Slxl1* are essential for fertility, palindrome-associated genes will likely prove to be a fruitful source of genes underlying these observations as palindrome-associated genes are rapidly evolving at the sequence level—a hallmark of genes involved in infertility and speciation.

Figure

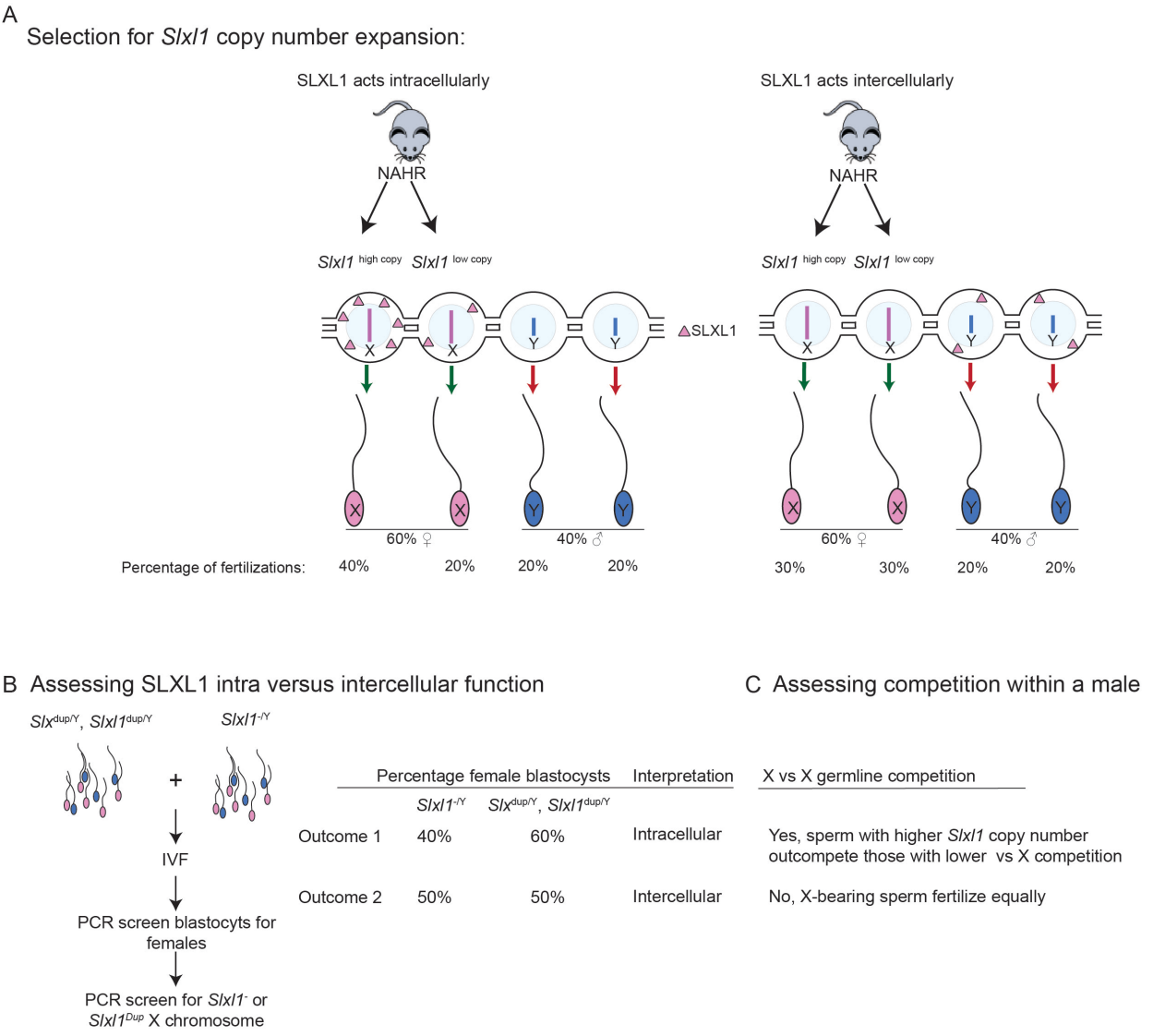

Figure 4-1. Evaluating if SLXL1 functions intracellular or intercellular and the impact on germline competition

A) Within a given male, non-allelic homologous recombination (NAHR) between sister chromatid *Slxl1* duplications could produce X chromosomes with greater (*Slxl1*$^{high\ copy}$) and fewer (*Slxl1*$^{low\ copy}$) gene copies of *Slxl1*. If *Slxl1* functions intracellularly, sperm with greater gene copies of *Slxl1* preferentially segregate over those with fewer (left panel), as SLXL1 protein is beneficial within X-bearing cells. If *Slxl1* functions intercellularly to disrupt Y-bearing sperm, X-bearing sperm with high and low copy number of *Slxl1* have the same capacity to fertilize (right panel). The bias towards female offspring is reflective of the fitness differential between X versus Y sperm. **B)** *Slxl1*$^{-/Y}$ versus *Slx*^{Dup}, *Slxl1*^{Dup} sperm competition to test the intra vs intercellular function of SLXL1 and assess in X versus X competition amongst sperm. **C)** Evaluation of X versus X sperm competition within the germline.

Bibliography

1. Rice, W.R. (1984). Sex Chromosomes and the Evolution of Sexual Dimorphism. Evolution *38*, 735-742.
2. Wang, P.J., McCarrey, J.R., Yang, F., and Page, D.C. (2001). An abundance of X-linked genes expressed in spermatogonia. Nat Genet *27*, 422-426.
3. Reinke, V. (2004). Sex and the genome. Nat Genet *36*, 548-549.
4. Khil, P.P., Smirnova, N.A., Romanienko, P.J., and Camerini-Otero, R.D. (2004). The mouse X chromosome is enriched for sex-biased genes not subject to selection by meiotic sex chromosome inactivation. Nat Genet *36*, 642-646.
5. Charlesworth, B., Coyne, J.A., and Barton, N.H. (1987). The Relative Rates of Evolution of Sex Chromosomes and Autosomes. The University of Chicago Press for The American Society of Naturalists *130*, 112-146.
6. Hu, Y.C., and Namekawa, S.H. (2015). Functional significance of the sex chromosomes during spermatogenesis. Reproduction *149*, R265-277.
7. Mueller, J.L., Mahadevaiah, S.K., Park, P.J., Warburton, P.E., Page, D.C., and Turner, J.M. (2008). The mouse X chromosome is enriched for multicopy testis genes showing postmeiotic expression. Nat Genet *40*, 794-799.
8. Mueller, J.L., Skaletsky, H., Brown, L.G., Zaghlul, S., Rock, S., Graves, T., Auger, K., Warren, W.C., Wilson, R.K., and Page, D.C. (2013). Independent specialization of the human and mouse X chromosomes for the male germ line. Nat Genet *45*, 1083-1087.
9. Soh, Y.Q., Alfoldi, J., Pyntikova, T., Brown, L.G., Graves, T., Minx, P.J., Fulton, R.S., Kremitzki, C., Koutseva, N., Mueller, J.L., et al. (2014). Sequencing the mouse Y chromosome reveals convergent gene acquisition and amplification on both sex chromosomes. Cell *159*, 800-813.
10. Treangen, T.J., and Salzberg, S.L. (2011). Repetitive DNA and next-generation sequencing: computational challenges and solutions. Nat Rev Genet *13*, 36-46.
11. Hughes, J.F., and Rozen, S. (2012). Genomics and genetics of human and primate y chromosomes. Annu Rev Genomics Hum Genet *13*, 83-108.
12. Vollger, M.R., Dishuck, P.C., Sorensen, M., Welch, A.E., Dang, V., Dougherty, M.L., Graves-Lindsay, T.A., Wilson, R.K., Chaisson, M.J.P., and Eichler, E.E. (2019). Long-read sequence and assembly of segmental duplications. Nat Methods *16*, 88-94.
13. Bellott, D.W., Skaletsky, H., Cho, T.J., Brown, L., Locke, D., Chen, N., Galkina, S., Pyntikova, T., Koutseva, N., Graves, T., et al. (2017). Avian W and mammalian Y chromosomes convergently retained dosage-sensitive regulators. Nat Genet *49*, 387-394.
14. Rozen, S., Skaletsky, H., Marszalek, J.D., Minx, P.J., Cordum, H.S., Waterston, R.H., Wilson, R.K., and Page, D.C. (2003). Abundant gene conversion between arms of palindromes in human and ape Y chromosomes. Nature *423*, 873-876.
15. Swanepoel, C.M., Gerlinger, E.R., and Mueller, J.L. (2020). Large X-linked palindromes undergo arm-to-arm gene conversion across Mus lineages. Mol Biol Evol.

16. Kuroda-Kawaguchi, T., Skaletsky, H., Brown, L.G., Minx, P.J., Cordum, H.S., Waterston, R.H., Wilson, R.K., Silber, S., Oates, R., Rozen, S., et al. (2001). The AZFc region of the Y chromosome features massive palindromes and uniform recurrent deletions in infertile men. Nat Genet *29*, 279-286.
17. Vogt, P.H., Edelmann, A., Kirsch, S., Henegariu, O., Hirschmann, P., Kiesewetter, F., Kohn, F.M., Schill, W.B., Farah, S., Ramos, C., et al. (1996). Human Y chromosome azoospermia factors (AZF) mapped to different subregions in Yq11. Hum Mol Genet *5*, 933-943.
18. Cocquet, J., Ellis, P.J., Mahadevaiah, S.K., Affara, N.A., Vaiman, D., and Burgoyne, P.S. (2012). A genetic basis for a postmeiotic X versus Y chromosome intragenomic conflict in the mouse. PLoS Genet *8*, e1002900.
19. Cocquet, J., Ellis, P.J., Yamauchi, Y., Mahadevaiah, S.K., Affara, N.A., Ward, M.A., and Burgoyne, P.S. (2009). The multicopy gene Sly represses the sex chromosomes in the male mouse germline after meiosis. PLoS Biol *7*, e1000244.
20. Cocquet, J., Ellis, P.J., Yamauchi, Y., Riel, J.M., Karacs, T.P., Rattigan, A., Ojarikre, O.A., Affara, N.A., Ward, M.A., and Burgoyne, P.S. (2010). Deficiency in the multicopy Sycp3-like X-linked genes Slx and Slxl1 causes major defects in spermatid differentiation. Mol Biol Cell *21*, 3497-3505.
21. Ellis, P.J., Bacon, J., and Affara, N.A. (2011). Association of Sly with sex-linked gene amplification during mouse evolution: a side effect of genomic conflict in spermatids? Hum Mol Genet *20*, 3010-3021.
22. Hurst, G.D., and Werren, J.H. (2001). The role of selfish genetic elements in eukaryotic evolution. Nat Rev Genet *2*, 597-606.
23. Werren, J.H. (2011). Selfish genetic elements, genetic conflict, and evolutionary innovation. Proceedings of the National Academy of Sciences of the United States of America *108 Suppl 2*, 10863-10870.
24. Agren, J.A., and Clark, A.G. (2018). Selfish genetic elements. PLoS Genet *14*, e1007700.
25. Helleu, Q., Gerard, P.R., and Montchamp-Moreau, C. (2014). Sex chromosome drive. Cold Spring Harb Perspect Biol *7*, a017616.
26. Courret, C., Chang, C.H., Wei, K.H., Montchamp-Moreau, C., and Larracuente, A.M. (2019). Meiotic drive mechanisms: lessons from Drosophila. Proc Biol Sci *286*, 20191430.
27. Lyttle, T.W. (1991). Segregation distorters. Annu Rev Genet *25*, 511-557.
28. Bravo Nunez, M.A., Nuckolls, N.L., and Zanders, S.E. (2018). Genetic Villains: Killer Meiotic Drivers. Trends Genet *34*, 424-433.
29. Schuh, M., and Ellenberg, J. (2008). A new model for asymmetric spindle positioning in mouse oocytes. Curr Biol *18*, 1986-1992.
30. Akera, T., Chmatal, L., Trimm, E., Yang, K., Aonbangkhen, C., Chenoweth, D.M., Janke, C., Schultz, R.M., and Lampson, M.A. (2017). Spindle asymmetry drives non-Mendelian chromosome segregation. Science *358*, 668-672.
31. Wu, T., Lane, S.I.R., Morgan, S.L., and Jones, K.T. (2018). Spindle tubulin and MTOC asymmetries may explain meiotic drive in oocytes. Nature communications *9*, 2952.
32. Chmatal, L., Gabriel, S.I., Mitsainas, G.P., Martinez-Vargas, J., Ventura, J., Searle, J.B., Schultz, R.M., and Lampson, M.A. (2014). Centromere strength provides the cell biological basis for meiotic drive and karyotype evolution in mice. Curr Biol *24*, 2295-2300.

33. Iwata-Otsubo, A., Dawicki-McKenna, J.M., Akera, T., Falk, S.J., Chmatal, L., Yang, K., Sullivan, B.A., Schultz, R.M., Lampson, M.A., and Black, B.E. (2017). Expanded Satellite Repeats Amplify a Discrete CENP-A Nucleosome Assembly Site on Chromosomes that Drive in Female Meiosis. Curr Biol *27*, 2365-2373 e2368.
34. Wei, K.H., Reddy, H.M., Rathnam, C., Lee, J., Lin, D., Ji, S., Mason, J.M., Clark, A.G., and Barbash, D.A. (2017). A Pooled Sequencing Approach Identifies a Candidate Meiotic Driver in Drosophila. Genetics *206*, 451-465.
35. Fishman, L., and Saunders, A. (2008). Centromere-associated female meiotic drive entails male fitness costs in monkeyflowers. Science *322*, 1559-1562.
36. Fishman, L., and Willis, J.H. (2005). A novel meiotic drive locus almost completely distorts segregation in mimulus (monkeyflower) hybrids. Genetics *169*, 347-353.
37. Buckler, E.S.t., Phelps-Durr, T.L., Buckler, C.S., Dawe, R.K., Doebley, J.F., and Holtsford, T.P. (1999). Meiotic drive of chromosomal knobs reshaped the maize genome. Genetics *153*, 415-426.
38. Dawe, R.K., Lowry, E.G., Gent, J.I., Stitzer, M.C., Swentowsky, K.W., Higgins, D.M., Ross-Ibarra, J., Wallace, J.G., Kanizay, L.B., Alabady, M., et al. (2018). A Kinesin-14 Motor Activates Neocentromeres to Promote Meiotic Drive in Maize. Cell *173*, 839-850 e818.
39. Dawe, R.K., Reed, L.M., Yu, H.G., Muszynski, M.G., and Hiatt, E.N. (1999). A maize homolog of mammalian CENPC is a constitutive component of the inner kinetochore. Plant Cell *11*, 1227-1238.
40. Yu, H.G., Hiatt, E.N., Chan, A., Sweeney, M., and Dawe, R.K. (1997). Neocentromere-mediated chromosome movement in maize. The Journal of cell biology *139*, 831-840.
41. Akera, T., Trimm, E., and Lampson, M.A. (2019). Molecular Strategies of Meiotic Cheating by Selfish Centromeres. Cell *178*, 1132-1144 e1110.
42. Sirajuddin, M., Rice, L.M., and Vale, R.D. (2014). Regulation of microtubule motors by tubulin isotypes and post-translational modifications. Nature cell biology *16*, 335-344.
43. Jain, M., Olsen, H.E., Turner, D.J., Stoddart, D., Bulazel, K.V., Paten, B., Haussler, D., Willard, H.F., Akeson, M., and Miga, K.H. (2018). Linear assembly of a human centromere on the Y chromosome. Nat Biotechnol *36*, 321-323.
44. Langley, S.A., Miga, K.H., Karpen, G.H., and Langley, C.H. (2019). Haplotypes spanning centromeric regions reveal persistence of large blocks of archaic DNA. Elife *8*.
45. Didion, J.P., Morgan, A.P., Clayshulte, A.M., McMullan, R.C., Yadgary, L., Petkov, P.M., Bell, T.A., Gatti, D.M., Crowley, J.J., Hua, K., et al. (2015). A multi-megabase copy number gain causes maternal transmission ratio distortion on mouse chromosome 2. PLoS Genet *11*, e1004850.
46. Didion, J.P., Morgan, A.P., Yadgary, L., Bell, T.A., McMullan, R.C., Ortiz de Solorzano, L., Britton-Davidian, J., Bult, C.J., Campbell, K.J., Castiglia, R., et al. (2016). R2d2 Drives Selfish Sweeps in the House Mouse. Mol Biol Evol *33*, 1381-1395.
47. Agulnik, S.I., Agulnik, A.I., and Ruvinsky, A.O. (1990). Meiotic drive in female mice heterozygous for the HSR inserts on chromosome 1. Genet Res *55*, 97-100.
48. Pardo-Manual de Villena, F., Slamka, C., Fonseca, M., Naumova, A.K., Paquette, J., Pannunzio, P., Smith, M., Verner, A., Morgan, K., and Sapienza, C. (1996). Transmission-ratio distortion through F1 females at chromosome 11 loci linked to Om in the mouse DDK syndrome. Genetics *142*, 1299-1304.

49. Pardo-Manuel de Villena, F., Naumova, A.K., Verner, A.E., Jin, W.H., and Sapienza, C. (1997). Confirmation of maternal transmission ratio distortion at Om and direct evidence that the maternal and paternal "DDK syndrome" genes are linked. Mamm Genome *8*, 642-646.
50. Yang, J., Zhao, X., Cheng, K., Du, H., Ouyang, Y., Chen, J., Qiu, S., Huang, J., Jiang, Y., Jiang, L., et al. (2012). A killer-protector system regulates both hybrid sterility and segregation distortion in rice. Science *337*, 1336-1340.
51. Chen, J., Ding, J., Ouyang, Y., Du, H., Yang, J., Cheng, K., Zhao, J., Qiu, S., Zhang, X., Yao, J., et al. (2008). A triallelic system of S5 is a major regulator of the reproductive barrier and compatibility of indica-japonica hybrids in rice. Proceedings of the National Academy of Sciences of the United States of America *105*, 11436-11441.
52. Rhoades, M.M., and Dempsey, E. (1957). Further studies on preferential segregation. Maize Genet. Coop. In Maize Genetics Cooperation Newsletter, Volume 31.
53. Kanizay, L.B., Albert, P.S., Birchler, J.A., and Dawe, R.K. (2013). Intragenomic conflict between the two major knob repeats of maize. Genetics *194*, 81-89.
54. Hiatt, E.N., Kentner, E.K., and Dawe, R.K. (2002). Independently regulated neocentromere activity of two classes of tandem repeat arrays. Plant Cell *14*, 407-420.
55. Morales, C.R., Lefrancois, S., Chennathukuzhi, V., El-Alfy, M., Wu, X., Yang, J., Gerton, G.L., and Hecht, N.B. (2002). A TB-RBP and Ter ATPase complex accompanies specific mRNAs from nuclei through the nuclear pores and into intercellular bridges in mouse male germ cells. Dev Biol *246*, 480-494.
56. Braun, R.E., Behringer, R.R., Peschon, J.J., Brinster, R.L., and Palmiter, R.D. (1989). Genetically haploid spermatids are phenotypically diploid. Nature *337*, 373-376.
57. Ventela, S., Toppari, J., and Parvinen, M. (2003). Intercellular organelle traffic through cytoplasmic bridges in early spermatids of the rat: mechanisms of haploid gene product sharing. Mol Biol Cell *14*, 2768-2780.
58. Fawcett, D.W., Ito, S., and Slautterback, D. (1959). The occurrence of intercellular bridges in groups of cells exhibiting synchronous differentiation. J Biophys Biochem Cytol *5*, 453-460.
59. Caldwell, K.A., and Handel, M.A. (1991). Protamine transcript sharing among postmeiotic spermatids. Proceedings of the National Academy of Sciences of the United States of America *88*, 2407-2411.
60. Umehara, T., Tsujita, N., and Shimada, M. (2019). Activation of Toll-like receptor 7/8 encoded by the X chromosome alters sperm motility and provides a novel simple technology for sexing sperm. PLoS Biol *17*, e3000398.
61. Zheng, Y., Deng, X., and Martin-DeLeon, P.A. (2001). Lack of sharing of Spam1 (Ph-20) among mouse spermatids and transmission ratio distortion. Biol Reprod *64*, 1730-1738.
62. Veron, N., Bauer, H., Weisse, A.Y., Luder, G., Werber, M., and Herrmann, B.G. (2009). Retention of gene products in syncytial spermatids promotes non-Mendelian inheritance as revealed by the t complex responder. Genes Dev *23*, 2705-2710.
63. Butler, A., Gordon, R.E., Gatt, S., and Schuchman, E.H. (2007). Sperm abnormalities in heterozygous acid sphingomyelinase knockout mice reveal a novel approach for the prevention of genetic diseases. Am J Pathol *170*, 2077-2088.
64. Bhutani, K., Stansifer, K., Ticau, S., Bojic, L., Villani, C., Slisz, J., Cremers, C., Roy, C., Donovan, J., Fiske, B., et al. (2019). Widespread haploid-based gene expression in

mammalian spermatogenesis associated with frequent selective sweeps and evolutionary conflict. bioRxiv.
65. Larracuente, A.M., and Presgraves, D.C. (2012). The selfish Segregation Distorter gene complex of Drosophila melanogaster. Genetics *192*, 33-53.
66. Dalstra, H.J., Swart, K., Debets, A.J., Saupe, S.J., and Hoekstra, R.F. (2003). Sexual transmission of the [Het-S] prion leads to meiotic drive in Podospora anserina. Proceedings of the National Academy of Sciences of the United States of America *100*, 6616-6621.
67. Seuring, C., Greenwald, J., Wasmer, C., Wepf, R., Saupe, S.J., Meier, B.H., and Riek, R. (2012). The mechanism of toxicity in HET-S/HET-s prion incompatibility. PLoS Biol *10*, e1001451.
68. Dalstra, H.J., van der Zee, R., Swart, K., Hoekstra, R.F., Saupe, S.J., and Debets, A.J. (2005). Non-mendelian inheritance of the HET-s prion or HET-s prion domains determines the het-S spore killing system in Podospora anserina. Fungal Genet Biol *42*, 836-847.
69. Long, Y., Zhao, L., Niu, B., Su, J., Wu, H., Chen, Y., Zhang, Q., Guo, J., Zhuang, C., Mei, M., et al. (2008). Hybrid male sterility in rice controlled by interaction between divergent alleles of two adjacent genes. Proceedings of the National Academy of Sciences of the United States of America *105*, 18871-18876.
70. Merrill, C., Bayraktaroglu, L., Kusano, A., and Ganetzky, B. (1999). Truncated RanGAP encoded by the Segregation Distorter locus of Drosophila. Science *283*, 1742-1745.
71. Kusano, A., Staber, C., and Ganetzky, B. (2001). Nuclear mislocalization of enzymatically active RanGAP causes segregation distortion in Drosophila. Dev Cell *1*, 351-361.
72. Brittnacher, J.G., and Ganetzky, B. (1989). On the components of segregation distortion in Drosophila melanogaster. IV. Construction and analysis of free duplications for the Responder locus. Genetics *121*, 739-750.
73. Lyttle, T.W. (1989). The effect of novel chromosome position and variable dose on the genetic behavior of the Responder (Rsp) element of the Segregation distorter (SD) system of Drosophila melanogaster. Genetics *121*, 751-763.
74. Wu, C.I., Lyttle, T.W., Wu, M.L., and Lin, G.F. (1988). Association between a satellite DNA sequence and the Responder of Segregation Distorter in D. melanogaster. Cell *54*, 179-189.
75. Gorlich, D., and Kutay, U. (1999). Transport between the cell nucleus and the cytoplasm. Annu Rev Cell Dev Biol *15*, 607-660.
76. Kusano, A., Staber, C., and Ganetzky, B. (2002). Segregation distortion induced by wild-type RanGAP in Drosophila. Proceedings of the National Academy of Sciences of the United States of America *99*, 6866-6870.
77. Hauschteck-Jungen, E., and Hartl, D.L. (1982). Defective Histone Transition during Spermiogenesis in Heterozygous SEGREGATION DISTORTER Males of DROSOPHILA MELANOGASTER. Genetics *101*, 57-69.
78. Seto, A.G., Kingston, R.E., and Lau, N.C. (2007). The Coming of Age for Piwi Proteins. Molecular Cell *26*, 603-609.
79. Nagao, A., Mituyama, T., Huang, H., Chen, D., Siomi, M.C., and Siomi, H. (2010). Biogenesis pathways of piRNAs loaded onto AGO3 in the Drosophila testis. RNA (New York, N.Y.) *16*, 2503-2515.

80. Gell, S.L., and Reenan, R.A. (2013). Mutations to the piRNA pathway component aubergine enhance meiotic drive of segregation distorter in Drosophila melanogaster. Genetics *193*, 771-784.
81. Katz, D.F., Erickson, R.P., and Nathanson, M. (1979). Beat frequency is bimodally distributed in spermatozoa from T/t12 mice. J Exp Zool *210*, 529-535.
82. Olds-Clarke, P., and Johnson, L.R. (1993). t haplotypes in the mouse compromise sperm flagellar function. Dev Biol *155*, 14-25.
83. Bauer, H., Schindler, S., Charron, Y., Willert, J., Kusecek, B., and Herrmann, B.G. (2012). The nucleoside diphosphate kinase gene Nme3 acts as quantitative trait locus promoting non-Mendelian inheritance. PLoS Genet *8*, e1002567.
84. Bauer, H., Veron, N., Willert, J., and Herrmann, B.G. (2007). The t-complex-encoded guanine nucleotide exchange factor Fgd2 reveals that two opposing signaling pathways promote transmission ratio distortion in the mouse. Genes Dev *21*, 143-147.
85. Bauer, H., Willert, J., Koschorz, B., and Herrmann, B.G. (2005). The t complex-encoded GTPase-activating protein Tagap1 acts as a transmission ratio distorter in mice. Nat Genet *37*, 969-973.
86. Charron, Y., Willert, J., Lipkowitz, B., Kusecek, B., Herrmann, B.G., and Bauer, H. (2019). Two isoforms of the RAC-specific guanine nucleotide exchange factor TIAM2 act oppositely on transmission ratio distortion by the mouse t-haplotype. PLoS Genet *15*, e1007964.
87. Herrmann, B.G., Koschorz, B., Wertz, K., McLaughlin, K.J., and Kispert, A. (1999). A protein kinase encoded by the t complex responder gene causes non-mendelian inheritance. Nature *402*, 141-146.
88. Rhoades, N.A., Harvey, A.M., Samarajeewa, D.A., Svedberg, J., Yusifov, A., Abusharekh, A., Manitchotpisit, P., Brown, D.W., Sharp, K.J., Rehard, D.G., et al. (2019). Identification of rfk-1, a Meiotic Driver Undergoing RNA Editing in Neurospora. Genetics *212*, 93-110.
89. Turner, B.C., and Perkins, D.D. (1979). Spore killer, a chromosomal factor in neurospora that kills meiotic products not containing it. Genetics *93*, 587-606.
90. Hammond, T.M., Rehard, D.G., Xiao, H., and Shiu, P.K. (2012). Molecular dissection of Neurospora Spore killer meiotic drive elements. Proceedings of the National Academy of Sciences of the United States of America *109*, 12093-12098.
91. Grognet, P., Lalucque, H., Malagnac, F., and Silar, P. (2014). Genes that bias Mendelian segregation. PLoS Genet *10*, e1004387.
92. Vogan, A.A., Ament-Velasquez, S.L., Granger-Farbos, A., Svedberg, J., Bastiaans, E., Debets, A.J., Coustou, V., Yvanne, H., Clave, C., Saupe, S.J., et al. (2019). Combinations of Spok genes create multiple meiotic drivers in Podospora. Elife *8*.
93. Nuckolls, N.L., Bravo Nunez, M.A., Eickbush, M.T., Young, J.M., Lange, J.J., Yu, J.S., Smith, G.R., Jaspersen, S.L., Malik, H.S., and Zanders, S.E. (2017). wtf genes are prolific dual poison-antidote meiotic drivers. Elife *6*.
94. Bravo Nunez, M.A., Lange, J.J., and Zanders, S.E. (2018). A suppressor of a wtf poison-antidote meiotic driver acts via mimicry of the driver's antidote. PLoS Genet *14*, e1007836.
95. Bravo Nunez, M.A., Sabbarini, I.M., Eickbush, M.T., Liang, Y., Lange, J.J., Kent, A.M., and Zanders, S.E. (2020). Dramatically diverse Schizosaccharomyces pombe wtf meiotic drivers all display high gamete-killing efficiency. PLoS Genet *16*, e1008350.

96. Hu, W., Jiang, Z.D., Suo, F., Zheng, J.X., He, W.Z., and Du, L.L. (2017). A large gene family in fission yeast encodes spore killers that subvert Mendel's law. Elife *6*.
97. Zanders, S.E., Eickbush, M.T., Yu, J.S., Kang, J.W., Fowler, K.R., Smith, G.R., and Malik, H.S. (2014). Genome rearrangements and pervasive meiotic drive cause hybrid infertility in fission yeast. Elife *3*, e02630.
98. Yu, X., Zhao, Z., Zheng, X., Zhou, J., Kong, W., Wang, P., Bai, W., Zheng, H., Zhang, H., Li, J., et al. (2018). A selfish genetic element confers non-Mendelian inheritance in rice. Science *360*, 1130-1132.
99. Chesley, P., and Dunn, L.C. (1936). The Inheritance of Taillessness (Anury) in the House Mouse. Genetics *21*, 525-536.
100. Schimenti, J. (2000). Segregation distortion of mouse t haplotypes the molecular basis emerges. Trends Genet *16*, 240-243.
101. Schimenti, J., Vold, L., Socolow, D., and Silver, L.M. (1987). An unstable family of large DNA elements in the center of the mouse t complex. J Mol Biol *194*, 583-594.
102. Coluccio, A., and Neiman, A.M. (2004). Interspore bridges: a new feature of the Saccharomyces cerevisiae spore wall. Microbiology *150*, 3189-3196.
103. Nuckolls, N.L., Mok, A.C., Lange, J.J., Yi, K., Kandola, T.S., Hunn, A.M., McCroskey, S., Snyder, J.L., Bravo Nunez, M.A., McClain, M.L., et al. (2020). The wtf4 meiotic driver utilizes controlled protein aggregation to generate selective cell death. bioRxiv.
104. Eickbush, M.T., Young, J.M., and Zanders, S.E. (2019). Killer Meiotic Drive and Dynamic Evolution of the wtf Gene Family. Mol Biol Evol *36*, 1201-1214.
105. Lindholm, A.K., Dyer, K.A., Firman, R.C., Fishman, L., Forstmeier, W., Holman, L., Johannesson, H., Knief, U., Kokko, H., Larracuente, A.M., et al. (2016). The Ecology and Evolutionary Dynamics of Meiotic Drive. Trends Ecol Evol *31*, 315-326.
106. Meiklejohn, C.D., and Tao, Y. (2010). Genetic conflict and sex chromosome evolution. Trends Ecol Evol *25*, 215-223.
107. Chang, C.H., Chavan, A., Palladino, J., Wei, X., Martins, N.M.C., Santinello, B., Chen, C.C., Erceg, J., Beliveau, B.J., Wu, C.T., et al. (2019). Islands of retroelements are major components of Drosophila centromeres. PLoS Biol *17*, e3000241.
108. Lin, C.J., Hu, F., Dubruille, R., Vedanayagam, J., Wen, J., Smibert, P., Loppin, B., and Lai, E.C. (2018). The hnRNP/RNAi Pathway Is Essential to Resolve Intragenomic Conflict in the Drosophila Male Germline. Dev Cell *46*, 316-326.
109. Kruger, A.N., Brogley, M.A., Huizinga, J.L., Kidd, J.M., de Rooij, D.G., Hu, Y.C., and Mueller, J.L. (2019). A Neofunctionalized X-Linked Ampliconic Gene Family Is Essential for Male Fertility and Equal Sex Ratio in Mice. Curr Biol *29*, 3699-3706 e3695.
110. Comptour, A., Moretti, C., Serrentino, M.E., Auer, J., Ialy-Radio, C., Ward, M.A., Toure, A., Vaiman, D., and Cocquet, J. (2014). SSTY proteins co-localize with the post-meiotic sex chromatin and interact with regulators of its expression. FEBS J *281*, 1571-1584.
111. Wong, H.W.S., and Holman, L. (2020). Fitness consequences of the selfish supergene *Segregation Distorter*. Journal of Evolutionary Biology *33*, 89-100.
112. Mueller, J.L., Skaletsky, H., Brown, L.G., Zaghlul, S., Rock, S., Graves, T., Auger, K., Warren, W.C., Wilson, R.K., and Page, D.C. (2013). Independent specialization of the human and mouse X chromosomes for the male germ line. Nat Genet *45*, 1083-1087.
113. Skaletsky, H., Kuroda-Kawaguchi, T., Minx, P.J., Cordum, H.S., Hillier, L., Brown, L.G., Repping, S., Pyntikova, T., Ali, J., Bieri, T., et al. (2003). The male-specific region

of the human Y chromosome is a mosaic of discrete sequence classes. Nature *423*, 825-837.
114. Turner, J.M., Mahadevaiah, S.K., Ellis, P.J., Mitchell, M.J., and Burgoyne, P.S. (2006). Pachytene asynapsis drives meiotic sex chromosome inactivation and leads to substantial postmeiotic repression in spermatids. Dev Cell *10*, 521-529.
115. Namekawa, S.H., Park, P.J., Zhang, L.F., Shima, J.E., McCarrey, J.R., Griswold, M.D., and Lee, J.T. (2006). Postmeiotic sex chromatin in the male germline of mice. Curr Biol *16*, 660-667.
116. Greaves, I.K., Rangasamy, D., Devoy, M., Marshall Graves, J.A., and Tremethick, D.J. (2006). The X and Y chromosomes assemble into H2A.Z-containing [corrected] facultative heterochromatin [corrected] following meiosis. Mol Cell Biol *26*, 5394-5405.
117. Turner, J.M., Mahadevaiah, S.K., Fernandez-Capetillo, O., Nussenzweig, A., Xu, X., Deng, C.X., and Burgoyne, P.S. (2005). Silencing of unsynapsed meiotic chromosomes in the mouse. Nat Genet *37*, 41-47.
118. Homolka, D., Ivanek, R., Capkova, J., Jansa, P., and Forejt, J. (2007). Chromosomal rearrangement interferes with meiotic X chromosome inactivation. Genome Res *17*, 1431-1437.
119. Baarends, W.M., Wassenaar, E., van der Laan, R., Hoogerbrugge, J., Sleddens-Linkels, E., Hoeijmakers, J.H., de Boer, P., and Grootegoed, J.A. (2005). Silencing of unpaired chromatin and histone H2A ubiquitination in mammalian meiosis. Mol Cell Biol *25*, 1041-1053.
120. Sin, H.S., and Namekawa, S.H. (2013). The great escape: Active genes on inactive sex chromosomes and their evolutionary implications. Epigenetics *8*, 887-892.
121. Akerfelt, M., Vihervaara, A., Laiho, A., Conter, A., Christians, E.S., Sistonen, L., and Henriksson, E. (2010). Heat shock transcription factor 1 localizes to sex chromatin during meiotic repression. The Journal of biological chemistry *285*, 34469-34476.
122. Akerfelt, M., Henriksson, E., Laiho, A., Vihervaara, A., Rautoma, K., Kotaja, N., and Sistonen, L. (2008). Promoter ChIP-chip analysis in mouse testis reveals Y chromosome occupancy by HSF2. Proceedings of the National Academy of Sciences of the United States of America *105*, 11224-11229.
123. Sassone-Corsi, P. (2002). Unique chromatin remodeling and transcriptional regulation in spermatogenesis. Science *296*, 2176-2178.
124. Betran, E., Demuth, J.P., and Williford, A. (2012). Why chromosome palindromes? Int J Evol Biol *2012*, 207958.
125. Brault, V., Pereira, P., Duchon, A., and Herault, Y. (2006). Modeling chromosomes in mouse to explore the function of genes, genomic disorders, and chromosomal organization. PLoS Genet *2*, e86.
126. Livak, K.J., and Schmittgen, T.D. (2001). Analysis of relative gene expression data using real-time quantitative PCR and the 2(-Delta Delta C(T)) Method. Methods *25*, 402-408.
127. Russell, L.D.E., R. A., Sinha Hikim, A. P., Clegg, E. D. (1990). Histological and Histopathological Evaluation of the Testis, (Cache River Press, Vienna, Austria).
128. Gaysinskaya, V., Soh, I.Y., van der Heijden, G.W., and Bortvin, A. (2014). Optimized flow cytometry isolation of murine spermatocytes. Cytometry A *85*, 556-565.
129. Merkin, J., Russell, C., Chen, P., and Burge, C.B. (2012). Evolutionary dynamics of gene and isoform regulation in Mammalian tissues. Science *338*, 1593-1599.

130. Necsulea, A., Soumillon, M., Warnefors, M., Liechti, A., Daish, T., Zeller, U., Baker, J.C., Grutzner, F., and Kaessmann, H. (2014). The evolution of lncRNA repertoires and expression patterns in tetrapods. Nature *505*, 635-640.
131. Margolin, G., Khil, P.P., Kim, J., Bellani, M.A., and Camerini-Otero, R.D. (2014). Integrated transcriptome analysis of mouse spermatogenesis. BMC Genomics *15*, 39.
132. Larson, E.L., Vanderpool, D., Keeble, S., Zhou, M., Sarver, B.A., Smith, A.D., Dean, M.D., and Good, J.M. (2016). Contrasting Levels of Molecular Evolution on the Mouse X Chromosome. Genetics *203*, 1841-1857.
133. Soumillon, M., Necsulea, A., Weier, M., Brawand, D., Zhang, X., Gu, H., Barthes, P., Kokkinaki, M., Nef, S., Gnirke, A., et al. (2013). Cellular source and mechanisms of high transcriptome complexity in the mammalian testis. Cell Rep *3*, 2179-2190.
134. Trapnell, C., Roberts, A., Goff, L., Pertea, G., Kim, D., Kelley, D.R., Pimentel, H., Salzberg, S.L., Rinn, J.L., and Pachter, L. (2012). Differential gene and transcript expression analysis of RNA-seq experiments with TopHat and Cufflinks. Nat Protoc *7*, 562-578.
135. Hughes, J.F., Skaletsky, H., Pyntikova, T., Graves, T.A., van Daalen, S.K., Minx, P.J., Fulton, R.S., McGrath, S.D., Locke, D.P., Friedman, C., et al. (2010). Chimpanzee and human Y chromosomes are remarkably divergent in structure and gene content. Nature *463*, 536-539.
136. Murphy, W.J., Pearks Wilkerson, A.J., Raudsepp, T., Agarwala, R., Schaffer, A.A., Stanyon, R., and Chowdhary, B.P. (2006). Novel gene acquisition on carnivore Y chromosomes. PLoS Genet *2*, e43.
137. Janecka, J.E., Davis, B.W., Ghosh, S., Paria, N., Das, P.J., Orlando, L., Schubert, M., Nielsen, M.K., Stout, T.A.E., Brashear, W., et al. (2018). Horse Y chromosome assembly displays unique evolutionary features and putative stallion fertility genes. Nature communications *9*, 2945.
138. Skinner, B.M., Sargent, C.A., Churcher, C., Hunt, T., Herrero, J., Loveland, J.E., Dunn, M., Louzada, S., Fu, B., Chow, W., et al. (2016). The pig X and Y Chromosomes: structure, sequence, and evolution. Genome Res *26*, 130-139.
139. Kuroda-Kawaguchi, T., Skaletsky, H., Brown, L.G., Minx, P.J., Cordum, H.S., Waterston, R.H., Wilson, R.K., Silber, S., Oates, R., Rozen, S., et al. (2001). The AZFc region of the Y chromosome features massive palindromes and uniform recurrent deletions in infertile men. Nature genetics *29*, 279-286.
140. Toure, A., Clemente, E.J., Ellis, P., Mahadevaiah, S.K., Ojarikre, O.A., Ball, P.A., Reynard, L., Loveland, K.L., Burgoyne, P.S., and Affara, N.A. (2005). Identification of novel Y chromosome encoded transcripts by testis transcriptome analysis of mice with deletions of the Y chromosome long arm. Genome Biol *6*, R102.
141. Gibbs, R.A., Weinstock, G.M., Metzker, M.L., Muzny, D.M., Sodergren, E.J., Scherer, S., Scott, G., Steffen, D., Worley, K.C., Burch, P.E., et al. (2004). Genome sequence of the Brown Norway rat yields insights into mammalian evolution. Nature *428*, 493-521.
142. Page, S.L., and Hawley, R.S. (2004). The genetics and molecular biology of the synaptonemal complex. Annu Rev Cell Dev Biol *20*, 525-558.
143. Reynard, L.N., Turner, J.M., Cocquet, J., Mahadevaiah, S.K., Toure, A., Hoog, C., and Burgoyne, P.S. (2007). Expression analysis of the mouse multi-copy X-linked gene Xlr-related, meiosis-regulated (Xmr), reveals that Xmr encodes a spermatid-expressed cytoplasmic protein, SLX/XMR. Biol Reprod *77*, 329-335.

144. Baier, A., Alsheimer, M., Volff, J.N., and Benavente, R. (2007). Synaptonemal complex protein SYCP3 of the rat: evolutionarily conserved domains and the assembly of higher order structures. Sex Dev *1*, 161-168.
145. Syrjanen, J.L., Pellegrini, L., and Davies, O.R. (2014). A molecular model for the role of SYCP3 in meiotic chromosome organisation. Elife *3*.
146. Sato, T., Katagiri, K., Yokonishi, T., Kubota, Y., Inoue, K., Ogonuki, N., Matoba, S., Ogura, A., and Ogawa, T. (2011). In vitro production of fertile sperm from murine spermatogonial stem cell lines. Nature communications *2*, 472.
147. Yuan, L., Liu, J.G., Zhao, J., Brundell, E., Daneholt, B., and Hoog, C. (2000). The murine SCP3 gene is required for synaptonemal complex assembly, chromosome synapsis, and male fertility. Mol Cell *5*, 73-83.
148. Chew, T.G., Peaston, A., Lim, A.K., Lorthongpanich, C., Knowles, B.B., and Solter, D. (2013). A tudor domain protein SPINDLIN1 interacts with the mRNA-binding protein SERBP1 and is involved in mouse oocyte meiotic resumption. PLoS One *8*, e69764.
149. Su, X., Zhu, G., Ding, X., Lee, S.Y., Dou, Y., Zhu, B., Wu, W., and Li, H. (2014). Molecular basis underlying histone H3 lysine-arginine methylation pattern readout by Spin/Ssty repeats of Spindlin1. Genes Dev *28*, 622-636.
150. Adams, S.R., Maezawa, S., Alavattam, K.G., Abe, H., Sakashita, A., Shroder, M., Broering, T.J., Sroga Rios, J., Thomas, M.A., Lin, X., et al. (2018). RNF8 and SCML2 cooperate to regulate ubiquitination and H3K27 acetylation for escape gene activation on the sex chromosomes. PLoS Genet *14*, e1007233.
151. Staub, E., Mennerich, D., and Rosenthal, A. (2002). The Spin/Ssty repeat: a new motif identified in proteins involved in vertebrate development from gamete to embryo. Genome Biol *3*, RESEARCH0003.
152. Presgraves, D.C. (2008). Sex chromosomes and speciation in Drosophila. Trends Genet *24*, 336-343.
153. Forejt, J. (1996). Hybrid sterility in the mouse. Trends Genet *12*, 412-417.
154. Zanders, S.E., and Unckless, R.L. (2019). Fertility Costs of Meiotic Drivers. Curr Biol *29*, R512-R520.
155. Larson, E.L., Kopania, E.E.K., and Good, J.M. (2018). Spermatogenesis and the Evolution of Mammalian Sex Chromosomes. Trends Genet *34*, 722-732.
156. Soh, Y.Q., Junker, J.P., Gill, M.E., Mueller, J.L., van Oudenaarden, A., and Page, D.C. (2015). A Gene Regulatory Program for Meiotic Prophase in the Fetal Ovary. PLoS Genet *11*, e1005531.
157. Necsulea, A., and Kaessmann, H. (2014). Evolutionary dynamics of coding and non-coding transcriptomes. Nat Rev Genet *15*, 734-748.
158. Hammoud, S.S., Low, D.H., Yi, C., Carrell, D.T., Guccione, E., and Cairns, B.R. (2014). Chromatin and transcription transitions of mammalian adult germline stem cells and spermatogenesis. Cell Stem Cell *15*, 239-253.
159. Chalmel, F., Lardenois, A., Evrard, B., Rolland, A.D., Sallou, O., Dumargne, M.C., Coiffec, I., Collin, O., Primig, M., and Jegou, B. (2014). High-resolution profiling of novel transcribed regions during rat spermatogenesis. Biol Reprod *91*, 5.
160. Bray, N.L., Pimentel, H., Melsted, P., and Pachter, L. (2016). Near-optimal probabilistic RNA-seq quantification. Nat Biotechnol *34*, 525-527.
161. Love, M.I., Huber, W., and Anders, S. (2014). Moderated estimation of fold change and dispersion for RNA-seq data with DESeq2. Genome Biol *15*, 550.

162. Haeussler, M., Schonig, K., Eckert, H., Eschstruth, A., Mianne, J., Renaud, J.B., Schneider-Maunoury, S., Shkumatava, A., Teboul, L., Kent, J., et al. (2016). Evaluation of off-target and on-target scoring algorithms and integration into the guide RNA selection tool CRISPOR. Genome Biol *17*, 148.
163. Scott, M.A., and Hu, Y.C. (2019). Generation of CRISPR-Edited Rodents Using a Piezo-Driven Zygote Injection Technique. Methods Mol Biol *1874*, 169-178.
164. Ahmed, E.A., and de Rooij, D.G. (2009). Staging of mouse seminiferous tubule cross-sections. Methods Mol Biol *558*, 263-277.
165. Perez-Riverol, Y., Csordas, A., Bai, J., Bernal-Llinares, M., Hewapathirana, S., Kundu, D.J., Inuganti, A., Griss, J., Mayer, G., Eisenacher, M., et al. (2019). The PRIDE database and related tools and resources in 2019: improving support for quantification data. Nucleic Acids Res *47*, D442-D450.
166. Hach, F., Hormozdiari, F., Alkan, C., Hormozdiari, F., Birol, I., Eichler, E.E., and Sahinalp, S.C. (2010). mrsFAST: a cache-oblivious algorithm for short-read mapping. Nat Methods *7*, 576-577.
167. Pendleton, A.L., Shen, F., Taravella, A.M., Emery, S., Veeramah, K.R., Boyko, A.R., and Kidd, J.M. (2018). Comparison of village dog and wolf genomes highlights the role of the neural crest in dog domestication. BMC Biol *16*, 64.
168. Guryev, V., Saar, K., Adamovic, T., Verheul, M., van Heesch, S.A., Cook, S., Pravenec, M., Aitman, T., Jacob, H., Shull, J.D., et al. (2008). Distribution and functional impact of DNA copy number variation in the rat. Nat Genet *40*, 538-545.
169. Cortez, D., Marin, R., Toledo-Flores, D., Froidevaux, L., Liechti, A., Waters, P.D., Grutzner, F., and Kaessmann, H. (2014). Origins and functional evolution of Y chromosomes across mammals. Nature *508*, 488-493.
170. Pavesi, G., Zambelli, F., Caggese, C., and Pesole, G. (2008). Exalign: a new method for comparative analysis of exon-intron gene structures. Nucleic Acids Res *36*, e47.
171. Ogura, A., Matsuda, J., Asano, T., Suzuki, O., and Yanagimachi, R. (1996). Mouse oocytes injected with cryopreserved round spermatids can develop into normal offspring. J Assist Reprod Genet *13*, 431-434.
172. Kishigami, S., and Wakayama, T. (2007). Efficient strontium-induced activation of mouse oocytes in standard culture media by chelating calcium. J Reprod Dev *53*, 1207-1215.
173. Ellis, P.J., Ferguson, L., Clemente, E.J., and Affara, N.A. (2007). Bidirectional transcription of a novel chimeric gene mapping to mouse chromosome Yq. BMC Evol Biol *7*, 171.
174. Russell, L.D., Ettlin, R.A., Sinha Hikim, A.P., Clegg, E.D. (1990). Histological and Histopathological Evaluation of the Testis, (Clearwater, FL: Cache River Press).
175. Hallast, P., Balaresque, P., Bowden, G.R., Ballereau, S., and M.A., J. (2013). Recombination dynamics of a human Y-chromosomal palindrome: rapid GC-biased gene conversion, multi-kilobase conversion tracts, and rare inversions. PLoS Genet *9*.
176. Kruger, A.N., Ellison, Q., Brogley, M.A., Gerlinger, E.R., and Mueller, J.L. (2018). Male mice with large inversions or deletions of X-chromosome palindrome arms are fertile and express their associated genes during post-meiosis. Sci Rep *8*, 8985.
177. Turner, J.M. (2007). Meiotic sex chromosome inactivation. Development *134*, 1823-1831.

178. Hasegawa, K., Sin, H.S., Maezawa, S., Broering, T.J., Kartashov, A.V., Alavattam, K.G., Ichijima, Y., Zhang, F., Bacon, W.C., Greis, K.D., et al. (2015). SCML2 establishes the male germline epigenome through regulation of histone H2A ubiquitination. Dev Cell *32*, 574-588.
179. Luo, M., Zhou, J., Leu, N.A., Abreu, C.M., Wang, J., Anguera, M.C., de Rooij, D.G., Jasin, M., and Wang, P.J. (2015). Polycomb protein SCML2 associates with USP7 and counteracts histone H2A ubiquitination in the XY chromatin during male meiosis. PLoS Genet *11*, e1004954.
180. Trinklein, N.D., Murray, J.I., Hartman, S.J., Botstein, D., and Myers, R.M. (2004). The role of heat shock transcription factor 1 in the genome-wide regulation of the mammalian heat shock response. Mol Biol Cell *15*, 1254-1261.
181. Hou, S., Xian, L., Shi, P., Li, C., Lin, Z., and Gao, X. (2016). The Magea gene cluster regulates male germ cell apoptosis without affecting the fertility in mice. Sci Rep *6*, 26735.
182. Doyle, J.M., Gao, J., Wang, J., Yang, M., and Potts, P.R. (2010). MAGE-RING protein complexes comprise a family of E3 ubiquitin ligases. Mol Cell *39*, 963-974.
183. Ernst, C., Eling, N., Martinez-Jimenez, C.P., Marioni, J.C., and Odom, D.T. (2019). Staged developmental mapping and X chromosome transcriptional dynamics during mouse spermatogenesis. Nature communications *10*, 1251.
184. Ward, M.A., and Burgoyne, P.S. (2006). The effects of deletions of the mouse Y chromosome long arm on sperm function--intracytoplasmic sperm injection (ICSI)-based analysis. Biol Reprod *74*, 652-658.
185. Greenbaum, M.P., Yan, W., Wu, M.H., Lin, Y.N., Agno, J.E., Sharma, M., Braun, R.E., Rajkovic, A., and Matzuk, M.M. (2006). TEX14 is essential for intercellular bridges and fertility in male mice. Proceedings of the National Academy of Sciences of the United States of America *103*, 4982-4987.
186. Miles, E.L., O'Gorman, C., Zhao, J., Samuel, M., Walters, E., Yi, Y.J., Sutovsky, M., Prather, R.S., Wells, K.D., and Sutovsky, P. (2013). Transgenic pig carrying green fluorescent proteasomes. PNAS *110*.
187. Zheng, Y., Deng, X., Zhao, Y., Zhang, H., and Martin-DeLeon, P.A. (2001). Spam1 (PH-20) mutations and sperm dysfunction in mice with the Rb(6.16) or Rb(6.15) translocation. Mamm Genome *12*, 822-829.
188. Haldane, J.B.S. (1922). Sex Ratio and Unisexual Sterility in Hybrid Animals. Journal of Genetics *12*, 101-109.
189. Kousathanas, A., Halligan, D.L., and Keightley, P.D. (2014). Faster-X Adaptive Protein Evolution in House Mice. Genetics *196*, 1131-1143.
190. Coyne, J.A. (1992). Genetics and speciation. Nature *355*.
191. Coyne, J.A., and Orr, H.A. (1989). Two rules of speciation: Speciation and its Consequences, (Sunderland, Mass: Sinauer Assoc).
192. Masly, J.P., and Presgraves, D.C. (2007). High-Resolution Genome-Wide Dissection of the Two Rules of Speciation in Drosophila. PLoS Biol *5*.